AFWAL-TR-82-2001

AD A117845

AUGMENTOR STABILITY MANAGEMENT PROGRAM

FINAL REPORT

R. Ernst
Pratt & Whitney Aircraft Group
Government Products Division
Division of United Technologies Corporation
P.O. Box 2691, West Palm Beach, Florida 33402

February 1982

Report for Periods: 1 September 1979 to 30 September 1981

Approved for Public Release; Distribution Unlimited

DTIC
ELECTED
AUG 5 1982

B

Aero Propulsion Laboratory
Air Force Wright Aeronautical Laboratories
Air Force Systems Command
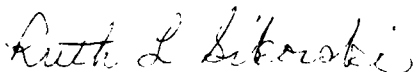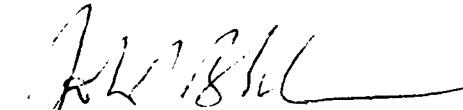Wright-Patterson Air Force Base, Ohio 45433

NOTICE

When Government drawings, specifications, or other data are used for any purpose other than in connection with a definitely related Government procurement operation, the United States Government thereby incurs no responsibility nor any obligation whatsoever; and the fact that the government may have formulated, furnished, or in any way supplied the said drawings, specifications, or other data, is not to be regarded by implication or otherwise as in any manner licensing the holder or any other person or corporation, or conveying any rights or permission to manufacture use, or sell any patented invention that may in any way be related thereto.

This report has been reviewed by the Office of Public Affairs (ASD/PA) and is releasable to the National Technical Information Service (NTIS). At NTIS, it will be available to the general public, including foreign nations.

This technical report has been reviewed and is approved for publication.

RUTH L. SIKORSKI
Project Engineer

JOHN BLACKMAN, Sqn Ldr, RAF
Acting Chief, Components Branch
Turbine Engine Division

FOR THE COMMANDER

H. I. BUSH
Director
Turbine Engine Division

"If your address has changed, if you wish to be removed from our mailing list, or if the addressee is no longer employed by your organization please notify AFWAL/POTC, W-PAFB, OH 45433 to help us maintain a current mailing list".

Copies of this report should not be returned unless return is required by security considerations, contractual obligations, or notice on a specific document.

SECURITY CLASSIFICATION OF THIS PAGE *(When Data Entered)*

REPORT DOCUMENTATION PAGE		READ INSTRUCTIONS BEFORE COMPLETING FORM
1. Report Number *AFWAL*-TR-82-2001	2. Govt Accession No. *AD-A117926*	3. Recipient's Catalog Number
4. Title *(and Subtitle)* AUGMENTOR STABILITY MANAGEMENT PROGRAM		5. Type of Report & Period Covered Final Report 1 Sept. 1979 to 30 Sept. 1981
		6. Performing Org. Report Number FR-15477
7. Author(s) R. C. Ernst		8. Contract or Grant Number(s) F33615-79-C-2059
9. Performing Organization Name and Address United Technologies Corporation Pratt & Whitney Aircraft Group Government Products Division P.O. Box 2691, West Palm Beach, FL 33402		10. Program Element, Project, Task Area & Work Unit Numbers 3066-06-35
11. Controlling Office Name and Address Air Force Wright Aeronautical Laboratories (AFWAL/POTC) Wright-Patterson Air Force Base, Ohio 45433		12. Report Date February 1982
		13. Number of Pages 107
14. Monitoring Agency Name & Address *(if different from Controlling Office)*		15. Security Class. *(of this report)* Unclassified
		15a. Declassification/Downgrading Schedule

16. Distribution Statement *(of this Report)*

Approved for public release; distribution unlimited.

17. Distribution Statement *(of the abstract entered in Block 20, if different from Report)*

18. Supplementary Notes

19. Key Words *(Continue on reverse side if necessary and identify by block number)*

Flameholder	Afterburner	Flame Speed
Combustion Stability	Combustion Efficiency	Flame Stability
Augmentors	Turbofan	

20. Abstract *(Continue on reverse side if necessary and identify by block number)*
   A model has been developed which predicts the efficiency and low frequency stability of a turbofan augmentor. The model evaluates the stability characteristics of the flameholders at low inlet temperature with a model for two-phase fuel flames. The driving potential for low frequency instability is identified with excessive flameholder wake fuel-air ratio. The model is compared to engine experience, available literature and other models with favorable results.

DD $_{1\ JAN\ 73}^{\ FORM}$ **1473** EDITION OF 1 NOV 65 IS OBSOLETE

SECURITY CLASSIFICATION OF THIS PAGE *(When Data Entered)*

FOREWORD

This final report was prepared in accordance with Contract F33615-79-C-2059, Augmentor Stability Management Program. The work was conducted under the direction of Lt. Donna J. Bess and Ms. Ruth L. Sikorski, Project Engineers, of the Air Force Wright Aeronautical Laboratories (POTC). This report presents the work conducted by Pratt & Whitney Aircraft Group, Government Products Division of United Technologies Corporation, during the period 1 September 1979 through 30 September 1981. The Program Manager for Pratt & Whitney Aircraft Group was Mr. R. C. Ernst. The principal investigators were Mr. E. A. Petrino, Dr. M. A. Glickstein and Mr. R. C. Ernst.

CONTENTS

ILLUSTRATIONS

ILLUSTRATIONS (Continued)

TABLES

LIST OF SYMBOLS

English Symbol	Definition	Typical Units
A	Area	$in.^2$
A	Stirred reactor mass loading	gm-mole/sec
A	Dummy variable in eqn. (128)	d'less
a	Reaction index in eqn. (111)	d'less
As	Surface area	sq in.
BPR	Bypass ratio	d'less
B/D	Wake width per unit flameholder	d'less
C	Activation energy constant in eqn. (111)	°K
c	Sonic velocity	in/sec
C_d	Drag coefficient	d'less
C_p	Specific heat at constant pressure	Btu/lbm/°R
C_v	Specific heat at constant volume	Btu/lbm/°R
C_v	Wake shape factor	$litre/in.^2$
C_1	Dummy variable in eqn. (85)	d'less
d	Diameter	in.
D_v	Diffusion coefficient	$in.^2/sec$
FA	Fuel-air ratio	d'less
H	Enthalpy	Btu/lbm
h_f	Film coefficient	$Btu/in.^2/sec/°R$
k	Reaction rate in eqn. (107)	d'less
k	Thermal conductivity in eqn. (91)	Btu/in./sec°R
K	Dummy variable in eqn. (71)	d'less
K1	Recirculation coefficient	d'less
L/D	Wake length per unit flameholder width	d'less
m	Mass	lbm
m	Mass flowrate	lbm/sec
M	Mach number	d'less
MW	Molecular weight	lbm/lb-mole
n	Reaction order in eqn. (107)	d'less
N	Flameholder width	in.
Nu	Nusselt number	d'less
p	Pressure	$lbf/in.^2$
Δp	Pressure drop	$lbf/in.^2$
PFSR	Sprayring fuel pressure	$lbf/in.^2$
Pr	Prandtl number	d'less
q	Volumetric heat release rate	$Btu/sec/in.^3$
q	Heat flux	$Btu/in.^2sec$
R	Gas constant	ft-lbf/lbm/°R
Re	Reynold's number	d'less
S	Entropy	Btu/lbm/°R
St	Turbulent flame speed	ft/sec
Sl	Laminar flame speed	ft/sec
T	Temperature	°F, °R, °K
Ti	Ideal temperature	°R
t	Time	sec
TFSR	Sprayring fuel temperature	°F
U	Flameholder lip velocity	ft/sec
u	Internal energy	Btu/lbm/°R
u	RMS turbulence velocity fluctuation	ft/sec

LIST OF SYMBOLS (Continued)

English Symbol	Definition	Typical Units
V	Velocity	ft/sec
Vo	Wake volume	litre
W	Duct width	in.
W	Mass flowrate	lbm/sec
WCOOL	Liner cooling flow/total engine flow	d'less
X	Axial distance	in.
Δx	Distance	in.
y	Stoichiometry factor in eqn. (108)	d'less
Δy	Flame penetration distance	in.
z	Defined in eqn. (76)	d'less
Z	Defined in eqn. (125)	d'less

Greek Symbol	Definition	Typical Units
α	Flameholder apex angle	deg
β	Defined in eqn. (75)	d'less
β_1	Droplet vaporization coefficient	d'less
β_2	Droplet collective coefficient	d'less
β_3	Surface vaporization coefficient	d'less
Γ	Blockage ratio	d'less
γ	Ratio of specific heats	d'less
ϵ	Wake reaction efficiency	d'less
ϵ_o	Turbulence intensity	d'less
η	Efficiency	d'less
λ	Latent heat or vaporization	Btu/lbm
μ	Viscosity	lbf/in.
χ_o	Oxygen concentration	gm-mole/litre
χ_{o2}	Oxygen volume fraction	d'less
χ_f	Fuel concentration	gm-mole/litre
ρ	Density	lbm/in.^{3}
τ	Wake residence time	sec
τ'	Normalized residence time	d'less
ℓ	Axial length between stations	in.
δ	Ratio of specific heats	d'less
τ	Sonic travel time	sec

Special Symbol:

Δ	Finite difference	

SECTION I

INTRODUCTION

The phenomenon of combustion instability has plagued all types of high heat release combustors from industrial furnaces to rocket engines. In general, however, the problem has been most severe in flight propulsion systems such as turbojets, ramjets, and rockets where weight considerations dictate highly efficient structures. In such applications, the pressure, vibration, and heat loads resulting from combustion instability, superimposed on the normal loading, are usually destructive.

In airbreathing engines, high frequency combustion instability problems were first encountered in the early 1950's, and solutions were sought through mathematical modeling and analytical studies directed toward an understanding of the phenomenon. Unfortunately, the computer technology and analytical techniques of 20 years ago proved inadequate, and "cut and try" empirical approaches involving changes in flameholders, combustion chamber shape, fuel injection, velocity profiles, and flame piloting were attempted. Fuel additives and combustion chamber baffles were also tested. Although some of these approaches, notably baffles, produced marginal improvement, the problem was not solved until damping devices in the form of acoustical absorbers (screech liners) were introduced. Screech liners are used routinely, and high frequency instability is no longer regarded as a problem.

Larger and more powerful turbopropulsion systems are presently being designed and developed. Because of the large physical dimensions of augmentors used in these systems, their natural acoustic modes have correspondingly long wavelengths; therefore, combustion instability can occur at very low frequencies, i.e., approximately 200 Hz or less.

The occurrence of instability at lower frequencies makes use of screech liners of conventional design difficult. To obtain adequate damping, the absorbing devices are designed so that the resonant frequency corresponds to the frequency of the expected mode of instability. The required cavity volume is inversely proportional to the square of the resonant frequency; therefore, low frequencies require large volumes. Large cavity volumes can be accommodated by increasing the augmentor envelope, but this produces an unacceptable increase in engine weight.

The problem of these very low frequencies, called rumble, have been reduced through combined experimental and analytical techniques. This experience has emphasized the necessity to understand the fundamental mechanisms involved in order to formulate a meaningful analytical effort and the necessity to relate this effort to physical hardware and processes.

The main feature which limits the usefulness of many combustion stability models is the absence of a direct correlation between the physical hardware of a real augmentor and combustion stability. Experience has shown that relatively subtle alterations in flameholder geometry can produce profound changes in rumble limits. For a usable design and evaluation tool, the model must be able to relate directly to such geometry changes.

Such a model was developed by Pratt & Whitney Aircraft under two previous Air Force contracts. These programs were:

(1) Flameholder Combustion Instability Study, F33615-76-C-2023
(2) Lo-Frequency Augmentor Instability Study, F33615-76-C-2024.

The model which resulted from these programs correctly predicted the major qualitative trends of augmentor rumble. There were, however, some areas of quantitative improvement desired and also some extensions of program capability.

The goals of this effort were to quantitatively improve the predictions of the model in the areas of combustion efficiency, rumble frequency and rumble limits. Also, this program added to the model the analytical capability to predict the augmentor fuel-air ratio distribution from the input injector geometry and flow conditions.

The resultant analytical models have been combined into one computer program which has three major modules as follows:

● The fuel injection module predicts the transient or steady-state behavior of an input fuel injection system of sprayrings or spraybars. The major output is a fuel flowrate distribution in an augmentor.

● The combustion module predicts the efficiency of a turbofan augmentor of known geometry and inlet flow conditions. The fuel-air ratio distribution may be input or calculated from the output of the fuel injection module. The major outputs are the predicted efficiency and the dynamic efficiency influence coefficients.

● The rumble module predicts the stability of the augmentor at known geometry and flow conditions. This module may use either specified combustion data or the results of the combustion module.

This final report is designed to provide a comprehensive description of the analytical formulation of all three modules in one document. Therefore, it contains information from the final reports of the previous studies as well as the results of this program. This report is a companion to the User's Manual for the Augmentor Stability Management Program (AFAPL-TR-81-   ).

SECTION II

TECHNICAL DISCUSSION

1. PROGRAM ORGANIZATION

The Augmentor Stability Management Program was structured as a continuation of two previous Air Force-sponsored programs which defined the fundamental models for flame stabilization and low-frequency stability in turbofan augmentors. There were two major goals to the current program. These were:

    a. Correct known deficiencies in the existing models for flame stabilization and system stability.

    b. Extend the capabilities of the models by including an analysis for the fuel injection system which is capable of predicting the augmentor fuel-air ratio as a function of time.

The program resulted in a computer program which has the capability of predicting the performance and stability of a given turbofan augmentor configuration at a specified operating condition. The computer program incorporates the three major models of the analysis which are:

    a. Augmentor Fuel Injection Model

    b. Augmentor Combustion Model

    c. Augmentor Rumble Model

The fundamental operational mode of the total program is as follows:

● Fuel injection model — for a specified fuel system geometry and specified augmentor conditions, the model predicts the fuel injection distribution as a function of time. A transfer subroutine converts this into the fuel-air ratio distribution approaching a user specified flameholder configuration. This is the primary output of this model.

● Augmentor combustion model — taking the now known fuel-air ratio distribution and input flameholder and augmentor geometries, this model will evaluate the level of combustion efficiency at specified augmentor inlet conditions. The model will also predict if any of the flameholder elements are beyond the local stabilization limit. The model then generates a series of normalized combustion gain factors which are to be used in the rumble analysis.

● Augmentor rumble model — using the given geometry, conditions, efficiency and gain factors, this model predicts the dynamic gain and phase angle of low-frequency oscillations. An instability exists whenever a gain of unity or more is shown with a phase angle of zero degrees.

The overall computer code includes all three of these models. They may, however, be run in any separate or sequential fashion if the user specifies the required transfer data.

3

This Final Report presents the results of the development and verification studies on each of these three major models in the following three sections. A detailed User's Manual was also written to document specific computer usage information.

B. TECHNICAL RESULTS

1. Augmentor Fuel Injection Model

a. *General*

Aircraft gas turbine engines with thrust augmentation share a common problem of requiring a fuel delivery system in a high-temperature environment. During nonaugmented operation, augmentor sprayrings or spraybars soak in the turbine exhaust gas and are heated to the gas temperature. During augmentation the fuel system is cooled by the flowing fuel. Problems can occur during the transition from nonaugmented to augmented operation. The transient start process requires the filling of hot fuel lines with fuel, and may result in fuel boiling, surging, and failure to achieve and sustain augmentor ignition. Depending on the particular fuel system configuration, different engines may have significantly different problems related to the transient start of augmentation.

b. *Physical System*

An augmentor fuel system, as defined in this model, consists of a fuel control system, a fuel distribution system, and necessary connecting plumbing. Two types of distribution systems are considered in the model, circumferential sprayrings and radial spraybars, and both types will henceforth be referred to generically as "injectors." A typical sprayring, shown in Figure 1, is supplied with fuel at one or more inlet locations along its circumference. Fuel spray jets may be either constant or variable area orifices, and are distributed along the sprayring. In a sprayring fuel system, multiple rings of different diameters are positioned coaxially in the augmentor, and may be supplied with fuel individually or in various multiple combinations.

In a spraybar system, radial spraybars are positioned circumferentially around the augmentor. Fuel supply is from one end, and spraybars may be jointly supplied in multiple combinations or zones.

Fuel control systems operate to control either fuel inlet flow rate, system pressure, or a combination of the two. Furthermore, provisions may be made for rapid system fill during start transient, or for sequenced starting of multiple zone systems.

During nonaugmented operation the augmentor fuel supply system is filled with air, and soaks in the hot turbine exhaust environment. During the transition to augmented operation, fuel fills the system, displacing the air and cooling the heated injector. The incoming fuel is heated and boils as it contacts the hot injector walls. The air and fuel vapor inside the injector are compressed by the incoming fuel, causing system pressure to rise, which in turn affects both the heat transfer to the fuel, and the rates of fuel flow and air flow out of the system. The transient phenomena associated with start of augmentation are controlled by the complex interaction of heat transfer, single and two-phase flow of air and fuel out of the system, and thermodynamic behavior of the system components.

Upper Inlet

Fuel Outflow

Air Outflow

Air

Two-Phase Boiling Fuel

Sprayring

Fuel Outflow

Lower Inlet

Supply Line

Fuel Inflow

Fuel Control
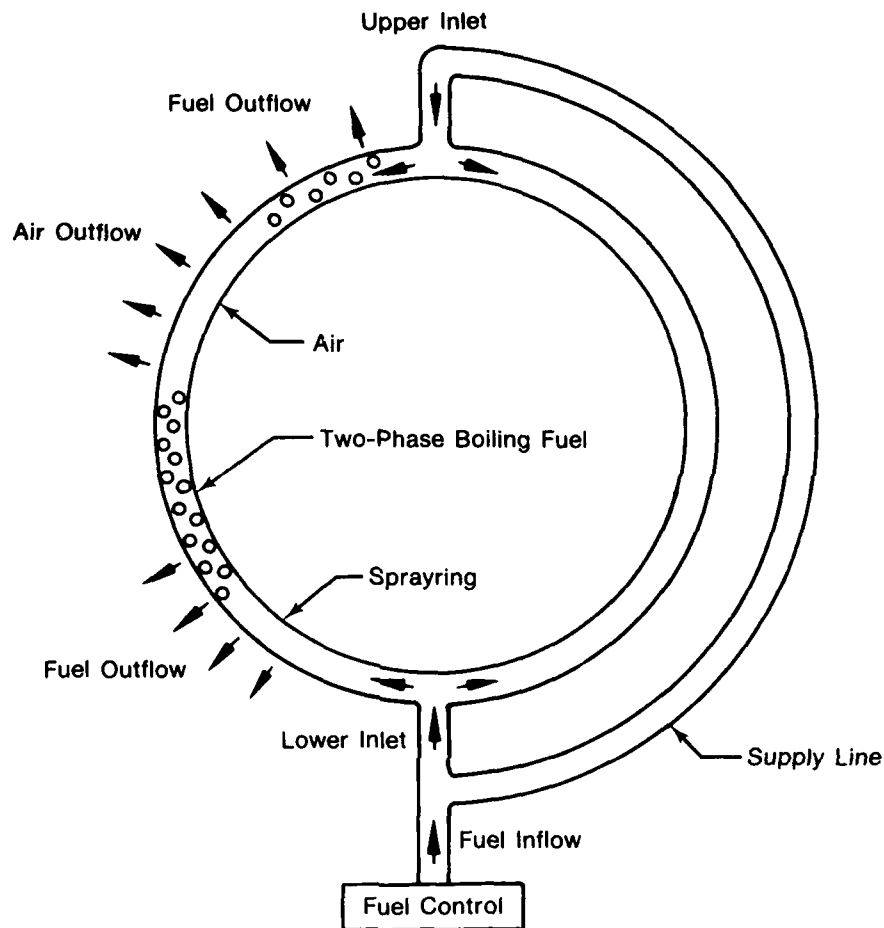
FD 230852

Figure 1.   Schematic of Sprayring During Fill Process

Several simplifications are made in describing the physical system by an analytical model. The three most signifcant assumptions are the following:

1. The fluid system can be described as three regimes: a liquid fuel, and two-phase fuel (liquid-vapor). These regimes do not mix.

2. The two-phase fuel regime can be described as a homogeneous mixture of liquid and vapor.

3. The pressure throughout the fuel system is uniform at any time (i.e., pressure losses within the system are small compared to temporal rates of pressure change).

6

Figure 2 illustrates the model assumptions as applied to a spraybar. The illustrated spraybar consists of two sections, a cold section oriented out of the hot turbine exhaust, and a heated section in the turbine exhaust. The fuel spray jets are assumed to be distributed uniformly over the entire length of the spraybar. The coordinates shown in Figure 2 define the length of the subcooled liquid regime (X_o), the length of the two-phase regime ($X - X_o$), and the length of the air regime (Z_a).
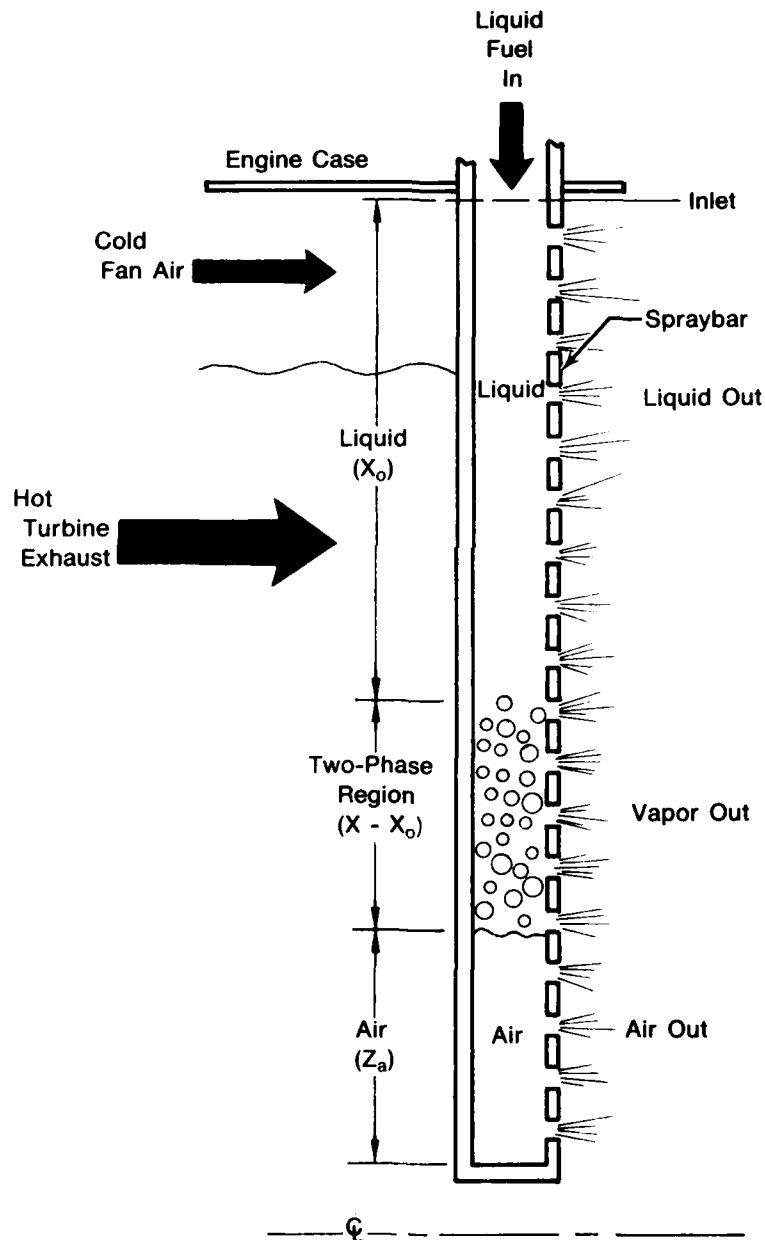
FD 165285

Figure 2. Schematic of Spraybar Showing Fluid Regimes

7

To begin the analysis of the augmentor start transient, the initial conditions must be specified. Initially, the injector is assumed to be air-filled and the metal temperatures are assumed equal to the local turbine exhaust temperatures. As fuel enters the system, the air is compressed and flows out through the spray jets. Fuel is heated, eventually boiling, and the fuel vapor adds to pressurization of the system. Air is gradually purged from the system, and the transient continues until the injector is cooled to the level determined by steady-state heat transfer rates.

c. Continuity and System Dynamics

Considering air, liquid fuel, and fuel vapor as separate species, mass continuity equations can be written for each specie. In an injector of cross sectional area A, the liquid fuel mass (M) is:

$$M_\ell = \rho A \, [X - \alpha(X - X_o)] \tag{1}$$

where ρ is the mean liquid density, α is the vapor void fraction, and (X, X_o) are regime lengths defined in Figure 2. Similarly, the masses of vapor and air in the system are:

$$M_v = \rho_v A \, \alpha \, (X - X_o) \tag{2}$$

$$M_a = \rho_a A \, Z_a \tag{3}$$

where ρ_v and ρ_a are the densities of vapor and air. Specie continuity is described by:

$$\frac{dM_\ell}{dt} = m_{li} - m_{lo} - m_v \qquad \text{(liquid)} \tag{4}$$

$$\frac{dM_v}{dt} = m_v - m_{vo} \qquad \text{(vapor)} \tag{5}$$

$$\frac{dM_a}{dt} = -m_a \qquad \text{(air)} \tag{6}$$

where (m_{li}, m_{lo}) are liquid flow rates in and out of the system. m_v is the rate of vapor generation, and (m_{vo}, m_a) are rates of vapor and air flow out of the system.

Combining Equations (1) through (6), assuming air compression to be isentropic, and vapor compression to be at constant quality, a set of continuity equations is produced relating system pressure and liquid and vapor volume. Solving the set of equations simultaneously for the interdependent variables results in a set of equations defining the rates of change of pressure, liquid volume, and vapor volume in the system. The resulting continuity set, written for a spraybar fed from one end is:

$$\frac{dP}{dt} = \frac{\dfrac{\dot{m}_{li}}{\rho} - \dfrac{\dot{m}_{lo}}{\rho} + \left(\dfrac{1}{\rho_v} - \dfrac{1}{\rho}\right)\dot{m}_v - \dfrac{\dot{m}_{vo}}{\rho_v} - \dfrac{\dot{m}_a}{\rho_a}}{\dfrac{AZ_a}{\gamma P} + \dfrac{A}{\rho_v}\left(\dfrac{\partial \rho_v}{\partial P}\right)\alpha(X - X_o)} \tag{7}$$

$$\frac{d\,\alpha(X - X_o)}{dt} = \frac{\dot{m}_v - \dot{m}_{vo}}{A\rho_v} - \frac{1}{\rho_v}\left(\frac{\partial \rho_v}{\partial P}\right)\alpha(X - X_o)\frac{dR}{dt} \tag{8}$$

$$\frac{dx}{dt} = \frac{d\,\alpha(X - X_o)}{dt} + \frac{\dot{m}_{li} - \dot{m}_{lo} - \dot{m}_v}{\rho A} \tag{9}$$

8

The dependent variables are system pressure (P), fuel-air interface location (X), two-phase interface (X_0), and vapor void fraction (α). From the nature of this equation set, it is apparent that heat transfer and flow calculations must be performed prior to, or simultaneously with, evaluation of the set, and are in turn dependent upon the results.

d. Heat Transfer Model

Because of the strong dependence of system performance on fuel vaporization rate (m_v), as evidenced in the continuity equations, provision of an accurate description of the fuel heat transfer characteristics is a prerequisite to the realistic simulation of the physical system.

Two principal heat transfer processes occur: heat flows from the injector to the fuel during the transient cooling of the system, and as the injector cools, heat flows from the hot turbine exhaust gases, establishing a steady-state process. The transient process is the primary source of heat flow during system fill and cooldown.

Heat transfer from the injector to the flowing fuel can occur in one of several modes, combining simple convection with various boiling modes. Because of the high initial temperature of the injector, film boiling of the fuel is possible. Because the heat source is from energy storage in the injector, the source temperature is the controlling parameter in the heat transfer process. As the system cools, heat transfer modes will vary from forced convection film boiling, to forced nucleate boiling, to simple convection. The local instantaneous difference between the injector temperature and the fuel liquid saturation temperature is considered to be the controlling parameter for determination of the heat transfer regime. Figure 3 shows the principal differences in the several heat transfer modes. Although vapor is generated by boiling in subcooled fuel, the vapor is rapidly condensed in the colder fluid away from the wall. Vapor accumulation only begins when the bulk fluid temperature equals the liquid saturation temperature (T_{sl}). During saturation boiling, the fuel bulk temperature (T_b) increases from the saturated liquid to the saturated vapor state at the location of total vaporization, or dryout. The various regimes are shown again in Figure 4 as a function of temperature difference between wall and saturated liquid state (ΔT_w). Three specified temperature differences are used to identify heat transfer regimes: the onset of nucleate boiling (ΔT_0), the maximum nucleate boiling condition (ΔT^*), and the minimum film boiling condition (ΔT_{CT}). In each heat transfer regime the liquid fuel may be in a thermodynamic state ranging from subcooled to saturated.
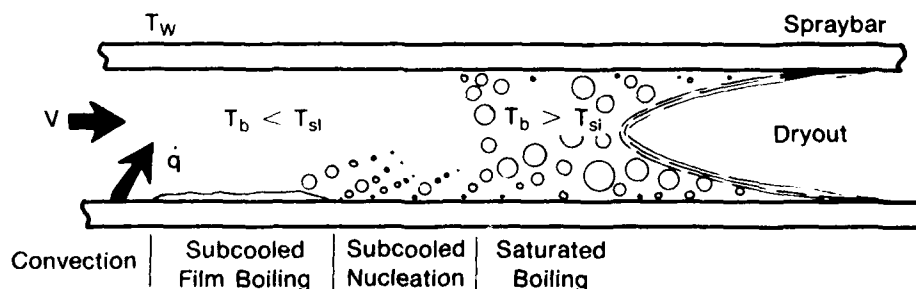
FD 230854

Figure 3. Heat Transfer Processes in Sprayring

9
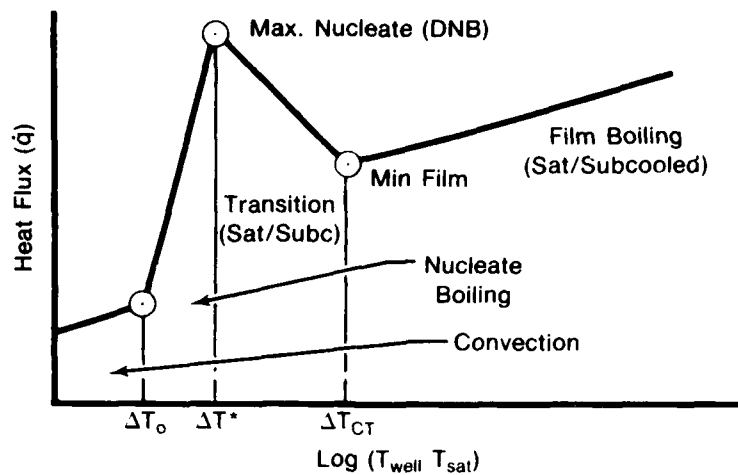
Figure 4. Fuel Heat Transfer Regimes

Figure 5 illustrates the thermodynamic process path as a blended hydrocarbon fuel (such as JP-5) is heated at constant pressure. The heat transfer characteristics in each heat transfer regime are defined by an empirical model. Figure 6 shows the logic for selection of the appropriate empirical model for description of the local heat transfer to the fuel.
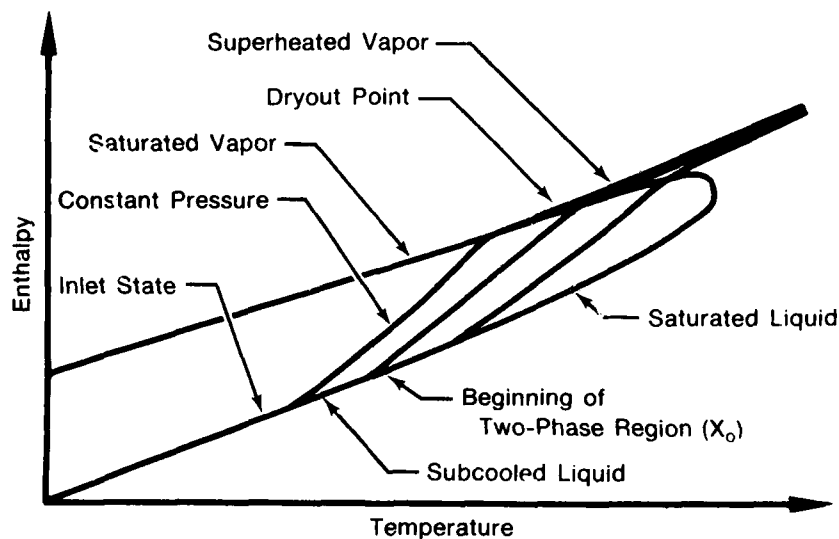
Figure 5. Path of Thermodynamic Process for Fuel Flow in Sprayring

10
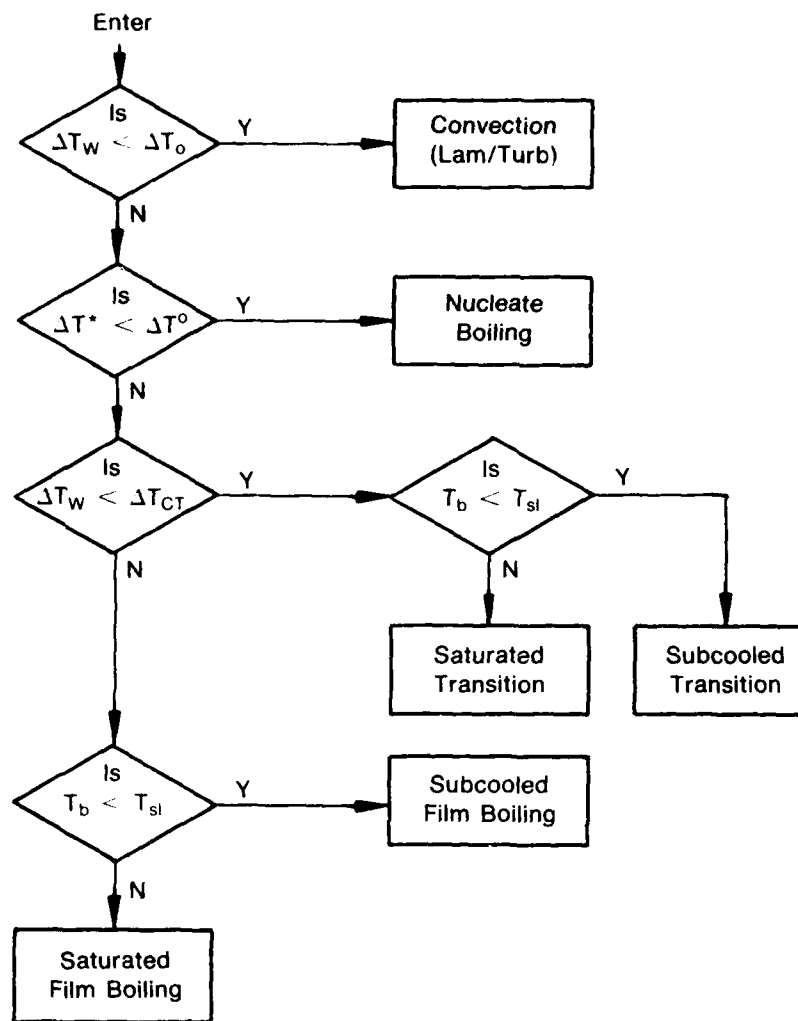
FD 230859

Figure 6. Logic for Heat Transfer Model

The specific models used are as follows:

1. Nonboiling convection is described by the Dittus-Boelter relation for turbulent flow, with a constant lower limit of the Nusselt number for laminar flow.

2. Nucleate boiling is described by interpolation between the convection model and the maximum nucleate boiling heat flux, described by Kaminski[1] for JP-5 by:

$$q_{max} = 27.4 + 0.351 \; \Delta T_{sc} \; V \; (Btu/hr\text{-}ft^2) \tag{10}$$

where

$\Delta T_{sc} = T_{sl} - T_b, \; °R$
$V = fuel \; velocity, \; ft/sec$

11

3. Saturated film boiling is described by Glickstein and Whitesides[2] for light hydrocarbons by:

$$Nu = 0.1058 \ Re_f^{0.641} \ Pr_f^{0.4} \ \left(\frac{\rho_b}{\rho_v}\right)^{0.5} \tag{11}$$

where the Reynolds number (Re_f) is based on the local fuel velocity and ρ_b is the bulk density.

4. Subcooled film boiling is described for JP-5 by a modified Dittus-Boelter equation of the form:

$$Nu = 0.529 \ Re_f^{0.8} \ Pr^{0.4} \ Sn^{0.8} \tag{12}$$

where Sn is the Sterman Number, defined by

$$S_n = \frac{q\left(\dfrac{1}{\rho_f} - \dfrac{1}{\rho_b}\right)}{V H_{fg}} \tag{13}$$

The vapor density (ρ_f) is evaluated at the arithmetic average film temperature, and H_{fg} is the constant pressure latent heat of vaporization.

5. Boiling in the transition regime is treated by interpolation between maximum nucleate boiling and minimum film boiling.

e. Flow Model

Accurate evaluation of the fuel and air flow rates out of the injector is an implicit requirement for the evaluation of the continuity equations. In addition, fuel velocity within the system is required for evaluation of the heat transfer to the fuel. Since the local internal velocity is dependent on the distribution of overboard flow (out of the system), and the local thermodynamic state, it is apparent that the overboard mass flow rates and internal heat transfer are implicitly related.

Characterization of the overboard flow is simplified by defining several flow regimes. Flow of air from the injector is described as one-dimensional compressible flow, and may be subsonic or choked flow. Fuel flow regimes are somewhat more complex, and may be distinguished by examining pressure potential throughout the injector. If P_{sb} is the bulk saturation pressure corresponding to the local fluid bulk temperature, then P_{sb} will vary throughout the system. Figure 7 shows the variation of P_{sb} over the length of a heated injector, compared with the system pressure (P) and the augmentor pressure (P_o). The regimes are defined, (I) $P_{sb} < P_o$, (II) subcooled with $P_{sb} > P_o$, and (III) two-phase flow:

1. *Regime I* — Fuel is subcooled and vapor pressure is less than augmentor pressure. Fuel flow is described as liquid flow through an orifice with the pressure difference ($P - P_o$).

2. *Regime II* — Fuel is subcooled, but vapor pressure exceeds augmentor pressure. Fuel is assumed to vaporize as it flows through the spray jets, limiting discharge pressure to P_{sb}. Flow is described as orifice flow with the driving pressure difference ($P - P_{sb}$).

12

3. *Regime III* - Two-phase flow with bulk boiling. Fuel flow is choked in the spray jets, the flow process being described as isentropic expansion from system pressure (P), to a critical pressure (P*). The ratio of critical to system pressure (P*/P) is a function of local vapor void fraction, described by Starkman,[3] et al. and ranges from 0.72 to approximately 0.5. The vapor fraction of the total flow in the two-phase regime is assumed to equal the initial local vapor quality.
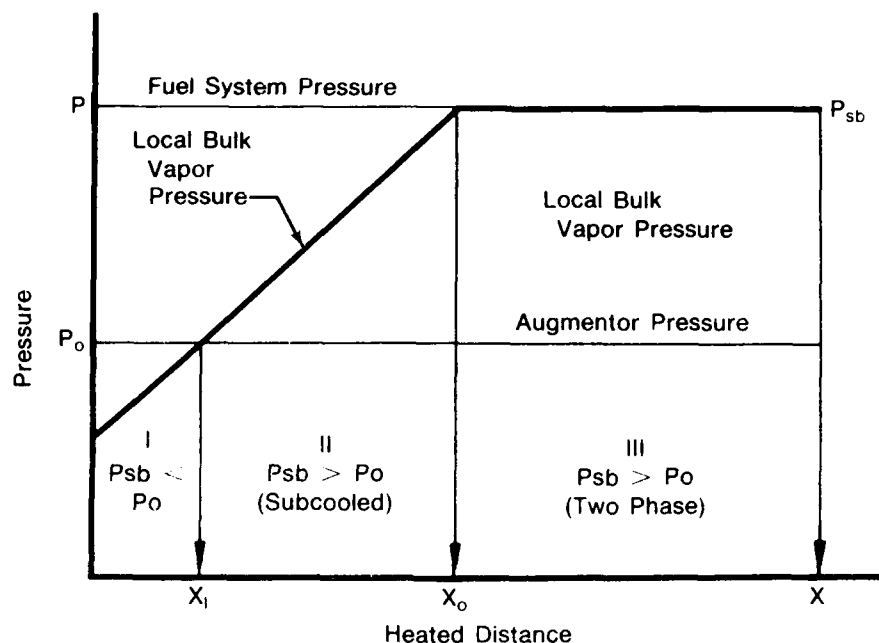
Figure 7. Definition of Fuel Flow Regimes

FD 230855

f. Program Logic

The described models for continuity, heat transfer, and mass flow have been programmed for computer evaluation. Required thermodynamic and thermophysical properties of several fuels have been incorporated in the program as empirical correlations. Although simultaneous evaluation of the various models would be desirable, sequential evaluation is used in the program because of its inherent simplicity.

Transient simulation of the augmentor start sequence begins with a defined initial system condition. Evaluation of the various models proceeds in a time-marching mode, with an update of all models and properties at each time step. Spatial evaluation of heat transfer, mass flow and injector and fuel temperature distributions are conducted with finite element analysis at each time step. The operational sequence of the computer evaluation is outlined in the logic diagram shown in Figure 8.

Time marching evaluation continues until the system becomes totally liquid-filled. Referring to Equation (7) for rate of pressure change, it is noted that the denominator tends to zero as the system becomes totally free of air and fuel vapor. For that case, the numerator of Equation (7) must be identically zero, defining the incompressible flow condition.

13

Enter

Input
- Fuel Type
- System Geometry
- Aero and Initial Conditions
- Control Mode
- Number of Zones (IT)

Initialize Sprayring Zone Index I = 1

Is t > t_max? — Yes → **Stop**; No

Increment Time Step t = t + Δt — Yes

Is I > IT? — No; Yes

Increment Zone Index I = I + 1

Calculate Sprayring Pressure

Control Routine
- Bookkeeping of Multizone Sprayring Variables
- Calculate Inlet Flow for Each Sprayring

Thermal Analysis
- Calculate Local Heat Fluxes in Fuel and Air
- Calculate Wall Temperature

Thermodynamic Analysis
Calculate:
- Fuel Temperature
- Location of Two-Phase Region
- Vaporization Rate
- Fuel Quality, Void Fraction

Flow Analysis
Calculate Fuel Flow Distribution Into Augmentor

Continuity
Calculate:
- Rate of System Pressure Change
- Rate of System Mass Change
- Rate of Liquid and Two-Phase Region Change

FD 165786

Figure 8. Flow Logic for Augmentor Fuel System Model

Continuity Equation (7) defines rate of change of system pressure as a function of several independent variables, including inlet fuel flow. As a result, the program can most conveniently be used to simulate fuel systems with inlet flow rate controlled as a function of time. The model can also be readily used for multiple zone systems. To allow evaluation of such systems, the program has been configured to operate in a multiplex mode, sequentially evaluating at each time step the characteristics of each zone. Operated in this mode, the program can simulate multiple augmentor fuel systems with different zones programmed to start in sequence, at the same time, or in any other combination.

14

g. Analytical Results

The program has been compared with engine test data at several different operating conditions, with good results. A single sprayring, with controlled inlet fuel flow, was exercised through the start sequence with the engine operating both at sea-level static and also at high altitude subsonic conditions. Figure 9 shows the inlet flow rate schedule used in the SLS test, and also used as program input. Figure 10 shows the resulting fuel system pressures, measured in the test and predicted by the simulation. Figure 11 and 12 show the same comparison for a test at Mach No. 0.8 and 50,000 ft altitude. In both comparisons the model results agree well with the engine data, although some differences are apparent in predicted pressure levels. Continuing model development is currently in progress to refine the quantitative accuracy of the model.
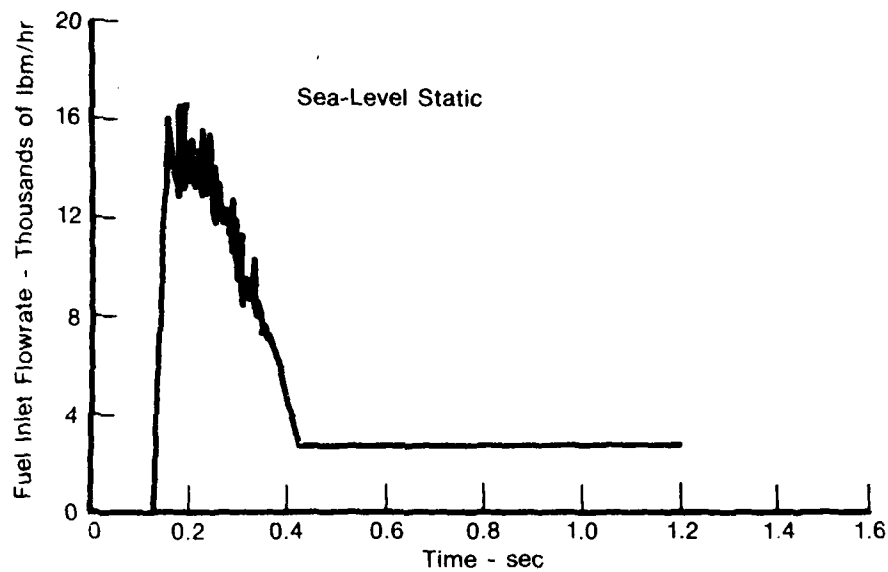
FD 230861

Figure 9. Inlet Fuel Flow in Sprayring Test at SLS Conditions

15
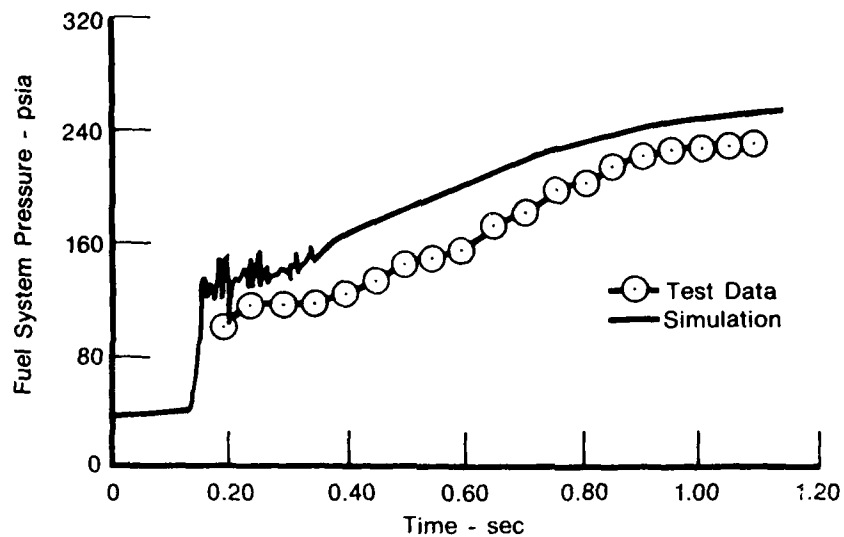
Figure 10. *Comparison of Measured and Predicted Pressures in Fuel System During Augmentor Start at SLS Condition*
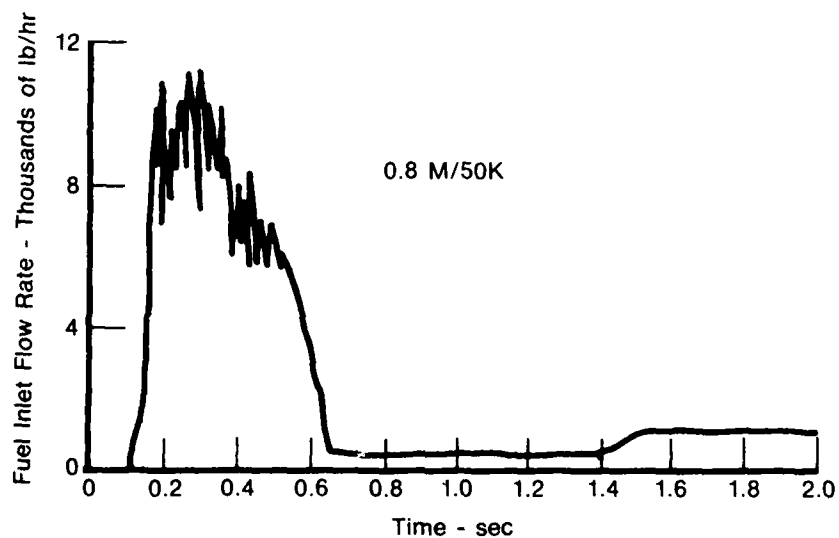
Figure 11. *Inlet Fuel Flow in Sprayring Test at Mach 0.8/50,000 ft Altitude Conditions*

16
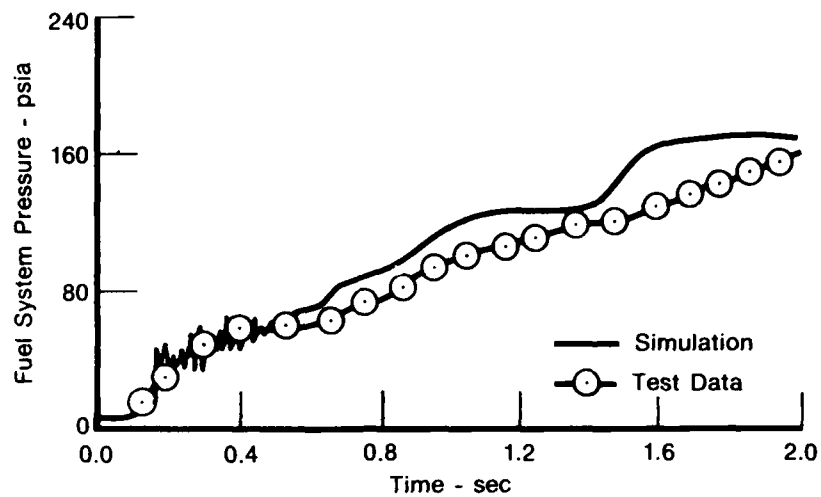
FD 230864

Figure 12. Comparison of Measured and Predicted Pressures in Fuel Systems During Augmentor Start at Mach 0.8/50,000 ft Altitude Conditions

2. Development of the Combustion Model

a. Rumble Mechanism

The nature of the feedback mechanism which drives rumble is the classical pressure and velocity response of the heat release mechanism causing variations in the average augmentor exit temperature. These variations result in oscillations in average nozzle inlet pressure through the choked flow relationships for a constant mass flowrate. This results in further oscillations in the flow conditions around the sprayring and flameholder region. The relative amplitudes and phase angles are functions of the geometry and operating conditions of the augmentor and fan duct.

The analysis and model for rumble were structured to rely as heavily as possible on analyses of the physical processes of the fuel preparation, flame stabilization and flame propagation. In this manner it was felt that maximum utility of the model would be realized. All too frequently combustion stability models are generated with built-in correlation constants which are generic to one form of combustor only. Whenever a geometry variation is performed there is no guideline for the required change in those constants, and the utility of the model is limited until sufficient experience is obtained. In this model format we have attempted to remove that restriction.

The mechanism of response of the heat release process to variations in pressure and velocity over the sprayring and flameholder region is described below with reference to Figure 13.

- A variation in pressure and velocity over the fuel injection spraybar results in a variation in the average air mass flowrate and thus local fuel-air ratio, since the fuel flowrate is essentially constant.

- At the flameholder, the pressure and velocity oscillation results in a variation in the rate of formation of the flameholder wake fuel-air ratio from the available liquid phase fuel.

- The pressure/velocity oscillation also results in a variation in the level of the wake reaction efficiency at the above level of fuel-air ratio. This results in a variation in the rate of initial flame propagation into the approach stream fuel-air mixture.

- The pressure/velocity oscillation also results in a variation in the rate of transverse flame spreading at the local flame speed due to the influences of local pressure and turbulence on flame speed.

- The final result is a variation in the average value of the nozzle inlet temperature due to the combined effects of the previous responses.

This variation occurs at a time delay equal to the transport delay between the sprayrings and the nozzle.

This process includes two major mechanisms which cause a response in nozzle inlet temperature to oscillations in augmentor inlet pressure or velocity. The variation in local fuel-air ratio (i.e., axial variation at fixed overall level) causes an axial variation in heat release which is felt as a temporal oscillation in nozzle inlet temperature. Imposed onto this variation is the variation in axially local heat release, at the value of fuel-air ratio, caused by response of the flame-holding process to the pressure or velocity oscillations.

18
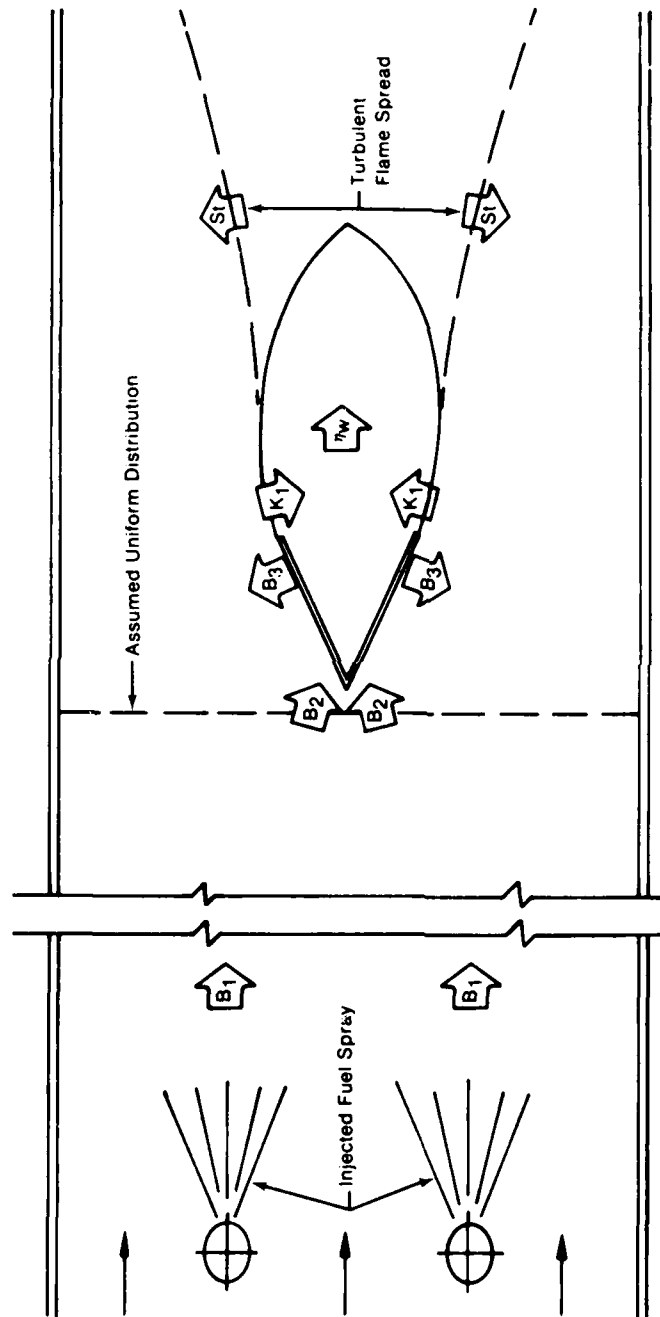
Nomenclature

B_1 — Droplet Varporization Fraction
B_2 — Flameholder Liquid Collection Coefficient
B_3 — Surface Vaporization Fraction
K_1 — Recirculation Rate Coefficient
N_w — Wake Reaction Efficiency
S_t — Turbulent Flame Speed

Figure 13. Two-Phase Fuel Ducted Flame Model

19

b. Combustion Model

The basic framework of the model will be described with references to Figure 13. This illustration may be visualized as representing a two-dimensional sector of a flameholder array. A full augmentor analysis would require a multistreamtube solution to represent the full flameholder.

The augmentor inlet conditions are known in terms of area, pressure, velocity, temperature, turbulence intensity and vitiation level (if any). The required overall fuel-air ratio and thus fuel flowrate from the spraybar is specified in terms of flowrate versus pressure drop and droplet size and distribution also versus pressure drop. Once specified, the flowrate of fuel or overall fuel-air ratio and duct static pressure will define a droplet size distribution.

At this point of injection a simple enthalpy balance is performed to evaluate the percentage of the fuel which vaporizes due to the adiabatic throttling process of injection from the high-pressure sprayring into the low-pressure augmentor. For this, the fuel properties and fuel temperature in the sprayring must be known. The fuel flowrate which remains in the liquid phase is placed into 5 or 10 fuel droplet size groups which represent equal mass flowrate distributions of the spray distribution curve for the particular sprayring injector.

These fuel droplets are allowed to accelerate with the airstream towards the flameholder with concurrent droplet vaporization. The vaporization analysis utilizes a forced convection model for combined heat and mass transfer. A finite difference scheme integrates the accelerating vaporizing droplet lifetime until either the flameholder plane is reached or the droplet diameter goes to zero. This is performed for each droplet size group. The droplets are treated as spherical for the acceleration and vaporization analysis.

It is at this location, the flameholder leading edge, that the combustion model deviates from classical flameholder or combustion analyses. The classical explanation for the mechanism by which a flameholder functions is that the wake of the bluff body serves as a volume for the reaction of the vapor phase mainstream fuel-air mixture. Ignition of the high-speed mainstream mixture is achieved by the hot wake reaction products in the shear layers aft of the flameholder. The degree of reaction achieved in the wake volume is dependent on the ratio of average residence time to average reaction rate. The reaction rate depends on the entering vapor fuel-air ratio and operating pressure and temperature, i.e., kinetic rate constants.

The problem is that in a relatively cool airstream, such as the 250 deg fan duct exit temperature, and overall fuel-air ratios which typically react well, the degree of droplet vaporization is very low. So low, in fact, that the vapor phase fuel-air ratio at the flameholder is well below the lean flammability limit for JP-type fuels. However, these conditions do produce stable flames in actual burners. Obviously, there is some additional mechanism by which vapor phase fuel is generated and mixed into the flameholder wake.

The mechanism which has been identified for this process is the formation of a liquid film on the surface of the flameholder by impingement of the fuel droplets. This surface film is partially vaporized by the heat flux from the hot wake through the surface of the flameholder into the film. This vaporized fuel enters the recirculation zone through the shear layer and provides the bulk of the vapor fuel for the wake reaction process.

For the purposes of the model, the process of fuel collection on the surface of the flameholder is analyzed as spherical droplet trajectories through the flow field as it moves around the flameholder. The analysis is performed for each of the initial drop size groups

20

utilizing the diameter which remains after the droplet has experienced partial vaporization between the spraybar and the flameholder. This analysis defines the fuel collection rate onto the surface of the flameholder, when integrated over the droplet size groups.

Once the film is established on the surface, the rate of vaporization is analyzed by assuming a Nusselt number form of forced mass transfer driven by the vapor pressure of the film. A combined film heating and vaporization solution is performed as a finite difference analysis along the surface. The heat flux is evaluated from a wake film coefficient and an assumed wake temperature. Since the wake temperature is a function of the fuel vaporization rate and the wake reaction level, an iterative solution is required between this initial guess of wake temperature and the calculated value.

As the finite difference solution proceeds, a certain amount of liquid fuel accumulates which has experienced heating but no vaporization. This fuel is lost to the near field stabilization process but does enter into the far field reaction during turbulent flame spreading. The energy required to raise this fuel from its collection temperature to the final film temperature represents a heat loss from the wake reaction.

For the evaluation of the wake reaction, the wake is treated as a well-stirred chemical reactor operating with gaseous fuel. To perform this calculation, the volume and mass influx rate must be known. These values are produced from published data on the relative size and recirculation rates behind bluff body stabilizers as functions of geometry and operating conditions. (Specific source references will be given as the analyses are developed in a later section of this report.) These data have been reduced to a series of empirical functions which relate wake volume and recirculation rate to flameholder blockage, geometry, approach flow conditions, and turbulence level.

The reaction efficiency in this known size wake reactor is analyzed assuming that the process proceeds as a single step, second order reaction with the inefficiencies represented as unreacted CO for lean operation or unreacted fuel for rich operation. The entering mass flowrate is balanced against the mass consumption rate at an unknown final level of efficiency. A straight-forward solution for the reaction efficiency and thus wake temperature proceeds. Any external heat gain or loss mechanisms are used to adjust the reaction rate and increase or reduce the final reactor efficiency.

At the known level of entering air and droplet vaporized fuel flowrate plus surface vaporized fuel, the iteration is performed as follows:

> Recirculation rate calculated
> Wake temperature assumed
> Surface vaporization calculated
> Wake fuel-air ratio thus known
> Wake reaction level at this f/a calculated
> Wake temperature thus known
> Iterate back through surface vaporization

At this point the wake conditions are known, and the fuel-air ratio distribution around the flameholder is known. The turbulent flame spreading into the free-stream is initiated in the shear layer by the hot wake products. The degree of perfect initiation depends on the excess thermal energy available from these products. Flame initiation is a go or no-go phenomenon and statistical in nature, since a lack of perfect initiation physically results in local regions along the surface of zero ignition. As the temperature of the wake products is

21

reduced, the percentage of the area which fails to ignite increases. As these regions increase in number and size, a greater portion of the heat liberated in those areas which do ignite is transferred into adjacent unlit regions rather than into transverse flame propagation. Since the model is based on uniform flame initiation, this process is observed as a slower rate of flame spreading. To produce this result, the model relates the flame speed to the ideal turbulent value and the wake efficiency level.

The form of the flame spreading model is a thin sheet flame front propagating into a fuel-air mixture at a velocity which was accelerated by the flameholder blockage. The specific analysis for the turbulent flame speed follows Karlovitz, where the turbulent flame speed is related to the laminar flame speed, at the approach conditions and the local fuel-air ratio, and the local value of turbulent velocity. This latter term is evaluated from the turbulence generated by the flameholder and axially decayed in a 10 L/D length, based on the width of the effective jet flow between the flameholders, as a function proportional to $x^{-1}2$. The final value after decay is the free-stream intensity.

An additional term is added to the calculated value of the turbulent flame speed to account for the sensitivity of the reaction rate to integrated efficiency and flame self-turbulence. These terms are modeled as a multiplier whose value depends on the local efficiency and has a value of 1 at zero and 100% efficiencies. The peak value is 2 at 50% efficiency.

The transverse position of the flame front is found by a finite difference integration of the local flame front into the approach flow. Due to the sustaining effect of the local heat release, the approach velocity is axially retained at the value accelerated by the flameholder.

The overall efficiency is found at the nozzle entrance through integration of the flame spreading heat release evaluated from the preceding analyses.

The combustion analyses are computerized into one cohesive pro am which combines the models for the various processes. The computerization approach selected is one which utilizes separate subroutines for each of the process sections of the model. Although this approach consumes slightly more computer run time than a full step-by-step calculation procedure it was selected for two reasons:

1. It allows easier alterations to each separate process should changes in any of the local analyses be desired, e.g., a revised reaction kinetics model. This reduces the chances for errors due to unforeseen interactions between sections of the program.

2. The iterative steps required between the wake analysis and the surface vaporization analysis is facilitated if they are isolated in the program.

The required input consists of a description of the geometry of the streamtube:

Blockage ratio
Flameholder width
Flameholder apex angle
Spraybar to flameholder spacing
Flameholder to exhaust spacing.

Those parameters which describe the operating conditions are:

Inlet pressure
Inlet velocity
Inlet temperature
Inlet turbulence intensity
Fuel-air ratio
Spraybar fuel pressure
Spraybar fuel temperature
Fuel type
Vitiation fuel-air ratio.

These inputs define the required flamework for the analysis. The program organization is shown in Figure 14. The various subroutines perform the analyses as follows:

INJECT   This performs the spray formation and throttling process vaporization analyses.

ACCEL   This evaluates the forced vaporization and acceleration of the droplets between the spraybar and flameholder. Done once per droplet size group.

COLLECT   This evaluates the collective rate of the liquid droplets onto the surface of the flameholder. Performed once per droplet size group.

RECIRC   This evaluates the size of the recirculation zone wake behind the flameholder and the rate of entry of gaseous components into this volume.

B3   This evaluates the rate of vaporization of the liquid film from the surface of the flameholder.

WAKE   For the results of RECIRC and B3, this solves for the wake reaction efficiency and temperature.

FLAME   This performs the solution for the transverse penetration of the turbulent flame from the wake shear layer into the free-stream mixture.

Currently, the input and output reflect the requirements to analyze a single case streamline analysis. The output defines the intermediate results of the various subroutines as well as the heat release profile between the flameholder and the exhaust nozzle. The program is capable of multiple case execution limited only by run time. This capability is utilized for multiple streamtube analysis and parametric studies. At present, there is no graphics output capability, but it could be added.

c.   Analyses and Results

The combustion model as formulated for the rumble mechanism essentially consists of two parts. These are a compositional analysis and a reaction analysis. The compositional analysis defines the manner in which a combustible fuel-air mixture is generated from the injected liquid fuel. The reaction analysis defines the manner in which this mixture actually burns to produce a final level of combustion efficiency.

Injector Characteristics

Droplet Vaporization and Acceleration

Droplet Capture

Recirculation

Surface Vaporization

Wake Reaction

Flame Propagation
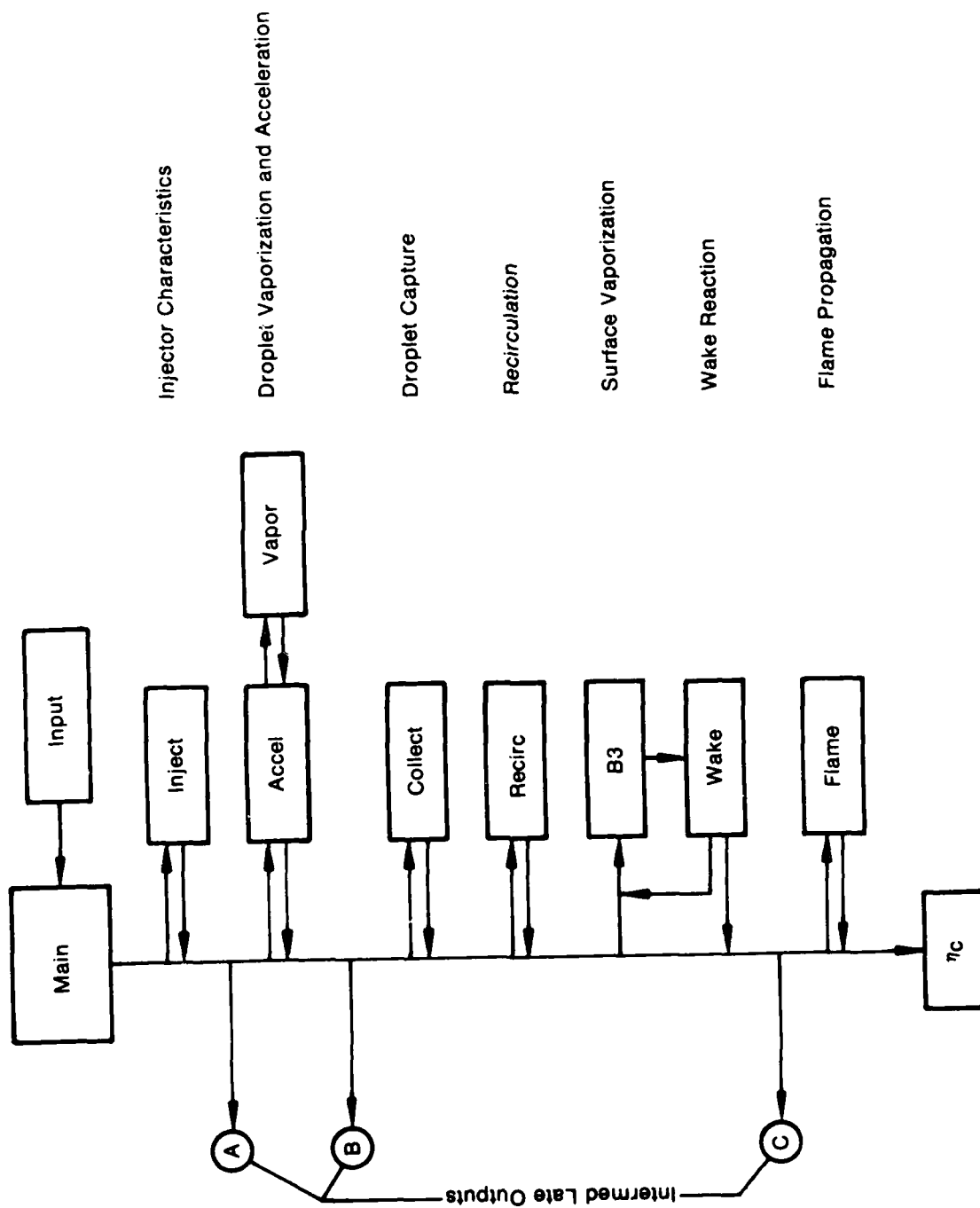
Figure 14. Ducted Flame Model Linkage Map

FD 134040

The analysis for the compositional portion is outlined below for the basic case of a two-dimensional duct with a bluff body stabilizer and liquid fuel injection source. For ease of development of the solutions, the following assumptions were used:

- The injected liquid fuel forms a homogeneously dispersed spray which fills the full cross section of the duct.

- The approach flow field is uniform in the transverse direction, i.e., transverse uniformity of velocity, pressure, and temperature.

Under these assumptions, the form of the compositional analysis was developed. The schematic of the processes is shown in Figure 15.
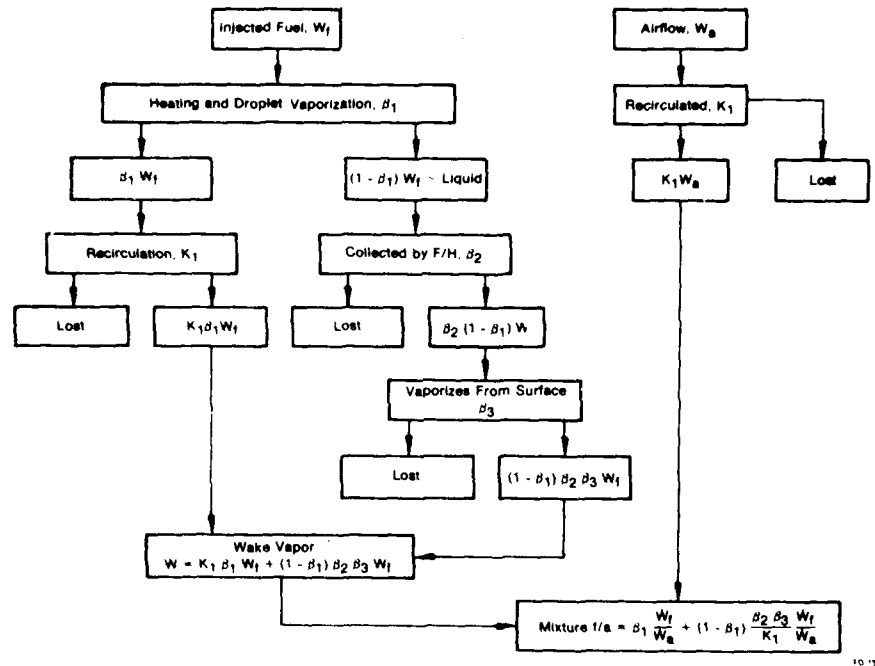
Figure 15. Schematic of Wake Mixture Formation

A certain portion of the injected fuel flowrate experiences flash vaporization during the injection process and forms a uniform flowrate of vapor phase fuel. This fuel flowrate is:

$$\dot{w}_{f_v} = \beta_{1_T}\dot{w}_f. \tag{14}$$

The remaining portion of fuel goes into a liquid droplet spray which undergoes spray vaporization. The vapor flowrate produced by this process is:

$$\dot{w}_{f_v} = \beta_{1_E}(1 - \beta_{1_T})\dot{w}_f. \tag{15}$$

Combining these processes into one influence coefficient we may write:

$$\dot{w}_{f_v} = \beta_1\dot{w}_f. \tag{16}$$

25

We continue to utilize the assumption that the vaporized fuel is homogeneously spread as it is produced. The next processes which are evaluated are those concerned with the formation of the liquid film vaporization rate.

At the flameholder plane, the mixture consists of a flowrate of air (w_a), vapor fuel (w_{f_v}) and liquid fuel ($w_{f\ell}$) defined as:

$$\dot{w}_a = \rho_a VA \tag{17}$$

$$\dot{w}_{f_T} = \theta \dot{w}_a \tag{18}$$

$$\dot{w}_{f_v} = \beta_1 \dot{w}_{f_T} = \beta_1 \theta \dot{w}_a \tag{19}$$

$$\dot{w}_{f\ell} = \dot{w}_{f_T} - \dot{w}_{f_v} = (1-\beta_1)\theta \dot{w}_a. \tag{20}$$

This leaves $(1-\beta_1)$ liquid fuel percentage available. Flowing through the flameholder area, then we have:

$$\dot{w}_{a\Gamma} = \Gamma \dot{w}_a = \Gamma \rho VA \tag{21}$$

$$\dot{w}_{f\ell_\Gamma} = (1-\beta_1) \theta \dot{w}_a \Gamma \tag{22}$$

$$\dot{w}_{f_v\Gamma} = \beta_1 \theta \dot{w}_a \Gamma. \tag{23}$$

The liquid and vapor fuel-air ratios at this point are:

$$(f/a)_v \frac{\dot{w}_{f_v\Gamma}}{\dot{w}_a \Gamma} = \frac{\beta_1 \theta \dot{w}_a \Gamma}{\dot{w}_a \Gamma} = \beta_1 \theta \tag{24}$$

$$(f/a)_\ell = (1-\beta_1)\theta. \tag{25}$$

A portion of the liquid fuel is now collected and vaporized from the surface. The collection rate of liquid fuel is:

$$\dot{w}_{f_c} = \beta_2 \dot{w}_{f\ell_\Gamma} = \beta_2(1-\beta_1) \theta \dot{w}_a \Gamma; \tag{26}$$

of this amount, β_3 percentage vaporizes from the surface and recirculates:

$$\dot{w} = \beta_3 \dot{w}_{f_c} = \beta_2 \beta_3 (1-\beta_1) \theta \dot{w}_a \Gamma. \tag{27}$$

The prevaporized fuel recirculates at a rate of K_1 percent which passes the blocked area:

$$\dot{w} = \dot{w}_{f_v\Gamma} K_1 = \beta_1 \theta \dot{w}_a \Gamma K_1. \tag{28}$$

Thus the total recirculated vapor fuel flowrate is:

$$\dot{w}_{f_{vw}} = \beta_1 \theta \dot{w}_a \Gamma K_1 + (1-\beta_1)\beta_2 \beta_3 \theta \dot{w}_a \Gamma \tag{29}$$

The air recirculation rate is K_1 of the flowrate through the blocked area:

$$\dot{w}_{a_w} = \dot{w}_a \Gamma K_1. \tag{30}$$

From Equations 16 and 17, the wake fuel-air ratio in vapor phase is:

$$\phi = \frac{\dot{w}_{l_{vw}}}{\dot{w}_{a_w}} \tag{31}$$

$$\phi = \beta_1 \theta + (1 - \beta_1)\theta \, \frac{\beta_2 \beta_3}{K_1} \tag{32}$$

$$\frac{\phi}{\theta} = \beta_1 + (1 - \beta_1) \frac{\beta_2 \beta_3}{K_1} \tag{33}$$

Equation 33 relates the wake vapor phase fuel-air ratio to the overall fuel-air ratio and, through the influence coefficients, to the geometric and aerothermodynamic situation under scrutiny. Each of these may now be evaluated from the available body of combustion literature to determine the overall form of the compositional model.

A comment on the implication of Equation 33 is in order here. This equation determines the mixture in the wake which then undergoes reaction to provide the ignition source for the mainstream reaction. As with any stirred chemical reactor, the most efficient process for a fixed volume occurs near the stoichiometric fuel-air ratio. Since the degree of this reaction efficiency strongly influences the overall augmentor efficiency, the wake fuel-air ratio should be kept near stoichiometric.

If we introduce the following values:

$$\beta_1 = 0.20$$
$$\beta_2 = 0.75$$
$$\beta_3 = 0.50$$
$$K_1 = 0.25$$

we find that Equation 33 yields:

$$\frac{\phi}{\theta} = 0.20 + (0.8) \frac{(0.75)(0.50)}{0.25}$$

$$\frac{\phi}{\theta} = 1.40$$

Thus, due to the relative fuel concentrating effect of the flameholder, the wake is 40% richer than the overall system. If the overall fuel-air ratio is 0.050, the wake is over stoichiometric at 0.070. Any further increase in fuel flowrate results in a drastic decrease in the wake reaction efficiency due to the increase in wake f/a.

The second portion of the analyses is the wake reaction efficiency and turbulent flame spreading. These analyses will be developed in the following sections.

(1) Fuel Vaporization Before Flameholder

As developed in the preceding analysis, the percentage of the liquid hydrocarbon fuel which vaporizes prior to reaching the flameholder consists of two mechanisms:

The formation of vapor due to the throttling process of injection (β_{1_T}).

The evaporation of fuel droplets due to forced convection (β_{1_E}).

Thus we define β_1 as:

$$\beta_1 = \beta_{1_T} + (1 - \beta_{1_T})\beta_{1_E} \tag{34}$$

The process of flash vaporization during the process of injection is treated as an adiabatic flow from a region of high pressure and moderate temperature (within the sprayring) to a low-pressure area (in the augmentor). This flow situation is analogous to the expansion valve process and is evaluated from knowledge of the final properties and operating conditions.

The process is evaluated assuming adiabatic expansion from known levels of fuel pressure and temperature within the sprayring to a known pressure level in the augmentor. If the sprayring pressure is sufficient to maintain the liquid fuel as a saturated liquid, the enthalpy level is defined for the given fuel type as a function of the sprayring fuel temperature only.

For adiabatic injection, the final mixture enthalpy equals the saturated liquid enthalpy at T_ι. The mixture enthalpy and a known static pressure will define the quality of the injected fuel. This process is readily evaluated from the enthalpy diagram of the particular fuel type.

An expanded diagram of the adiabatic process for JP-4 is shown in Figure 16. This example is for injection of 250°F fuel into a 7.5 psia environment. The parametric results for JP-4 fuel are shown in Figure 17.
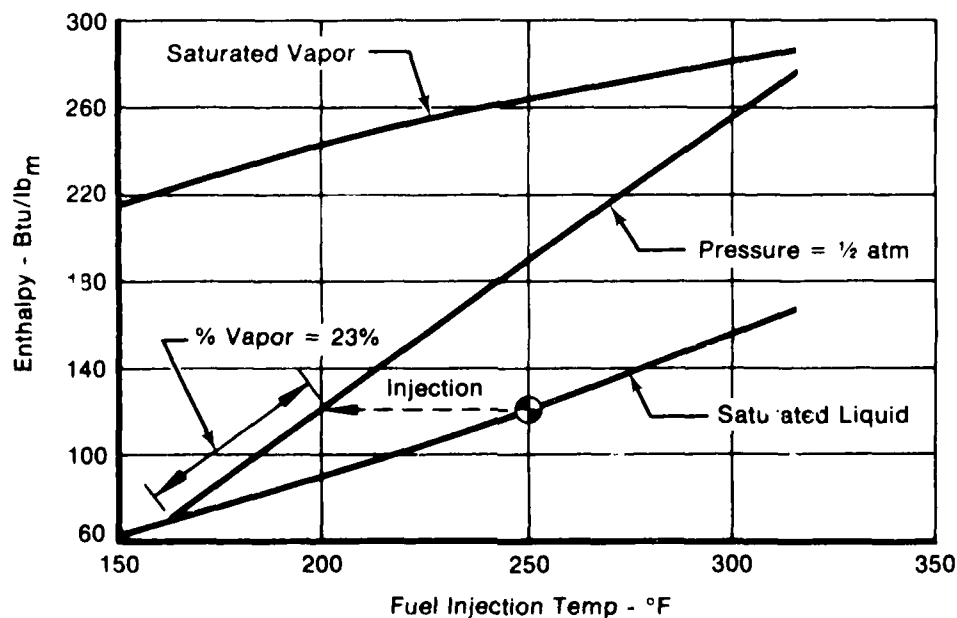
FD 134044

Figure 16. Constant Enthalpy Fuel Injection of JP-4 Fuel

28
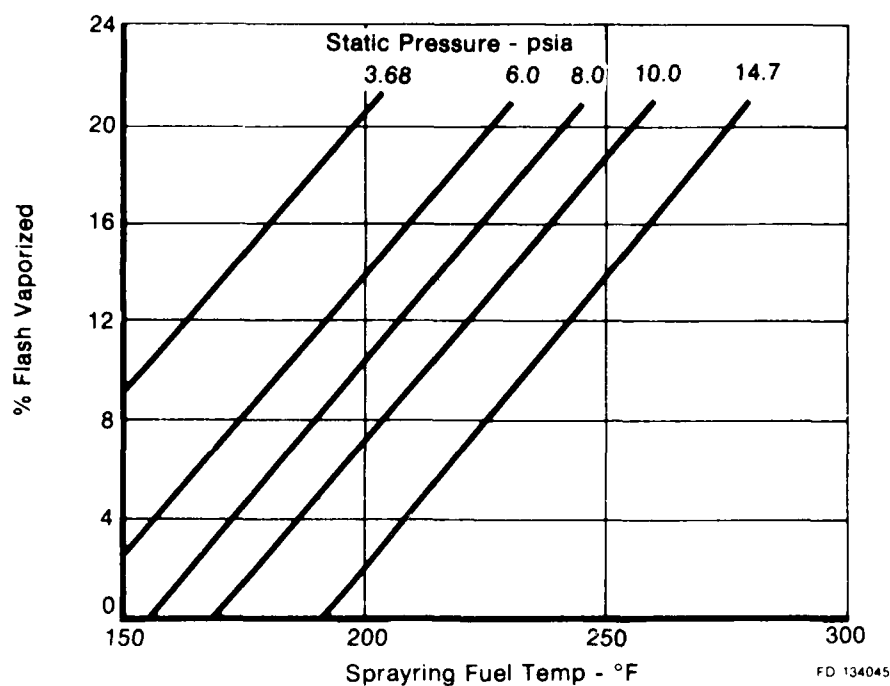
Figure 17   Throttling Process. % Vaporized vs Fuel Temperature (JP-4 Fuel)

The remaining liquid fuel is partitioned into the droplet size groups on a 5 or 10 group equal flowrate basis. For this, the droplet size distribution must be known. Due to the large number of spray systems available to the augmentor designer, no attempt was made to model this droplet formation process. Rather, a distribution function is built into the program which describes the size distribution as a function of the fuel pressure drop. The curve used in the program represents the droplet distributions for variable area pintle spraybars. Figure 18 shows this function.

If 5 size groups are to be used, each one represents 20% of the liquid flowrate. The sizes used in the analysis would be the 10, 30, 50, 70 and 90% diameters. Once these sizes are known, the program performs the solution to the forced convection droplet vaporization between the spraybar and the flameholder.

The basis for the droplet vaporization solution is the form of the Nusselt number devised for spherical droplets by Ranz and Marshall and subsequently improved by Preim and Heidmann. The assumed forms are:

$$Nu_H = 2 + 0.6 \ Re \ Pr \tag{35}$$

$$Nu_M = 2 + 0.6 \ Re \ Sc \tag{36}$$

29

for heat and mass transfer. For the assumption of Lewis No. = 1, i.e., Pr = Sc, these become identical. The fuel droplet mass efflux rate is calculated from:

$$\dot{w} = KA_s \, p_s \ln \left(\frac{p_s}{p_s - p_v} \right) \qquad (37)$$

$$K = \frac{Nu \, D_v \, MW}{R \, d_\ell \, T_a} \, . \qquad (38)$$
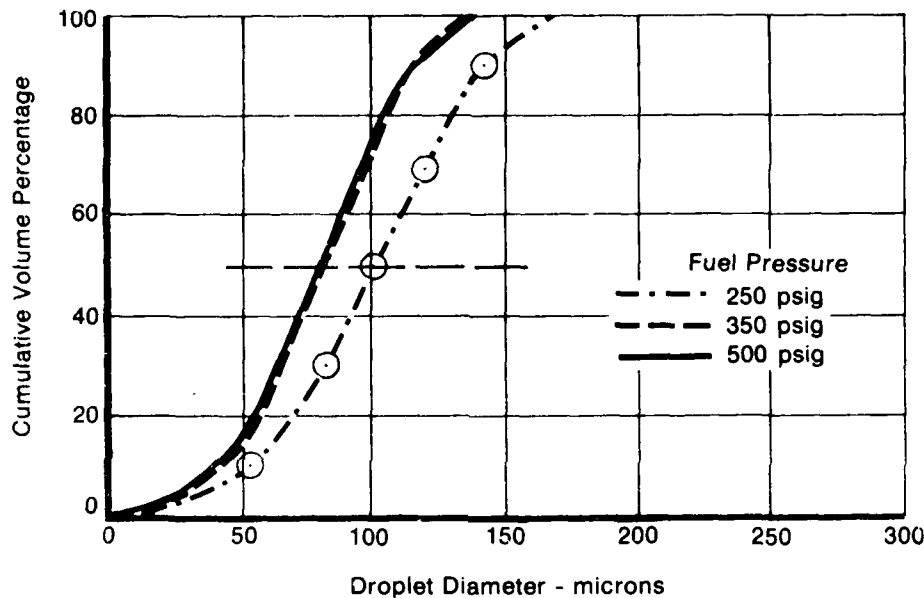
FD 134046

Figure 18. Typical Spray Distribution

During the transient droplet heating period between injection at $T_\ell = T_{\ell_0}$ and achievement of the wet-bulb temperature, the droplet temperature is evaluated from the heat input and the diffusion driven mass efflux. The difference between the heat required to generate the mass efflux and the heat which actually reaches the surface of the droplet is assumed to go towards alteration of the droplet bulk temperature. This assumption is essentially a statement that the droplet internal circulation is sufficiently rapid compared to the thermal input that significant droplet radial thermal gradients do not exist.

In evaluation of the net heat flux into the liquid surface, the mass efflux blocking term introduced by Preim is used. This term evaluates the loss in net flux due to the vapor superheating which occurs as the evolved fuel vapor achieves thermal equilibrium at the free-stream gas temperature. The transient solution proceeds as follows, after evaluation of the fuel mass efflux rate, w, from Equation 37.

The thermal film coefficient, h_f, is:

$$h_f = \frac{k \, Nu_H}{d_\ell} \qquad (39)$$

where Nu_H is from Equation 35.

30

The net heat flux to the droplet liquid surface, q, is calculated with allowance for the thermal blocking due to vaporizing fuel heating (β):

$$\dot{q} = h_l A_s (T_a - T_\ell) \beta \tag{40}$$

where

$$\beta = \frac{z}{e^z - 1} \tag{41}$$

and

$$z = C p_v \dot{w} / \pi k d_\ell \, Nu_H. \tag{42}$$

The net amount of heat which is available for sensible heating of the droplet is the net liquid surface flux minus the latent heat required to generate the vapor mass flux:

$$\Delta \dot{q} = \dot{q} - \dot{w}_v \lambda. \tag{43}$$

This net flux is used to raise the liquid bulk temperature, T_ℓ, as:

$$\frac{dT_\ell}{dt} = \frac{\Delta \dot{q}}{m_l \, Cp_\ell} = \frac{\Delta \dot{q}}{4/3 \, \pi \, (d_\ell/2)^3 \, \rho_\ell \, Cp_\ell} . \tag{44}$$

This change in T_ℓ may be positive or negative depending on the relative values of w and q.

The wet-bulb temperature is defined as *that liquid droplet temperature where the thermal net input is just sufficient to generate the mass efflux at that temperature and vapor pressure*. As such, it is a function of effective Nusselt number and local static pressure and temperature. Coincident with this transient heating and vaporization, the liquid droplet is being accelerated by the faster free stream gas velocity. The acceleration is evaluated from the standard equation:

$$\frac{dV_\ell}{dt} = \frac{3}{4} \frac{C_d}{d_\ell} \frac{\rho_a}{\rho_\ell} (V_a - V_\ell)^2. \tag{45}$$

Since the Reynolds number used in the Nusselt number formulation is defined as:

$$Re = \frac{\rho_a d_\ell (V_a - V_\ell)}{\mu_g} , \tag{46}$$

a simultaneous solution of Equations 44 to 46 is required. In the computer analysis, this is accomplished by a finite difference solution utilizing small time intervals. The ordinary differential equations are rewritten as delta terms, e.g.,

$$\frac{dV_\ell}{dt}$$

becomes

$$\frac{\Delta V_\ell}{\Delta t}.$$

31

For each time increment, the initial values are used to calculate Re, Nu_H, Nu_M, P_v, etc. Equations 37 to 44 are solved which yields $\Delta\dot{w}_v$ and ΔT_ℓ. Equation 45 is solved to yield ΔV_ℓ. At the end of this step, $\dot{w}_v$ is incremented by $\Delta\dot{w}_v$, T_ℓ by ΔT_ℓ and V_ℓ by ΔV_ℓ. The average value of V_ℓ over this Δt yields a delta axial travel distance.

The procedure is repeated in small time steps until either the total axial travel exceeds the spraybar-to-flameholder separation distance or the liquid is fully vaporized. At the start of each new time increment, the input values reset to reflect the effect of the previous step; e.g., ρ_v is evaluated at $T_\ell + \Delta T_\ell$, d_ℓ is evaluated to reflect less liquid mass, etc.

Some typical results for the vaporization portion of the analysis are presented in Figure 19. Figure 19 also shows the transient bulk liquid temperature for a 100 micron droplet in a 400°F, 250 ft/sec gas stream. The decrease in temperature from the initial 80°F injection temperature for the 0.5 atmosphere pressure reflects the fact that the initial mass efflux by convection exceeds the available net heat input.

For a situation described as follows:

V_a = 250 fps
T_a = 275°F
T_ℓ = 80°F
P_v = 10 psia
d_ℓ = 25 to 125 microns.

The amount of JP-4 which will vaporize in a typical distance of 6 inches is shown in Figure 20. These results are typical for fan duct conditions at high altitude and low flight Mach number.
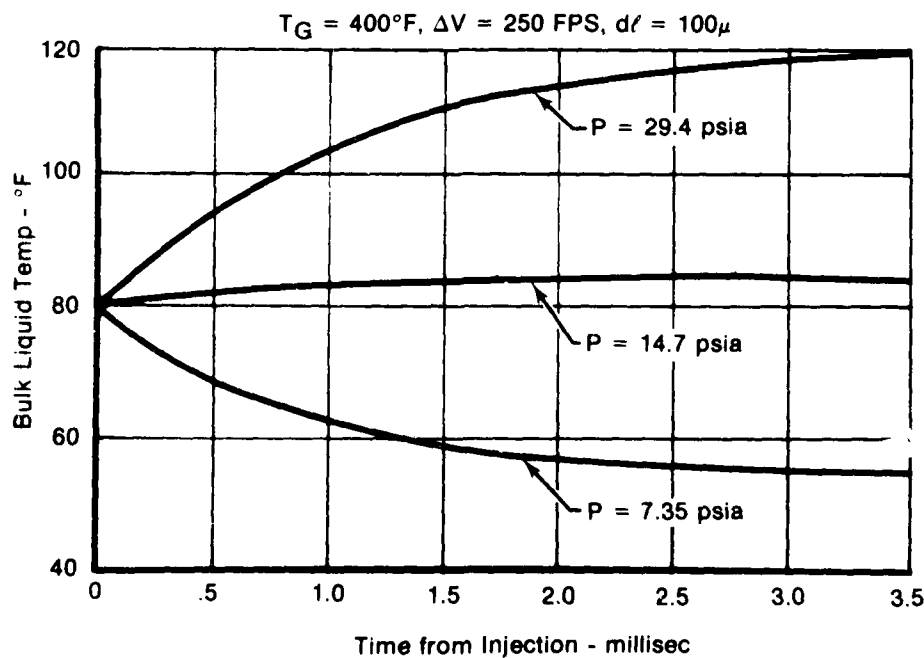
FD 134047

Figure 19. JP-4 Droplet Transient Temperature

32
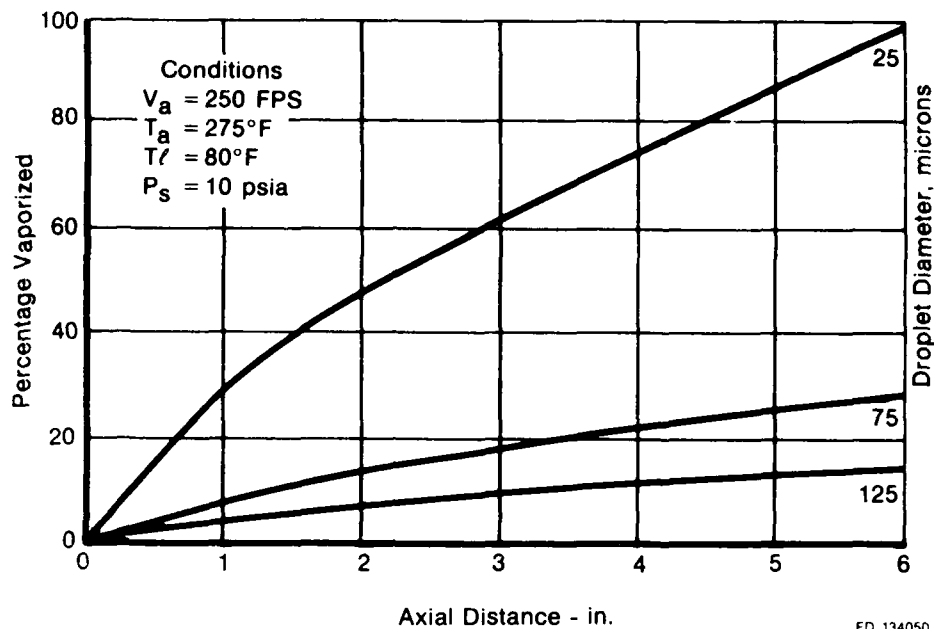
Figure 20. Vaporization of JP-4 Fuel Droplets vs Axial Length

(2) Flameholder Fuel Collection Efficiency

The output from the ACCEL subroutine defines a spray of droplet diameters at a plane with the flameholder leading edge. The diameters are defined from the final step in the forced vaporization analysis as is the droplet axial velocity. The spray field is still assumed to be homogeneous in the transverse direction in terms of size and volume flowrate distribution.

As the flow stream approaches the stabilizer, the suspended droplets are unable to fully follow the divergence of the flow streamlines and a portion of them impinge on the bluff body. The evaluation of this "capture rate" is done in nondimensionalized terms as β_2:

$$\dot{w}_{fc} = \dot{w}_{fv} \Gamma \beta_2 \tag{47}$$

$$\beta_2 = \frac{\dot{w}_{fc}}{\Gamma \dot{w}_{fv}} \tag{48}$$

where

$\dot{w}_{fc}$ = fuel liquid capture rate
$\dot{w}_{fv}$ = fuel liquid flowrate at F/H plane
Γ = F/H blockage.

β_2 is also the ratio of the separation of the droplet capture limit streamlines to the F/H width:

$$\dot{w}_{fc} = \rho_v V_v \delta^* \tag{49}$$
$$\dot{w}_{fv} = \rho_v V_v A$$
$$= \rho_v V_v \frac{N}{\Gamma} .$$

33

Substituting yields:

$$\beta_2 = \frac{\delta^*}{N} \qquad\qquad (50)$$

where $\delta^* \sim$ droplet capture width. This is shown schematically in Figure 21.

$$B_2 = \frac{\delta^*/N}{2} \qquad \text{where: } N = \text{Flameholder Width} \\ \delta^* = \text{Limit Streamline}$$

FD 134080

Figure 21. Droplet Capture Schematic

This analysis will be performed once for each size group exiting the vaporization analysis. If 10 groups are used initially, each size represents 10% of the liquid fuel at plane A, since the smaller sizes will have higher vaporization rates between the injection plane and plane A. The overall collection rate is thus:
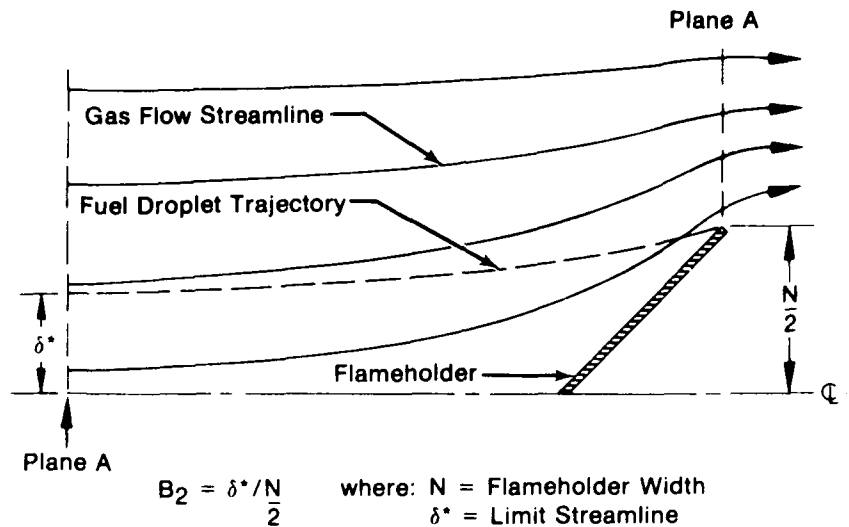
$$\beta_2 = \frac{1}{m_{f,t} \, A} \sum_{i=1}^{10} m_{f,i} \, A\beta_{2i}. \qquad\qquad (51)$$

Evaluation of β_2, requires, therefore, evaluation of δ^* for any value of droplet diameter. Additionally, the streamline divergence rate will be a function of the flameholder geometry (apex angle, blockage). The droplet acceleration rate in the x and y directions will be a function of the flow conditions (pressure, temperature, velocity) and initial fuel droplet velocity (output from β_1, subroutine).

An earlier analysis for collection into a cylindrical bar was performed by Langmuir. The collection efficiency was found to be dominated by air velocity and droplet diameter. The influence of diameter is exceptionally strong. Typical results are shown for vee-gutter flameholders in Table 1. Going from 25 to 75 micron droplets doubles the collection rate from ~30% to ~70%.

The effect reinforces the dependence of the low air temperature stabilization process on the surface film analysis. As the air temperature is reduced, the level of droplet vaporization is also reduced and the droplet diameter at the flameholder is increased. This not only increases the liquid flowrate available for collection but also increases the percentage collected. This doubling effect produces a much greater dependence of the wake fuel-air ratio on the surface film.

34

TABLE 1. COLLECTION EFFICIENCY vs
DROPLET DIAMETER

Gutter Apex Angle (deg)	Blockage Ratio (%)	Droplet Diameter (microns)	Collection Efficiency (%)
60	15	25	0.35
60	15	50	0.59
60	15	75	0.70
60	15	100	0.76
60	30	25	
60	30	50	0.65
60	30	75	0.73
60	30	100	0.78
40	30	25	0.30
40	30	50	0.55
40	30	75	0.63
40	30	100	0.71

(3) Fuel Film Surface Vaporization Evaluation

The liquid droplets which contact the surface of the flameholder are assumed to generate a uniform liquid film. This liquid film experiences heat transfer from the hot wake through the flameholder as shown in Figure 22.
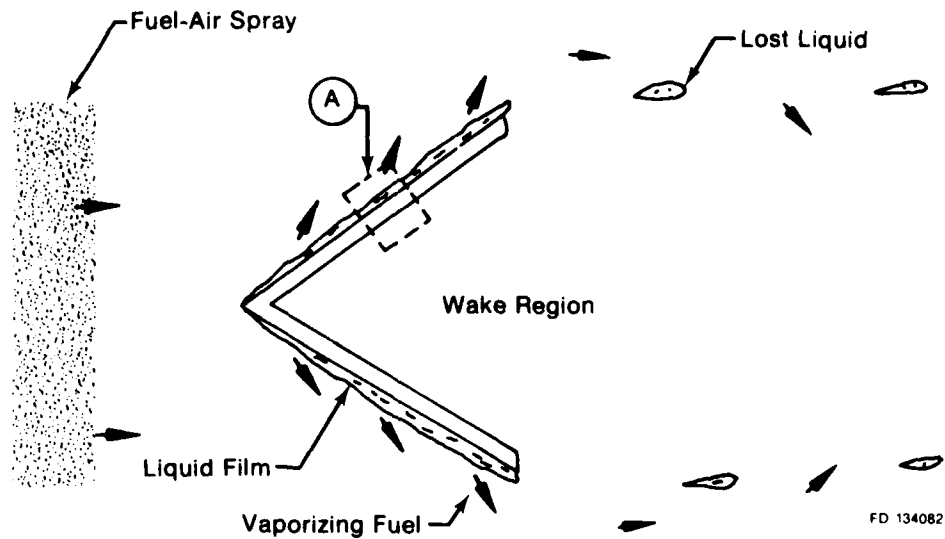

Figure 22. Flameholder Surface Vaporization Schematic

The liquid film vaporization rate is used to calculate the surface vaporization efficiency, β_{λ}. This efficiency is the percentage of the collected liquid fuel which is vaporized from the flameholder surface and recirculated into the wake reaction.

The controlling parameter becomes a forced diffusion process. The controlling equation may thus be written as:

$$\dot{w}_{fc} = \dot{w}_v + \dot{w}_s + \frac{dm}{dt} \tag{52}$$

$$\dot{w}_v = fcn(Nu_m, p_v, A_s) \tag{53}$$

$$p_v = fcn(T_f) \tag{54}$$

$$T_f \cong T'_{fc} + {}^1\!/_2\, \Delta T_f \tag{55}$$

$$\dot{q} = \dot{w}_v \lambda + \dot{w}_{fc}\, C_p\, \Delta T_f \tag{56}$$

$$\dot{q} = fcn\, (Nu_H, T_a, T_w). \tag{57}$$

In these equations, the collected mass flowrate, w_{fc}, is the result of the β_2 subroutine. We assume that the liquid film total mass does not change with time unless the entry flowrate alters, i.e.,

$$\frac{dm}{dt} = 0.$$

The various film properties are functions of the fuel type and temperature. Suitable curves are used in the program for JP-4 and JP-5 fuel.

This situation is a forced mass transfer from the surface represented by a Nusselt number function driven by the film vapor pressure and Nusselt number form of heat flux from the wake into the film.

The formulation of the rate of liquid fuel vaporization from the surface of the flameholder has been programmed as a finite element solution to the nonuniform forced diffusion process. The diffusion process is evaluated from the surface Nusselt number for mass transfer:

$$\dot{w}_v = C_1 A_s p_s \ln\left(\frac{p_s}{p_s - p_v}\right) \tag{58}$$

$$C_1 = \frac{Nu_m\, D_v\, MW}{R\, \Delta x\, T_a}. \tag{59}$$

The Nusselt number is functionally identical for heat flux and mass flux when the Prandtl number in the thermal Nusselt number is replaced with the Schmidt number for mass transfer.

The heat flux from the recirculation zone is evaluated directly from a Nusselt number formulation for recirculation wakes behind bluff bodies as:

$$Nu_w = \frac{h_f N}{k_m} = 0.99\, Re^{0.5}\, P_r^{0.33}. \tag{60}$$

For a known value of heat flux through the flameholder, the rate of surface vaporization is evaluated by breaking the liquid film into 10 subgroups. In each subgroup, the vaporization process is assumed to be controlled by the vapor pressure corresponding to the mean liquid film temperature within that subgroup (see Figure 23).

The heat flux into each subgroup is responsible for two physical effects. The heat is used to provide the latent heat of vaporization and provide sensible heat to elevate the bulk liquid temperature.

For the initial subgroup, the entrance mass flowrate is the prorated portion of the fuel collection rate. Thereafter, the entry flowrate consists of the prorated collection rate plus the unvaporized liquid fuel from the preceding subgroup.

The entrance fuel temperature for the initial subgroup is the droplet bulk temperature as evaluated in the spray vaporization subroutine. For succeeding subgroups, the initial fuel temperature is evaluated from the mixture of captured fuel at droplet temperature and liquid fuel film at elevated temperature.

The solution in each subgroup for the liquid temperature rise and vaporization rate requires an iteration process. The initial guess on vaporization is evaluated at the fuel entry temperature. The latent heat required to accommodate this vaporization is subtracted from the heat flux and the excess used to increase the bulk film temperature. A new vaporization rate is calculated at a mean fuel temperature between entry and exit. The solutions for vaporization and temperature rise are repeated until convergence occurs.

This process of finite element solution, if the subdivisions are fine enough, allows a relatively simple evaluation of the vaporization rate for nonadiabatic walls and a nonuniform liquid film temperature. It may be made as exact as desired by decreasing the subgroup size. This may be very desirable for solutions to multicomponent fuels (such as JP-4) where the latent heat of vaporization and surface vapor pressure are strong functions of the bulk liquid temperature.

The partitioning of the heat flux, Equation 56, and the forced diffusion process, Equations 58 and 59, may be combined to yield:

$$\dot{q} = \dot{w}_{f_e} \, \dot{C}_p \, (T_{\ell \, f} - T_{\ell \, i}) + \lambda \, \left(\frac{Nu_m \, D_v \, MW}{R \Delta_x T_a} \right) \, A_s p_s \ln \left(\frac{p_s}{p_s - p_v} \right) \tag{61}$$

where $\dot{C}p$, λ and p_v are all functions of T_ℓ.

The functional unknown in this group is T_ℓ, the average film temperature. Once T_ℓ is known, the mass efflux is known from Equation 58. The form of the efflux response to T_ℓ is such that a critical film temperature exists, when $p_v = p_s$, where infinite flux exists. For JP-4 and 10 psia static pressure this is 180°F. A very careful analysis is required to iterate to a successful answer. A typical result is shown in Figure 24 for JP-4 and flow conditions of 250 fps, 275°F, 10 psia.

37
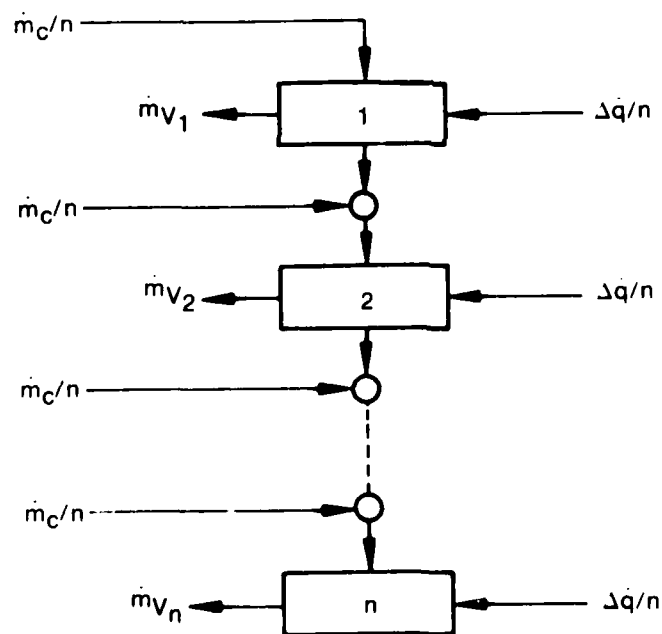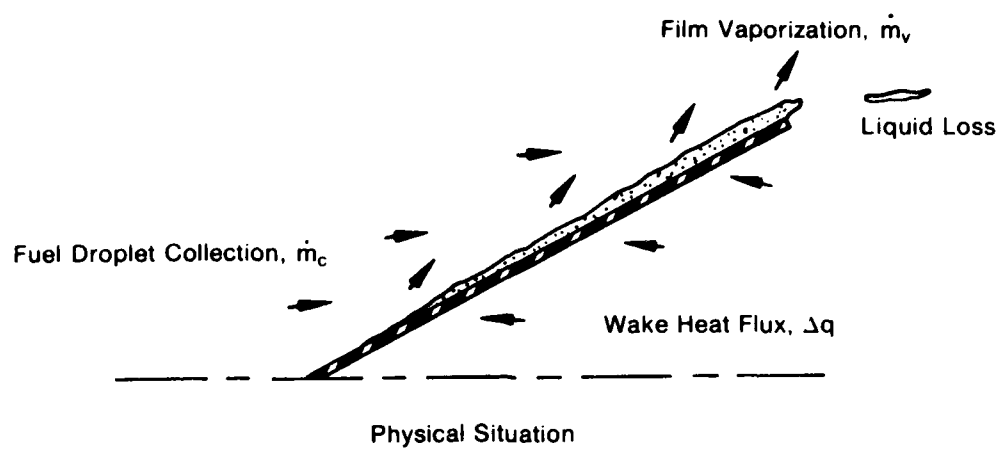
$$\dot{m}_V = \sum_{i=1}^{n} \dot{m}_{V_i} \qquad \beta_3 = \dot{m}_V / \dot{m}_c$$

Figure 23. Finite Difference Solution Procedure
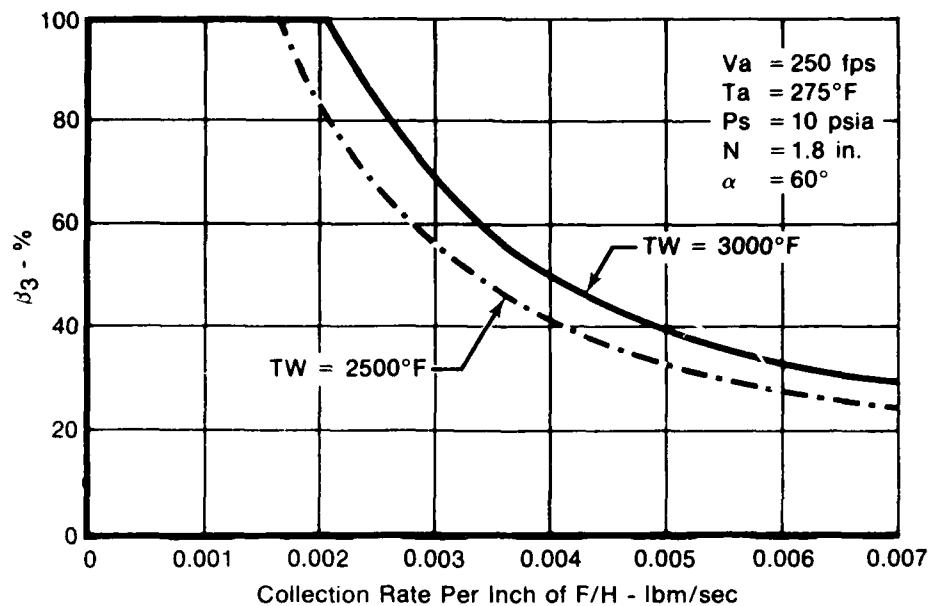
Figure 24. *Surface Vaporization vs Fuel Collection Rate for Two Levels of Wake Temperature*

(4) Flameholder Wake Recirculation Ratio

In a manner analogous to the definition of the collection efficiency, we will define a recirculation efficiency, K_1. This efficiency relates the mass flowrate into the wake of the flameholder to the mass which flows through the projected blocked area of the flameholder:

$$\dot{w}_{a_r} = \rho_a V_a N K_1. \tag{62}$$

This recirculation flowrate is the mass which is transferred by turbulent diffusion across the free shear layers aft of the flameholder. These layers form the boundaries of the backflow wake aft of the bluff body. If we look at this wake volume as a homogeneous region with mass transfer across the boundaries, the recirculation rate may also be written as:

$$\dot{w}_{a_r} = \frac{\rho_a V_0}{\tau}. \tag{63}$$

If the wake volume and residence time may be evaluated as a function of the geometric and flow variables, then the recirculation rate may be evaluated from the known variables without resorting to the much more difficult solution to the effective transport across the shear layers.

The approach relates the wake volume and residence time to the controlling aerodynamic and geometric variables, such as:

Blockage ratio
Vee-gutter apex angle
Flow Mach number
Pressure, velocity, temperature.

39

Once these are known, the recirculation rate calculation proceeds as follows:

$$\dot{w}_{a_r} = \rho_a \, V_o / \tau \tag{64}$$

$$V_o = C_V(L/D)(B/D)N^2. \tag{65}$$

If we nondimensionalize the residence time with respect to velocity and characteristic dimension, flameholder width, we have:

$$\tau' = \frac{\tau V_a}{N} \tag{66}$$

$$\dot{w}_{a_r} = \frac{V_a}{N} \, \frac{\rho_a V_o}{\tau'}. \tag{67}$$

Now, from Equations 65 and 67, we have:

$$\dot{w}_{a_r} = \frac{\rho_a V_a C_V(L/D)(B/D)N}{\tau'}. \tag{68}$$

From this and Equation 62, we may write:

$$K_1 = C_V(L/D)(B/D)(\tau')^{-1}. \tag{69}$$

The value of the shape coefficient, C_V, was determined by assuming that the wake was similar to a two-dimensional ellipse which is truncated by the flameholder at its forward edge. The value used is 0.80.

The data presented were reduced to a series of curves which describe the effect of various parameters on recirculation rate. The functional groupings and the corresponding figures are:

L/D	vs Blockage	(Figure 25)
L/D	vs Apex Angle	(Figure 26)
B/D	vs Blockage	(Figure 27)
B/D	vs Apex Angle	(Figure 28)
τ'	vs Blockage	(Figure 29)
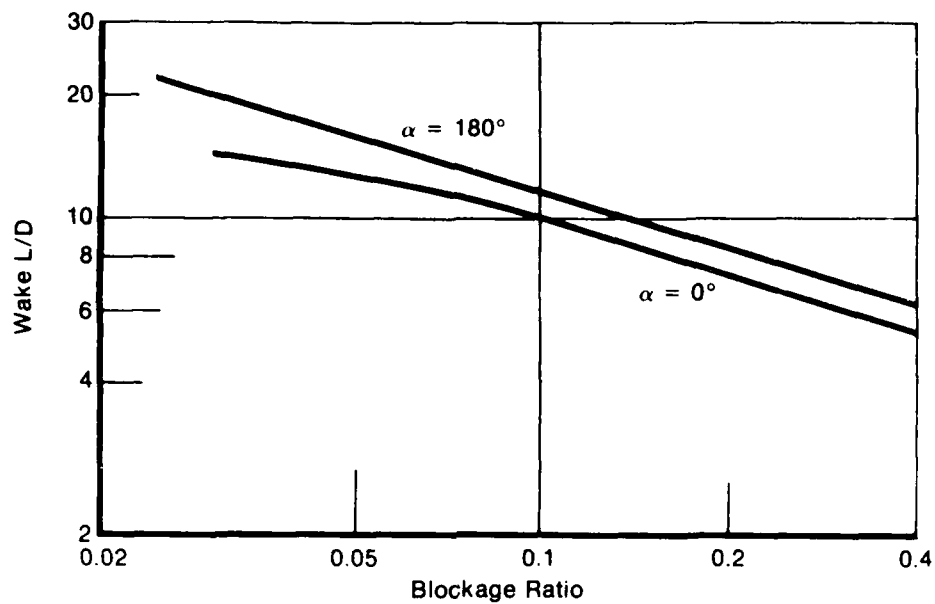
Figure 25. Wake L/D vs Blockage Ratio
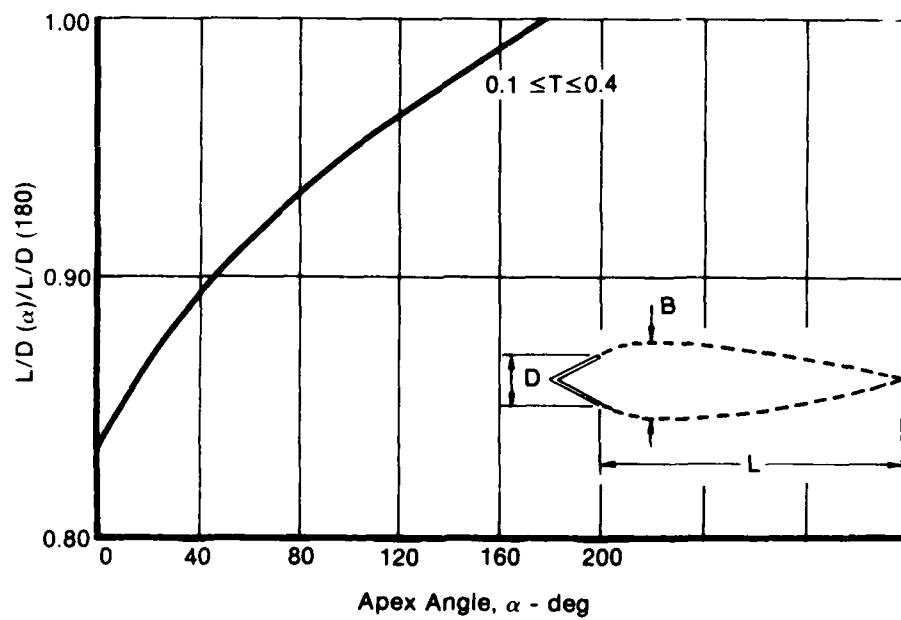
Figure 26. Wake L/D vs Apex Angle

41
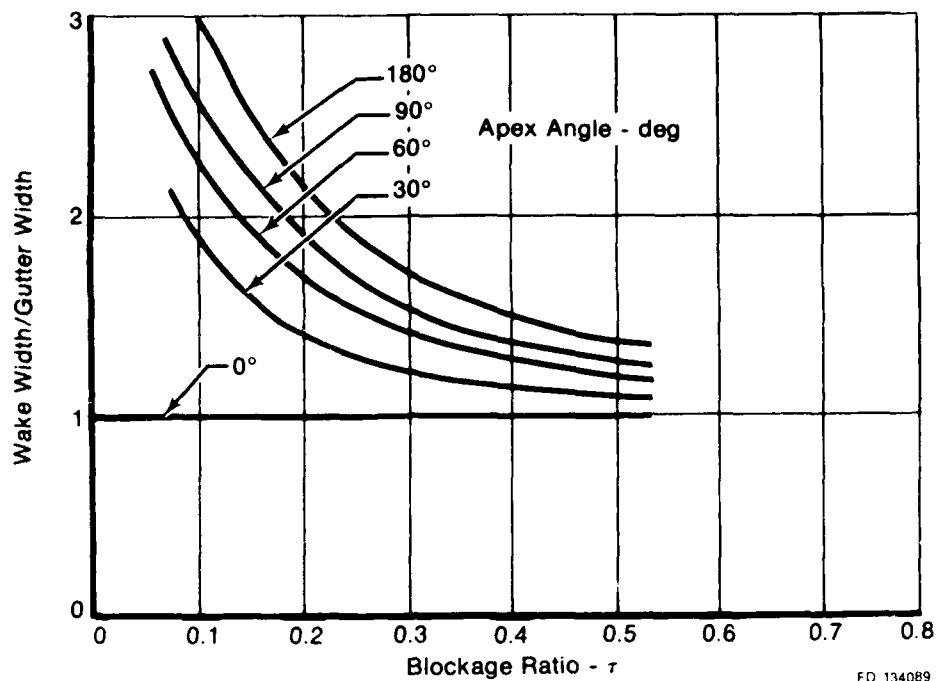
Figure 27. Wake B/D vs Blockage Ratio
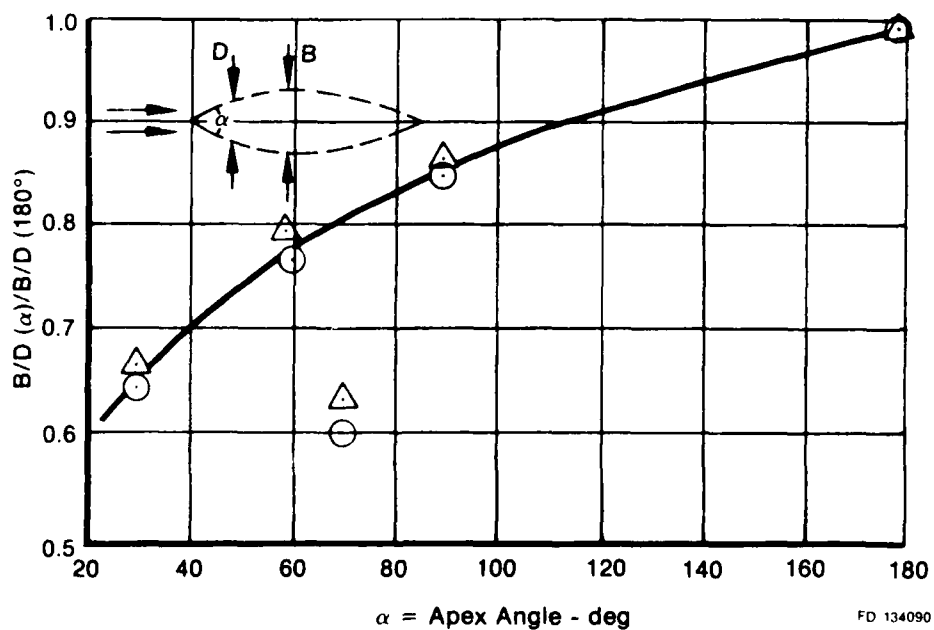
Figure 28. Effect of Apex Angle on Wake B/D

42
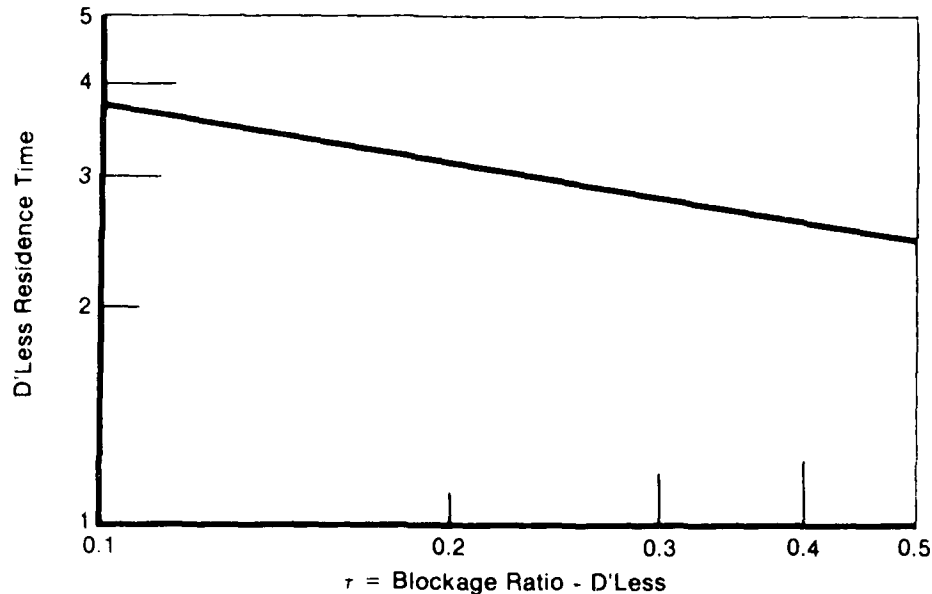
Figure 29. Wake Residence Time vs Blockage Ratio

(5) Recirculation Zone Reaction Kinetics

The recirculation zone wake of the bluff body stabilizer is analyzed by assuming that it behaves similarly to a well-stirred reactor with the volume and mass entry rate known from the results of the RECIRC analyses.

Analyses of well-stirred reactors have been presented by numerous investigators and the analogy to actual combustors and bluff body wakes studied. The basic thesis of these studies is that the performance of the reactor may be evaluated from a balance between the mass entry rate and the kinetic conversion rate. For the purpose of these studies, we assume that the entire wake volume is available for reaction and that the mixing is very rapid. These assumptions result in an optimistic evaluation of the kinetic limits which we will correct later.

The following analysis follows the development of Kretschmer and Odgers for lean wake fuel-air ratios. The general form of the reaction of hydrocarbon fuels proceeds in essentially two major steps. The first is the pyrolysis and partial oxidation of the virgin fuel to form short-lived intermediate species. At the end of this stage, the maximum concentration of carbon monoxide is present. The second stage is the oxidation of carbon monoxide to form carbon dioxide. This latter step is much slower and serves as the rate-controlling process. The slower CO oxidation results in the very close similarity of reaction rates for a wide range of saturated hydrocarbons.

The general form of the conversion equation may be written as:

$$\frac{dm_o}{dt} = \frac{k}{R_a^n} \chi_o a \; \chi_f^{n \; a} \; V_o p^n \frac{e^{C/T}}{T^{n \; 0.5}}; \tag{70}$$

for gaseous flow into a well-stirred reactor, this becomes:

$$\frac{A}{V_o p^n} = \frac{k(m+1)}{R_1^n y_\epsilon} \; \chi_o^a \chi_f^{n \; a} \; \frac{e^{C/T}}{T^{n \; 0.5}}. \tag{71}$$

43

For the assumed single-step reaction process postulated here, the reaction mass balance is (for propane fuel):

$$\phi C_3 H_8 + 5O_2 + 5mN_2 \rightarrow 3y\epsilon\ CO_2 + 4y\epsilon H_2 O + \tag{72}$$
$$(\phi - y\epsilon)\ C_3 H_8 + 5(1 - y\epsilon)\ O_2 + 5mN_2.$$
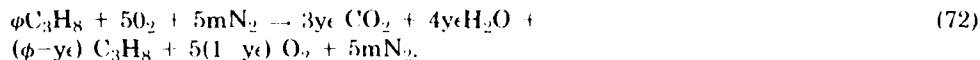
Also, a linear efficiency vs temperature function is assumed:

$$T = T_i + \epsilon\Delta T. \tag{73}$$

From these equations, the stirred reactor loading capability may be written as:

$$\frac{A}{V_o p^n} = \frac{k(m+1)\ [5(1-y\epsilon)]^a\ [\phi - y\epsilon]^{n-a}\ e^{-C/(T_i + \epsilon\Delta T)}}{R_1^n y\epsilon\ [5(m+1) + \phi + y\epsilon]^n\ [T_i + \epsilon\Delta T]^{n-0.5}}. \tag{74}$$

Based on comparison of predicted results with available stirred reactor data, Reference 21 recommends the following values for this reaction:

    n: for $\phi < 1$, $n = 2\phi$
               for $\phi > 1$, $n = 2/\phi$
    a: $a = n/2$.

This yields:

$$\frac{A}{V_o p^{2\phi}} = \frac{1.29 \times 10^{10}\ (m+1)\ [5(1-y\epsilon)]^\phi\ (\phi - y\epsilon)^\phi\ e^{-C/(T_i + \epsilon\Delta T)}}{(0.08206)^{2\phi}\ y\epsilon [5(m+1) + \phi + y\epsilon]^{2\phi}\ [T_i + \epsilon\Delta T]} \tag{75}$$

for lean mixtures.

While the results presented above are from one reference, similar results have been obtained by others for the same problem.

Longwell and Weiss (Reference 4) present the following results for lean and rich operation.

    Lean:

$$\frac{A}{V_o p^{1.8}} = 430\ k_1\ \frac{e^{-E/T_f}}{T_f^{1.3}}\ \frac{[2\phi(1 - \epsilon)]^{0.8}\ (1 - \phi\epsilon)}{\phi\epsilon[4.76 + \phi\ (1.36 - \epsilon)]^{1.8}} \tag{76}$$

    Rich:

$$\frac{A}{V_o p^{1.8}} = 430\ k_2\ \frac{e^{-E/T_f}}{T_f^{1.3}}\ \frac{(0.080\ \phi)^{0.8}}{\epsilon}\ \left\{ \frac{1 - \epsilon}{4.76 - \epsilon + 0.08\phi\ (1 + 16\epsilon)} \right\}^{1.8} \tag{77}$$

where

    $k_1 = 1.67 \times 10^{10}$ litre$^{0.8}$/°K$^{0.5}$ gm-mole$^{0.8}$ sec
    $k_2 = 1.11 \times 10^{11}$ litre$^{0.8}$/°K$^{0.5}$ gm-mole$^{0.8}$ sec
    $E = 42,000$ gm-cal/gm-mole.

The solution procedure utilized in the WAKE subroutine utilizes the results of RECIRC as a definition of the entry rate, A, and the zone Volume, V_o. The equivalence ratio is from Equation 33 and the results of $\beta 1$, $\beta 2$, $\beta 3$ and RECIRC. The ideal temperature rise, ΔT, is read from curves of ΔT versus wake fuel-air ratio, inlet temperature, and static pressure for

this specified fuel type. An iterative solution procedure solves for the efficiency, ϵ, where the known value of $A/V_0 p^2$ agrees with the predicted value as a function of ϵ. The complexity of Equation 76 or 77 requires this sort of reverse solution.

The behavior of the solution is shown in Figure 30 for inlet temperatures of 300 and 400°K and equivalence ratios of 0.8 and 1.0. The wake efficiency decreases at an increasing rate until the decay slope becomes infinite. At this point, the wake reaction process is said to have blownout. If we plot the locus of the blowout points as $A/V_0 p^2$ versus equivalence ratio, we obtain a classical blowout curve. This curve, except for magnitude, represents the classical results for gaseous fuel data from wake-stabilized flames. This is shown in Figure 31.
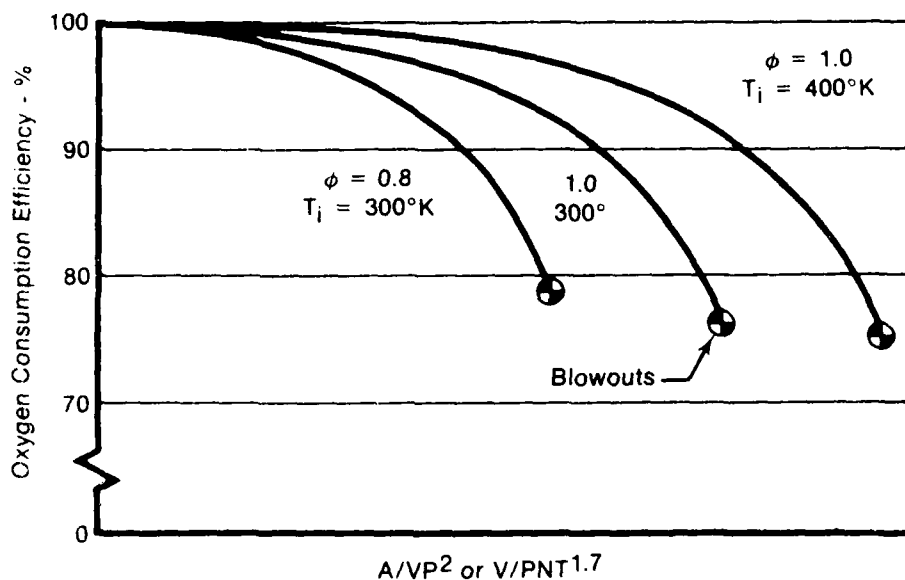
FD 134095

Figure 30.   Stirred Reactor Kinetic Efficiency vs Loading Rate

This analysis tends to overestimate the limits of blowout velocity when compared to available data. To reconcile this, comparisons were made between predicted limits and actual limits for available data. The correlating ratio between predicted and actual was 3.55, i.e.:

$$\frac{\left(\dfrac{A}{V_0 p^2} \right)_{\text{max. pred}}}{\left(\dfrac{A}{V_0 p^2} \right)_{\text{max. data}}} = 3.55. \tag{78}$$

In the analysis, the calculated recirculation rate per unit volume is multiplied by this factor before solving for ϵ. In this manner, the predicted limits and available data are numerically equal, and the efficiency response towards blowout follows the theoretical curve.

The reason for this error is most likely either imperfect mixing or lack of full utilization of the wake volume for reaction. The approach used above will account for either one of these.
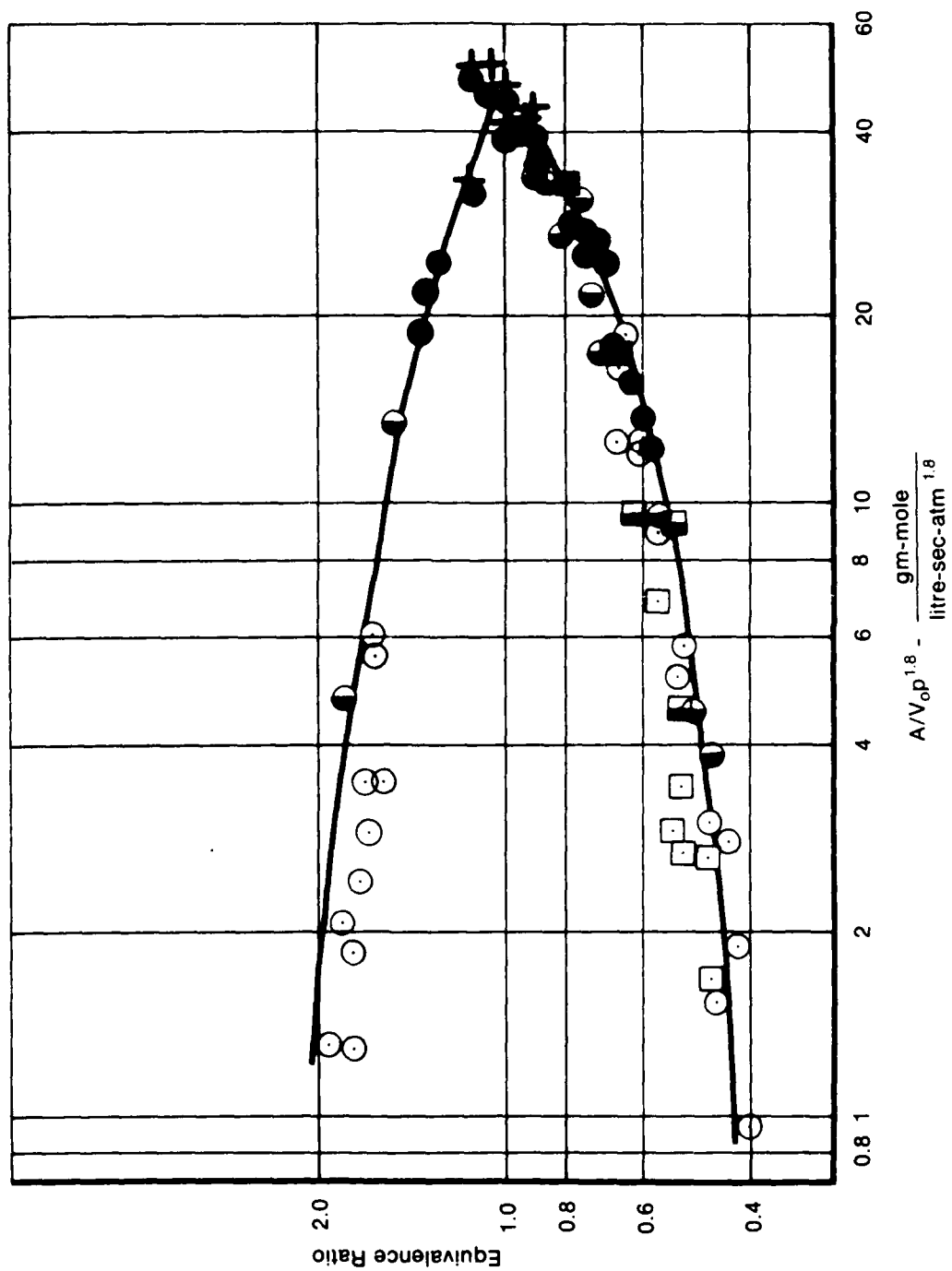
Figure 31. Focus of Stirred Reactor Blowout Limits

$$A/V_o p^{1.8} - \frac{\text{gm-mole}}{\text{litre-sec-atm}^{1.8}}$$

Equivalence Ratio

FD 134396

46

(6) Turbulent Flame Spreading Rate

The turbulent flame propagation into the unreacted free-stream is initiated in the shear layers of the wake. The model used (subroutine ST) relates the local turbulent flame speed to the local aerothermodynamic conditions and performs a finite difference integration of the flame front penetration starting in the wake and proceeding to the exhaust nozzle.

For the purposes of current analysis, the following assumptions were made:

1. Uniform air flow profiles

2. Uniform fuel-air ratio

3. Incompressible acceleration of free air velocity by the flameholder blockage with no induced profile

4. Known wake size and reaction efficiency

5. Two-dimensional ducted flame.

The schematic of the situation which is analyzed is shown in Figure 32.

The approach flow, at known levels of pressure, temperature, velocity and fuel-air ratio, is accelerated by the blockage of the flameholder to velocity U, where:

$$U = \frac{V_a}{(1-\Gamma)} \tag{79}$$

where:

    $U \sim$ Velocity at flameholder tip
    $V_a \sim$ Approach velocity
    $\Gamma \sim$ Blockage ratio.

At this point, Station 1 of Figure 31, an induced turbulence level is calculated from:

$$\epsilon_0 = \left[C_d\Gamma + \left(\frac{\Gamma}{1-\Gamma}\right)^2 \frac{1}{6}\right]^{1/2} \tag{80}$$

This equation (Reference 12) relates the turbulence intensity, ϵ_0, to the blockage ratio and the flameholder zero blockage drag coefficient, C_d.

At this location, the turbulent flame velocity calculations are initiated. The equation used for the local flame speed is the Karlovitz equation:

$$St = S_\ell + (2u'S_\ell)^{1/2} \tag{81}$$

where:

    $St \sim$ Turbulent flame speed, ft/sec
    $S_\ell \sim$ Laminar flame speed, ft/sec
    $u' \sim$ RMS turbulence velocity, ft/sec.

The value of u' is:

    $u' = \epsilon_0 U$.

47

Air Velocity
Held Constant

Air Velocity Accelerated
By Blockage - Uniform
Profile Assumed

Turbulence Generated
By F/H = Fan (γ, C_d)

Turbulence
Decays as $1/\sqrt{X}$

Uniform Flow at
Known V_a, T_a, p_s, f/a

Final
$\bar{\eta}_c = \Delta y/w$

S_t

U

2.) Local η_c Equal to
Local Flame Front
Propagation Distance
% of Duct Width, i.e.,
"Step Flame" of Zero
Width

1.) Local Flame Speed =
FCN of Local Turbulence
Level, FA, and Local
Avg η_c Value

1.) Initial Flame Velocity
Calculated from Karlovitz
S_t Equation at FA Times
Wake Efficiency

$S_t = [S_\ell + (2S_\ell \epsilon X \mu^{1/2}] \eta_w$

1.) Wake Reaction
Level Calculated
2.) Initial η_c Set
Equal to
$\bar{\eta}_w \times \dfrac{mr}{ma}$

0

1

2

3

4

FD 134091

Figure 32. Schematic of Flame Spreading Analysis

48

An additional term is required to relate the resultant flame speed to the level of recirculation zone reaction efficiency. As the wake efficiency and temperature decrease, local areas in the flame sheet appear where ignition does not occur. Since the model assumes a continuous flame sheet, we model these local areas of no ignition by reducing the overall flame speed. A reduced flame speed results in lower overall combustion efficiency which is similar to the effect of locally zero ignition. The model uses the following equation:

$$St' = St \cdot \eta_w. \tag{83}$$

The initial value for the augmentor efficiency is the wake reaction level on a mass weighted basis. Expressed as an equation this is:

$$\eta_{c_o} = \eta_w \cdot \frac{\dot{m}_r}{\dot{m}_a} \tag{84}$$

where:

η_{c_o} $\sim$ Initial efficiency
η_w $\sim$ Wake efficiency
$\dot{m}_r$ $\sim$ Wake mass flowrate
$\dot{m}_a$ $\sim$ Total duct flowrate.

The type of flame utilized in this model is a zero thickness flame which separates a region of unreacted propellants from a region of completely reacted products. From this setup the average local augmentor efficiency is simply the ratio of the transverse flame penetration, Δy, to the duct width, W (see Figure 32).

To be consistent, the transverse location of the flame front at the initial calculation station is taken to be:

$$\Delta y_o = \eta_{c_o} \cdot W. \tag{85}$$

This value is assigned to the first axial station, which is assumed to occur halfway down the length of the recirculation zone. From visual observations of wake-stabilized flames, this is the approximate location of transverse flame initiation.

From this location downstream to the exhaust nozzle, the flame front transverse location is calculated by a finite difference integration of the local flame speed. Several axial profiles are introduced as the integration proceeds. These are:

- The turbulence intensity is decayed from the value generated at the aft flameholder lip (Equation 80) at a rate inversely proportional to the square root of axial distance over an effective jet length. The final value is set at the initial turbulence level. The effective jet length is set at 10 L/D where the D is the open area distance between adjacent flameholders.

- The velocity of the unreacted fuel-air mixture is retained at the level generated at the flameholder lip. Measured profiles from several ducted flame test rigs support this assumption.

- A term is introduced which relates the local flame speed to the local average duct combustion efficiency, peaking at 50%. This treats the counteracting influences of reduced heat loss as efficiency increases and the reduced free oxygen concentration. Local rates which follow roughly a sine wave function have been reported from duct data.

49

Analysis of the terms utilized for evaluation of the laminar flame speed term, S'_ℓ, has resulted in the following:

$$S'_\ell = S_\ell (\phi) \left(\frac{T_a}{540}\right)^{1.5} \left(\frac{X_{O_2}}{0.21}\right)^3 \qquad (86)$$

where:

S_ℓ = laminar flame speed at 1 atm and 540 deg

ϕ = equivalence ratio

T_a = air temperature °F

X_{O_2} = oxygen mole fraction.

The influence of pressure is indeterminate at this time and has been incorporated as $\sqrt{p}$ for subatmospheric data and no influence for pressures above 1 atmosphere.

d. Phase I Results

The first efforts to improve the combustion model were directed at the solution methodology for the fan stream flameholder wakes. The solution technique for a given fan streamtube utilizes two sets of equations with the flameholder wake temperature and flameholder wake fuel-air ratio as independent variables.

The first equation set is called the composition solution. For a given geometry and operating point, the wake fuel-air ratio (ϕ) is related to the streamtube fuel-air ratio (θ) by the equation:

$$\frac{\phi}{\theta} = \beta_1 + (1-\beta_1)\frac{\beta_2\,\beta_3}{K_1}$$

In this equation, all terms are independent of the wake temperature except β_3. Since β_3 is controlled by the heat flux through the flameholder surface, the wake fuel-air ratio will increase as the wake temperature increases.

The solution technique arbitrarily increases the wake temperature through a range from 1000°F to 5000°F and calculates the resultant value of wake fuel-air ratio as β_3 increases. Such solutions are shown in Figure 33 for one geometry and operating point for three levels of streamtube fuel-air ratio.

The vertical portion of the composition solution curve for 0.020 streamtube fuel-air ratio occurs because β_3 reached a value of 1.0 at about 2600°F. Since all the surface fuel film was vaporized here, further increases in wake temperature resulted in no further increase in wake fuel entry or fuel-air ratio.

The second equation set reverses the order of fuel-air ratio and temperature to produce a curve of wake temperature versus fuel-air ratio. In this case, the wake fuel-air ratio is arbitrarily increased from a very low value. The wake reaction is evaluated at this fuel-air ratio and the given set of geometry and inlet conditions. For the initial low values of fuel-air ratio, no wake kinetic solution will exist. The first fuel-air ratio value which produces a wake reaction solution establishes the lean limit for the given conditions. The solution technique continues to increase the wake fuel-air ratio, establishing a wake temperature for each fuel-air ratio, until a value of wake fuel-air ratio is tried which does not yield a solution. This establishes the wake rich limit.

50

The curve which results from this approach is shown in Figure 33 labeled kinetics solution.
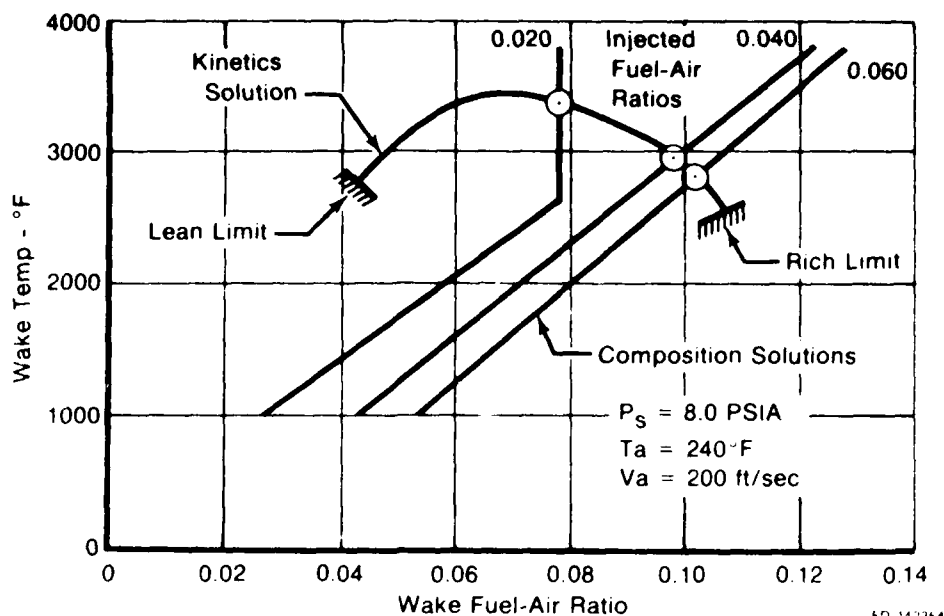

Figure 33. Duct Stream Flameholder Wake Solution

The final step in the solution for the fan duct streamtube is to locate the simultaneous solution of these two procedures. The intersection defines the possible solution to the fan duct streamtube wake fuel-air ratio and wake temperature. It is also possible, however, that there is no intersection of these two curves. The composition curve may miss the kinetics curve on either the lean or rich side. These situations reflect the use of input variables for which no stable flame is possible. Since it is not possible to a priori determine the lean and rich limits for all configurations, the intersection solution must recognize that failure to intersect is not an error but a valid blowout.

The solution which is used in the computer program was found to have several serious flaws which were directly responsible for inconsistent answers from the program. The program required that variations in overall efficiency with changes in inlet pressure, temperature, velocity and fuel-air ratio should be smooth curves. The solution technique originally employed resulted in a variation as shown in Figure 34.

The problems were traced to several defects. First, the two sets of curves were stored in arrays which were not dimensioned large enough to store the full range of data at some points. This resulted in a true solution which existed beyond the range of the array, but was solved using the last array value. As a result, the "solution" would vary depending on exactly where the array started.

The second problem was related to the solution for wake reaction efficiency as a function of the wake aerodynamic loading parameter ($V/PsT^{1.7}$). This function, for a given loading and fuel-air ratio, has two possible solutions, one of which is invalid. Therefore, provisions were made to assure selection of the proper solution. Unfortunately, the provisions covered all possibilities but one. That possibility was when an initial guess on the solution was greater than a failure solution but within the convergence tolerance. This problem was eliminated by using the slope of the function at convergence to determine if the solution is valid.
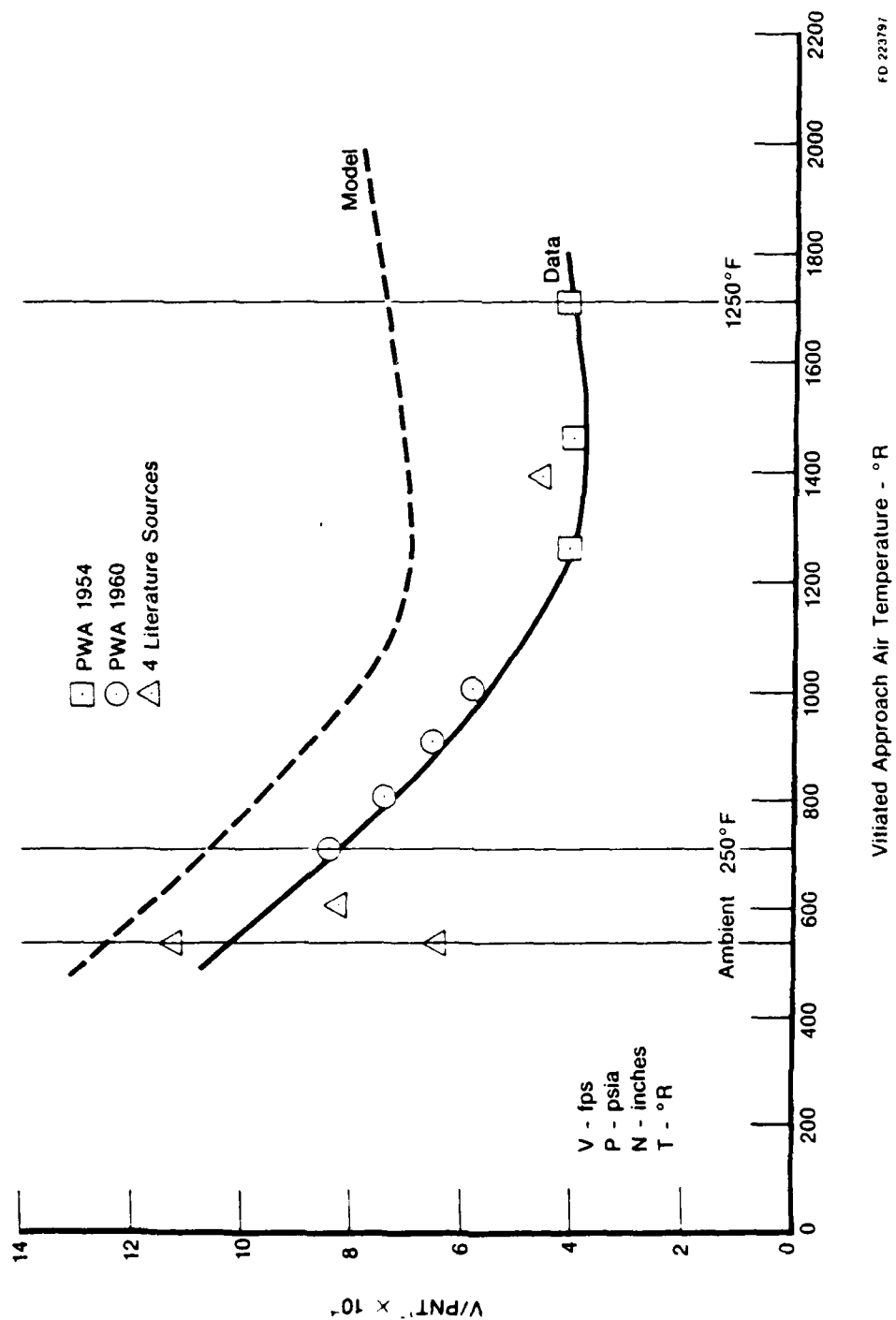
51

Figure 34. Comparison of Blowout Data to Model

52

A reaction kinetics solution curve was generated by incrementing fuel-air ratio and solving for wake temperature until a point failed. From that point, the f/a was reduced in very small increments until a point solved. This was defined as the rich limit. The problem occurred when the rich limit point was actually the last solved point (i.e. f/a reduced a full increment).

In this case, a round-off error occurred in the seventh decimal place in f/a causing the curve interpolating routine to return erroneous temperature information when evaluating near the rich limit. This problem was resolved by eliminating this extra solution information whenever the error occurred.

Also, the slight waviness in the results was eliminated by tightening the tolerance on all iterative solutions from 0.005 to 0.0001. Graphic examples of the results of these efforts are shown in Figures 34 through 37. The data points used are from the engine data taken under contract F33615-76-C-2024 and presented in AFAPL-TR-78-82. Variations are shown plotted versus static pressure (P,) and fuel-air ratio (f/a).

FD 230860
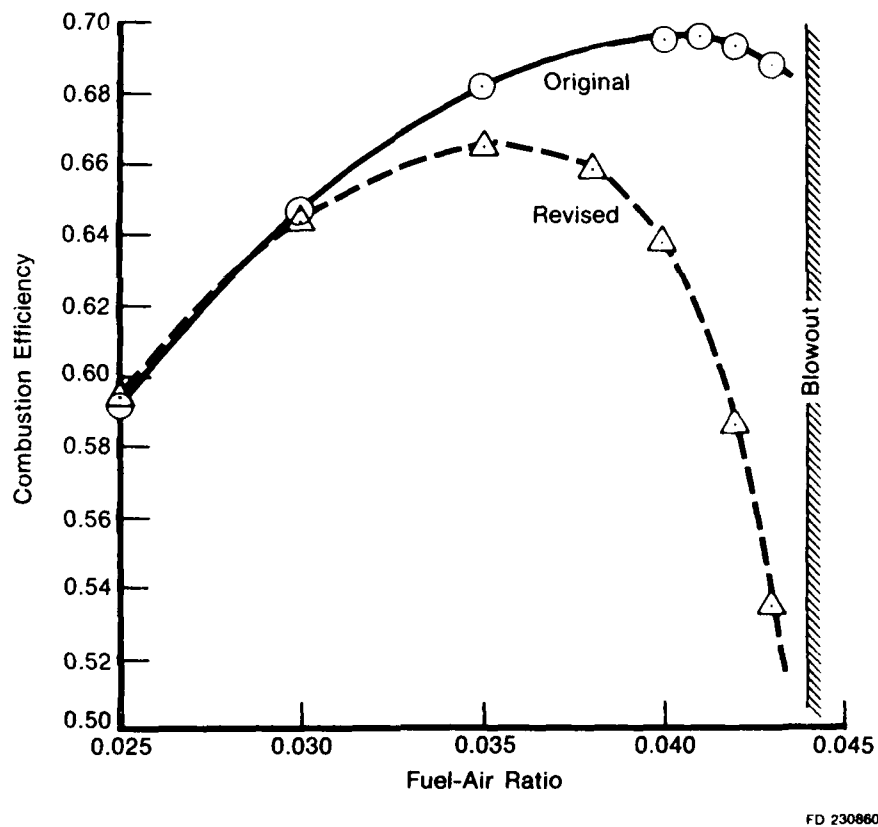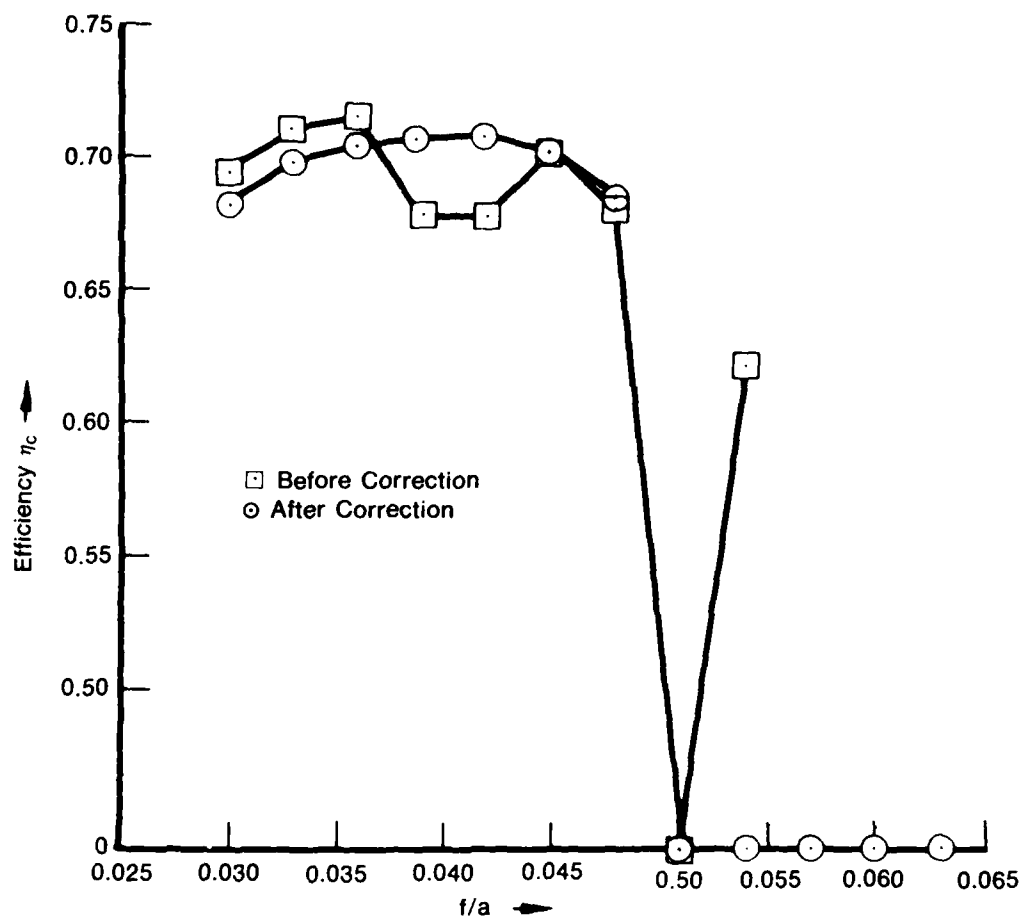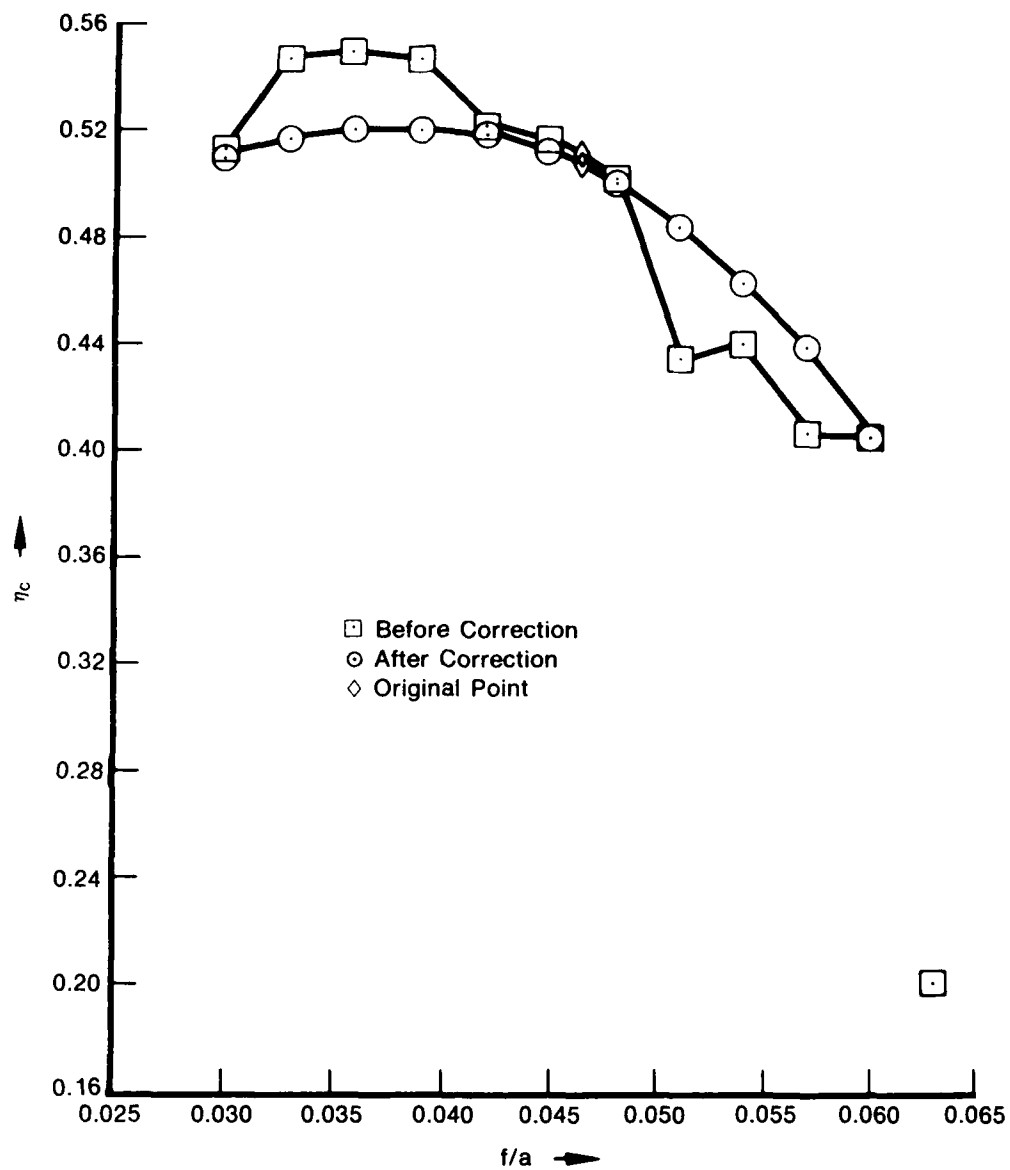
Figure 35. Revised Combustion Model Results, Fan Stream Case

53

Figure 36. Sample Case: Data Pt 0.504 HB1

FD 230856

54

Figure 37. Sample Case: Data Pt 195 B/M

FD 230853

55

The revised solution technique also eliminated the problem of a blowout prediction (η > 0) in-between two valid solutions. Now, once the flame blows out it stays out.

The next area of investigation was to determine why the surface vaporization model would not execute for approach air temperatures in excess of approximately 350°F. The original surface vaporization model was formulated and calibrated for approach air temperatures in the range of 200 to 250°F. One of the heat transfer modes which was included in the model was heat transferred from the airstream to the surface fuel film on the flameholder.

As test cases were run to evaluate the range of applicability of the model, it was found that premature rich wake blowouts were predicted above 350F and by 500F virtually no stable flame was possible. This result is, of course, in opposition to observed flame stability behavior. The investigation into the reson for this failure focused on the formulation for the vaporization rate of a liquid exposed to high velocity airflow with subsurface heating.

The results of this study showed that the Nusselt number formulation for the heat transfer from the air flow to the liquid film was in error on the high side. The result of this error was that the majority of the heat which was responsible for the liquid vaporization was due to the air flow and not due to the heat from the flameholder wake. As the air temperature increased, the degree of surface vaporization increased (larger β_0) and the wake fuel-air ratio exceeded the rich limit.

The equations were revised to reduce the dependence on the air heat transfer mode. This reduced the amount of surface vaporization considerably and resulted in converged solutions to well beyond 800°F. However, another problem arose. The converged solutions were now quite a bit leaner and very large values of approach fuel-air ratio were required for blowout, due to the low percentage of heat flux through the wake

Additionally, when a fuel other than JP4 was used, specifically JP5, the model refused to converge. The lower volatility of JP5, coupled with the lower heat flux into the liquid, did not yield enough vaporized fuel to achieve wake fuel-air ratios above the lean limit. The situation was thus that there was apparently another mode of transfer of liquid fuel into the flameholder wake which was not accounted for originally and the excessive air heat flux gave about the correct level of extra fuel at about 250°F.

This missing mechanism was discovered in a paper by Gater and L'Ecuyer (Reference 1) on liquid-film cooling mass transfer. Two modes of liquid mass transfer to the local shear layer are postulated. The first is vaporization as was used in the model. The second employed the direct transfer of liquid from the film to the shear layer due to roughness of the liquid surface.

This mechanism was added to the calculation routine for β_0 in the model. Since there is little dependence on the air temperature, excessive wake enrichment is avoided. Since the direct transfer is also not volatility dependent, the extremely lean results previously obtained with JP5 fuel shifted to reasonable wake fuel-air ratio values.

A significant problem was discovered in the combustion model during the course of evaluation of multiple streamtube configurations. A streamtube was used in the core stream to represent a location in the flameholder where no reaction was present. To model this, the user input an extremely narrow flameholder, which should have been past the blowout limit. The model predictions, however, resulted in stable flames to well below experience limits. The wake stability model was severely overpredicting the blowout limits at the higher levels of approach gas temprature which exists in the turbine discharge air flow or core region. A reexamination of the formulation for the blowout limits was started.

The formulation for the core region flameholder wake consisted of a recirculation calculation and the wake kinetics calculation. The basic thesis is that the wake region could be treated behaviorally as a stirred reactor whose volume was equal to the recirculation zone size and whose mass loading rate was equal to the recirculation rate. This reactor was assumed to have a fuel-air ratio equal to the injected fuel flowrate divided by the approach air flowrate.

The problems which were discovered included an inappropriate temperature exponent on the recirculation rate which reduced the effective reactor loading at elevated temperatures. This reduced loading calculation permitted higher levels of wake reaction efficiency and thus improved blowout limits. Additionally, the analysis originally did not account for the effect of the vitiation of the core stream approach flow upon the reaction zone equivalence ratio or adiabatic flame temperature.

The recirculation rate and the reactor loading rate were originally related as follows:

- The reactor loading parameter, after Longwell (Reference 4) is:

$$\frac{A}{V_o p^2}$$

where:

A	=	mass entry rate
V_o	=	reactor volume
p	=	static pressure

- The recirculation rate is:

$$A = K_1 \, \rho V_g N = K_1 \frac{p}{RT_g} V_g N$$

- The reactor volume is:

$$V_o = \text{Constant} \cdot (L/d)(B/d)N^2$$

Combining yields:

$$\frac{A}{V_o p^2} = \text{Constant} \times K_1 \frac{p}{RT_g} V_g N \cdot \frac{1}{(L/d)(B/d)N^2} \cdot \frac{1}{p^2}$$

$$\frac{A}{V_o p^2} = \text{Constant} \cdot K_1 \frac{V_g}{pNT_g}$$

- An air viscosity term was added to account for the assumed dependence of recirculation rate in approach viscosity through temperature, yielding

$$\frac{A}{V_o p^2} \propto \frac{V_g}{pNT_g^{1.7}}$$

This relationship has the form of the classical blowout correlations and was thought to be correct. What was overlooked was the allowable limit on reactor loading would increase as the approach temperature increased. Since blowout occurs when the calculated recirculation or loading exceeds the limit value, the result of this oversight was to raise the blowout limits quite rapidly at elevated temperatures. The model would predict a stability limit which would correlate with $T_g^{3.5}$ as opposed to the experimental data range of $T_g^{1.2}$ to $T_g^{1.5}$.

The corrections were twofold. First, the assumed viscosity term was deleted. Secondly, an effect of approach temperature on the wake volume was noted and included. The addition of these two corrections resulted in a loading parameter as:

$$\frac{A}{V_o p^2} = Constant \cdot \frac{V}{pNT^{0.5}}$$

when coupled with the $T^{1.8}$ increase in the limit value the stability correlation term became

$$\frac{V}{pNT^{2.7}} \quad .$$

This was better, but still overpredicted the stability limit increase due to Tg increase when compared with available data.

The final correction was made when it was noticed that the flameholder wake kinetics analysis was being performed using a fuel-air ratio which was based on the injected fuel flowrate only and ignored the effect of the vitiation which occurs in the main combustor. This effect was modeled in the wakes as an increase in the diluent fraction of the recirculated air flow with ie reaction fuel-air ratio based on the available oxygen mole fraction.

This revised analysis had the effect of offsetting the increase in stability limit as temperature increased since the available oxygen decreased. This effect is noted only for the situation where the approach gas temperature is raised by direct vitiation.

To evaluate tne success of this revised model, a series of stability limit calculations were performed. The peak of the blowout curve was plotted as a function of vitiated approach gas temperature. The resultant curve was then compared to several gaseous stability limits from open literature and internal data. It was expected that the resultant curve would have a temperature exponent near the value of 1.7.

The result is shown in Figure 38. The stability limit does not show the expected trend but neither did the data. The model does show the same trend as the data indicated. The conclusion is that the model represents a realistic evaluation of the fundamental physics of bluff body flame stabilization. Also, at least for vitiated air flow, there is no single value of the exponent on temperature.

The final modification which was made to the combustion model was in the area of the initialization of the turbulent flame speed from the shear layers of the recirculation zone. This interaction is necessary to couple the effects of inlet dynamics on wake conditions to the ultimate level of overall efficiency. The working thesis is that as the inlet conditions are altered, e.g., pressure decrease, velocity increase, the wake reaction efficiency also changes. This change in inlet conditions affects the turbulent flame speed directly through the flame propagation model and indirectly through the process of ignition from the wake.
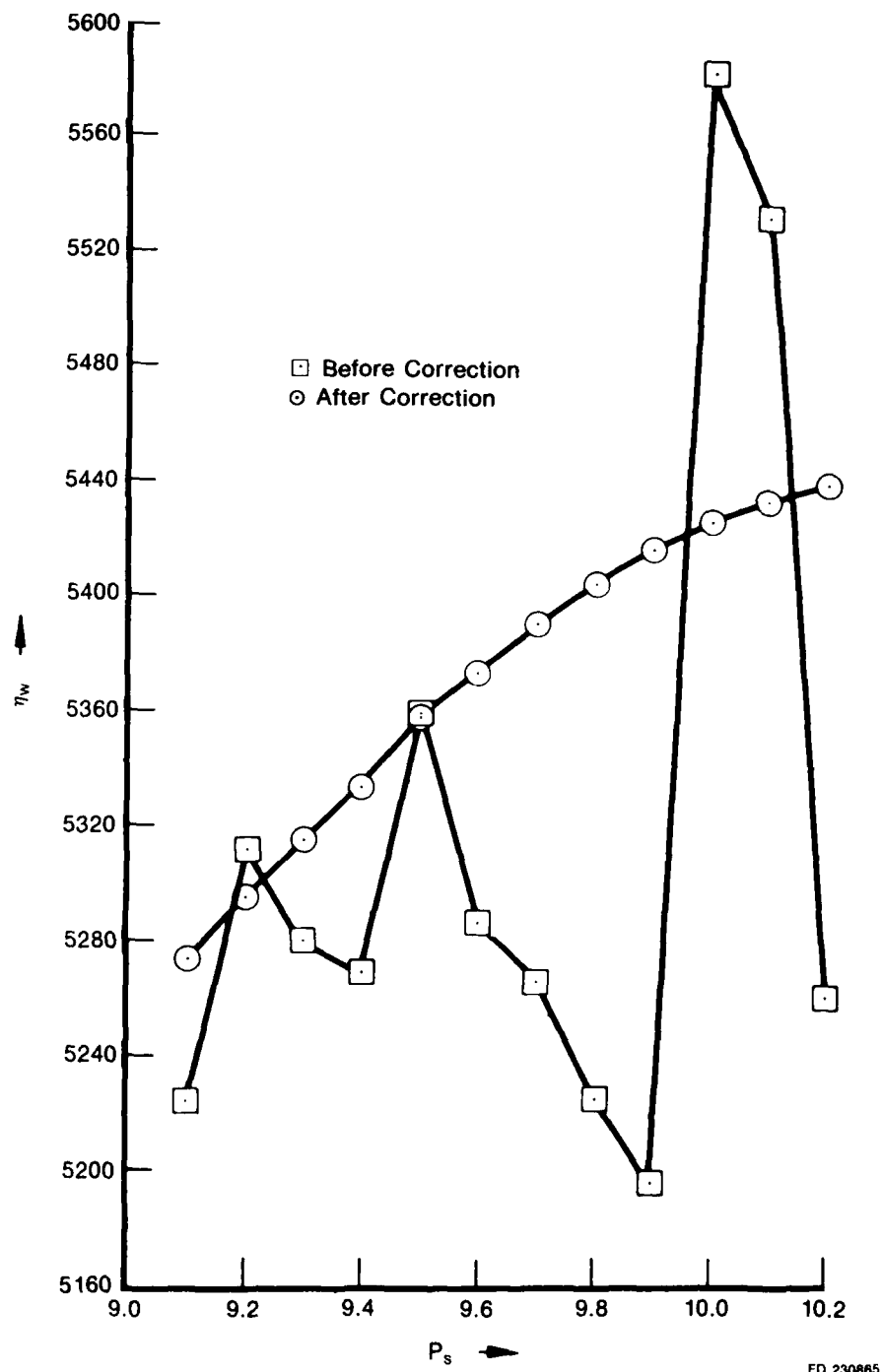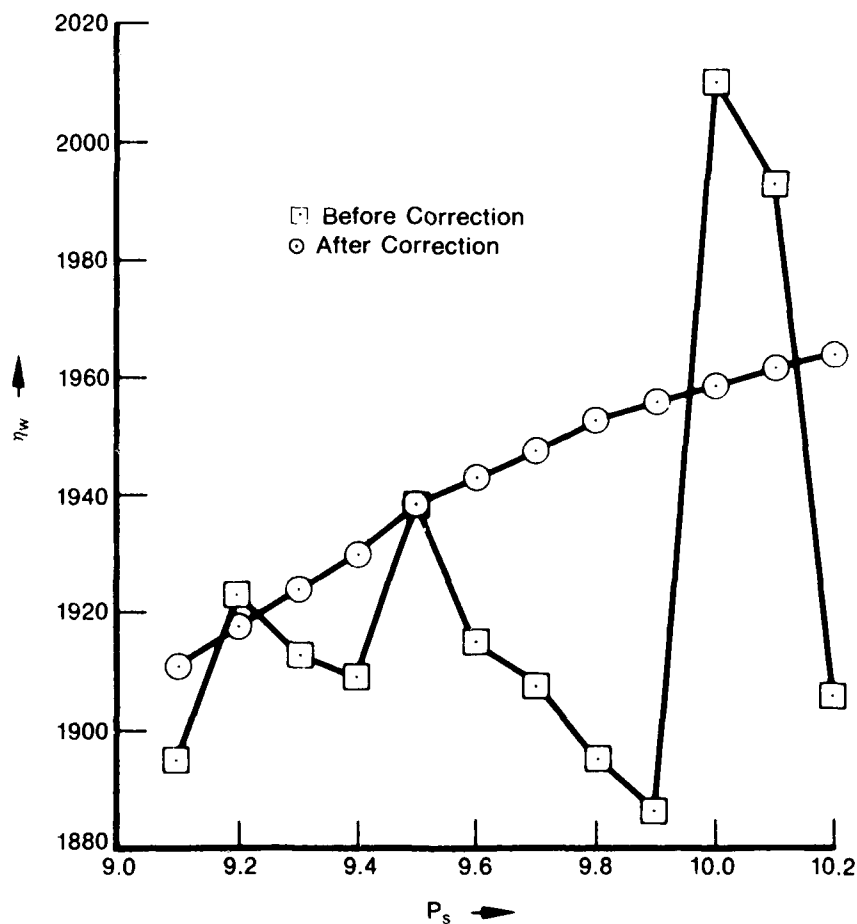
Figure 38.   Sample Case: Data Pt 195 B/M

59

If, for example, the inlet velocity were increased, the wake efficiency and thus shear layer temperature would decrease. This would result in a lower energy level for ignition of the bulk gas flow and a greater potential for ignition failure. The combustion analysis models this effect through an equation which relates the initial turbulent flame speed to the wake efficiency and shear layer temperature.

The original analysis used a term which decreased the turbulent flame speed by the linear factor of wake efficiency and surface vaporization percentage. The vaporization was used to account for the quenching effect of liquid fuel present in the shear layer. This simple model did not result in the dramatic decrease in overall efficiency, as the blowout was approached, which was required to drive the rumble instability.

A revised coupling model was used in the final version of the program. This model uses a strong nonlinear functional relationship between shear layer temperature and initial flame speed. This is felt to be a more accurate description of the initial steps in the ignition process. The results of this revised model are shown in Figure 39. The increased dependence of the overall efficiency on the wake conditions is seen as the stronger decrease rate near blowout. The ultimate stability limit is not altered by this revision, since the wake blowout limit is unchanged. The rumble onset point is moved away from the blowout point sufficiently to allow a less critical evaluation by the user.

FD 230866

Figure 39.   Sample Case: Data Pt 504 HB1

60

A further modification in the model was made to calculate the wake recirculation time constant which is used in the stability analysis. This constant represents the time lag between which a dynamic flow perturbation is seen at the flameholder trailing edge and the effect is transferred to the turbulent flame propagation rate.

The original model assumed that the effects of flow perturbations were transferred across this interface instantaneously. The revised model accounts for the time which is required for the wake region to respond to a flow shift. This time constant is already calculated as the wake residence time in the combustion recirculation rate solution.

The revision consisted of evaluating the average value of this constant over the streamlines used and placing the value in storage for use by the stability analysis.

e. Computer Program Description

The computer code is currently set to analyze a conventional turbofan augmentor with vee-gutter flameholders. The liquid fuel is injected through a spraybar located a specified distance upstream of the flameholder. The combustion process is stabilized by the bluff body recirculation zone, and a turbulent flame sheet propagates into the approach fuel-air mixture. The geometry is two-dimensional and would represent one streamtube of a multiple stream augmentor system.

The various analyses which were developed previously and referenced in the following paragraphs are written as subroutines in the computer program. This results in a modular program with a supervisory MAIN executing subroutines as required. This approach allows easy modification of the various analyses without disturbing the overall program operational logic.

The program first reads the input in NAMELIST format. From the input the two-dimensional model format is set up. Total air and fuel flowrates are calculated and the core stream or duct stream option is exercised. The following description details the duct stream analysis procedure.

From the fuel conditions in the spraybar and the flow field conditions in the duct, the degree of flash vaporization which occurs during injection is calculated. This percentage of fuel is allocated to the initial vapor phase.

The fuel which remains liquid is assigned to five equal mass flowrate groups. These groups are each assigned a mean droplet diameter. The droplet diameters generated by the program represent the spray formation characteristics of a variable area pintle spraybar. The controlling size parameter is the fuel injection pressure drop. These data are empirical from Pratt & Whitney Aircraft data. These five groups thus represent the flowrate versus size distribution unique to this spraybar type. If a different type of injector is to be analyzed, the droplet sizing subroutine must be rewritten.

The program then performs a finite difference solution to the droplet acceleration and vaporization equations by selecting a small time step and solving for the deltas of liquid velocity, temperature and a delta vaporized from the drag and vaporization/heating equations. The axial travel of the liquid droplet during this time increment is calculated from the initial and final liquid velocities. The analysis continues this small time step solution until the axial distance value equals the spraybar to flameholder separation distance. The acceleration/vaporization model assumes that the isolated droplet vaporization rate exceeds the rate in spray clouds by a factor of two. The calculation sums the amount of fuel which vaporizes from all the droplet size groups and adds this to the amount of fuel vaporized during injection. The sum of these represents the total term in the wake compositional equation.

The analysis next calculates the percentage of each of these size groups which is collected by impingement onto the flameholder surface. The collection rate is calcuated for each size group individually utilizing the droplet diameter which exists for each group after the vaporization calculations. The total collected liquid flowrate is summed from the collection efficiency for each group and the liquid flowrate which exists in each group after the vaporization calculations. The collecting rate calculation for each droplet size group is evaluated from droplet trajectory analyses which were performed and correlated against the geometric variables of the flameholder system. The details of this were presented in the earlier Phase I results.

The wake recirculation rate is next evaluated, again following the earlier reported analyses. The influence curves were reduced to a series of equations or curve reading routines within the RECIRC subroutine. This subroutine evaluates the aerodynamic loading of the idealized recirculation zone based on the empirical data earlier presented. The recirculation coefficient, K_1, is calculated, and the loading is stored for transfer to the wake kinetics subroutine.

At this point the solution proceeds along the parallel paths of exercising the flameholder surface vaporization subroutine, BETA 3, and the wake kinetics subroutine.

For the solution of BETA 3, values of wake temperature are assumed for every 200°F increment from 1000 to 5000°F. For each of these values, the heat flux from the recirculation zone through the flameholder into the liquid film is calculated. The surface vaporization is calculated utilizing a 20-step finite difference solution to the forced convection vaporization problem. The solution technique is the same as presented earlier. A 20-step solution was found necessary for convergence of numerical accuracy and to assure a smooth evaluation as the vaporization rate passes through to 100%. A check is made in the calculation for the ratio of heat flux to the liquid latent heat at collection conditions. Whenever the ratio exceeds unity, the vaporization is set at 100%.

For each value of wake temperature, the calculated vaporization rate is used in conjunction with the previous compositional coefficients to define a wake vapor phase fuel-air ratio. This temperature versus fuel-air ratio array is stored for later use.

The program transfers next the WAKE subroutine for the kinetics solution utilizing the recirculation rate from RECIRC and the Longwell reactor model presented earlier. The subroutine is exercised over a range of fuel-air ratios. The fuel-air ratios are started at 0.020 and increased by 0.0045. The solution is stored in an array of efficiency and wake temperature versus wake fuel-air ratio between the lean and rich limits.

These limits are evaluated at the level of aerodynamic loading for the case being analyzed. The lean limit is the first fuel-air ratio where a kinetic solution is found. The rich limit is found by a fine grid search backwards from the first fuel-air ratio which fails to produce a solution on the rich side. The increased accuracy of definition of the rich limit was found necessary since the rich blowout is the significant failure mode of duct flameholders.

Once this array is generated, the program searches for array intersection between the BETA 3 and WAKE results. If none is found, appropriate failure messages are printed and execution stops. If intersection is found, the convergent results of the wake compositional solution are printed.

The next subroutine, FLAME, performs the finite difference solution to the two-dimensional flame propagation problem presented earlier. The flame speed base value is altered by the level of wake reaction efficiency and by the percentage of liquid fuel which is sloughed from the flameholder trailing edge. This influence accounts for two real effects in the augmentor transferred to the pseudo-two-dimensional analysis. The wake efficiency is assumed uniform and continuous as is the flame sheet. In reality, as the efficiency decreases, local regions are generated where flame initiation in the shear layer fails. Decreasing the transverse speed of the idealized flame sheet is a method of describing this effect to account for the requirement of flame propagation normal to the duct into these unignited regions.

63

Similarly, the sloughed fuel serves to quench local regions of ignition in the shear layers which also require more normal flame penetration. The inclusion of a vaporization/sloughing term accounts for this in a two-dimensional analysis.

Once the flame is initiated, the subroutine performs a finite difference solution to the transverse propagation into the free-stream allowing for the axial variations in velocity, turbulence, etc. This continues until the exhaust nozzle is reached.

For the analysis of a core stream segment the procedure is simplified greatly due to the complete fuel vaporization. The program sets the wake fuel-air ratio equal to the total fuel-air ratio and performs the wake kinetics solution at this value and the calculated value of recirculation. A gaseous phase turbulent flame is initiated, corrected by wake efficiency, and evaluated downstream as before.

3. Development of Rumble Model Equations

a. General

The augmentor math model consists of a set of time-dependent equations describing the longitudinal dynamics of the flowing air stream and the axially distributed combustion process in the augmentor, coupled with a solution technique for determining stability. These equations are linearized, through the assumption of small perturbations, and transformed from the time-domain to the Laplace transform "S" domain. The solution technique is based upon the Nyquist stability criterion and consists of determining whether the time response of the system to a small disturbance would display oscillatory behavior with a growing amplitude. The result is a determination of stability at a given operating point, regions of operation which will cause rumble, and changes to the augmentor to make it rumble free.
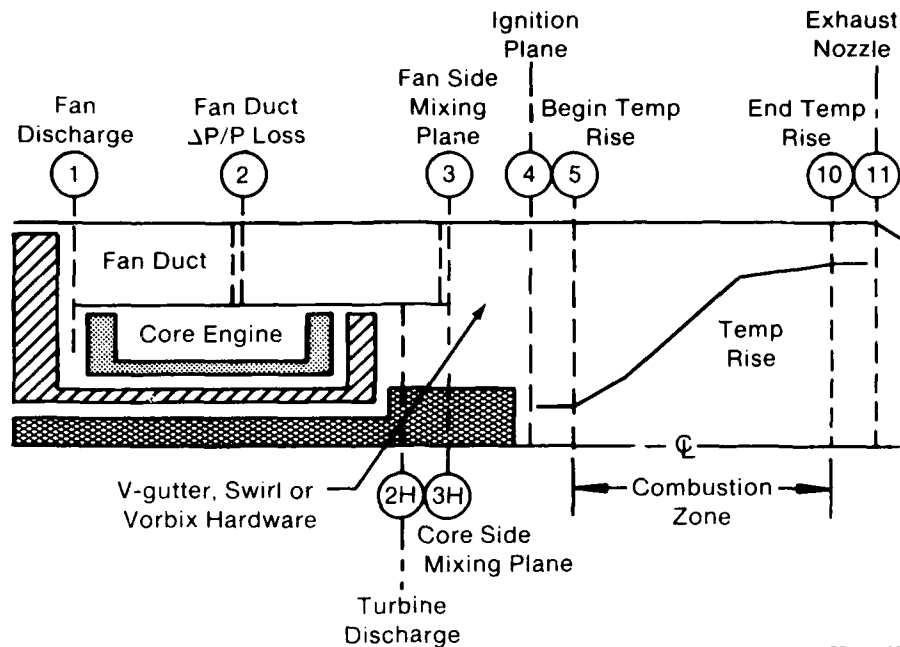
b. Development of Acoustic Equations

In this section equations are developed to describe how velocity, pressure, and density at every point in the augmentor respond to a combustion disturbance, which is treated as a heat input to a flowing inviscid ideal gas stream. Knowing how these three parameters (velocity, pressure, density) respond allows calculation of any other parameter needed, such as mass flowrate or temperature. The first equations to be developed are the three longitudinal wave equations, which are applicable between boundaries and discontinuities. Then equations for the boundaries and discontinuities are developed. The wave equations plus the boundary and discontinuity equations are referred to as the "acoustic" equations. The "combustion" equations needed to complete the rumble model are developed in part c.

Symbols used below are defined in the List of Symbols. For any section of augmentor with rigid walls and constant cross-sectional area, such as shown in Figure 40, through which an invicid fluid (viscosity is zero) is flowing, the one-dimensional momentum, continuity, and energy equations are:

$$\frac{\partial P}{\partial x} + \rho V \frac{\partial V}{\partial x} + \rho \frac{\partial V}{\partial t} = 0$$

$$\rho \frac{\partial V}{\partial x} + V \frac{\partial \rho}{\partial x} + \frac{\partial \rho}{\partial t} = 0 \tag{87}$$

$$q + \frac{PV}{\rho} \frac{\partial \rho}{\partial x} + \frac{P}{\rho} \frac{\partial \rho}{\partial t} = \rho V \frac{\partial u}{\partial x} + \rho \frac{\partial u}{\partial t}$$

For an ideal gas, these equations reduce to the following non-linear wave equations:

$$(V+C) \left[\frac{1}{P} \frac{\partial P}{\partial x} + \frac{\gamma}{C} \frac{\partial V}{\partial x} \right] + \left[\frac{1}{P} \frac{\partial P}{\partial t} + \frac{\gamma}{C} \frac{\partial V}{\partial t} \right] = (\gamma - 1) \frac{q}{P}$$

$$(V-C) \left[\frac{1}{P} \frac{\partial P}{\partial x} - \frac{\gamma}{C} \frac{\partial V}{\partial x} \right] + \left[\frac{1}{P} \frac{\partial P}{\partial t} - \frac{\gamma}{C} \frac{\partial V}{\partial t} \right] = (\gamma - 1) \frac{q}{P} \tag{88}$$

$$V \left[\frac{1}{P} \frac{\partial P}{\partial x} - \frac{\gamma}{\rho} \frac{\partial \rho}{\partial x} \right] + \left[\frac{1}{P} \frac{\partial P}{\partial t} - \frac{\gamma}{\rho} \frac{\partial \rho}{\partial t} \right] = (\gamma - 1) \frac{q}{P}$$

Figure 40. Rumble Model Station Identification

The wave equations are linearized by the small perturbation substitutions:

$$
\begin{aligned}
P(x,t) &= \hat{P}(x) + \Delta P(x,t) \\
\rho(x,t) &= \bar{\rho}(x) + \Delta\rho(x,t) \\
C(x,t) &= \bar{C}(x) + \Delta C(x,t) \\
V(x,t) &= \bar{V}(x) + \Delta V(x,t) \\
q(x,t) &= \bar{q}(x) + \Delta q(x,t)
\end{aligned}
\tag{89}
$$

Second order terms are neglected in making the substitutions.

To simplify notation, the following substitutions are made which normalize the change in each variable by its steady-state value:

$$
P' = \frac{\Delta P}{\hat{P}}, \ V' = \frac{\Delta V}{\bar{V}}, \ \rho' = \frac{\Delta\rho}{\bar{\rho}}, \ q' = \frac{\Delta q}{\bar{q}}
\tag{90}
$$

The linearized version of equations (88) becomes:

$$
(\bar{V}+\bar{C}) \frac{\partial}{\partial x}\left[P'+\gamma\bar{M}V' \right] + \frac{\partial}{\partial t}\left[P'+\gamma\bar{M}V' \right] + (\gamma-1)\frac{\bar{q}}{\hat{P}}\beta_F' = (\gamma-1)\frac{\bar{q}}{\hat{P}} q'
$$

$$
(\bar{V}-\bar{C})\frac{\partial}{\partial x}\left[P'-\gamma\bar{M}V' \right] + \frac{\partial}{\partial t}\left[P'-\gamma\bar{M}V' \right] + (\gamma-1)\frac{\bar{q}}{\hat{P}}\beta_G' = (\gamma-1)\frac{\bar{q}}{\hat{P}} q'
\tag{91}
$$

$$
\bar{V} \frac{\partial}{\partial x}\left[P'-\gamma\rho' \right] + \frac{\partial}{\partial t}\left[P'-\gamma\rho' \right] + (\gamma-1)\frac{\bar{q}}{\hat{P}}\beta_E' = (\gamma-1)\frac{\bar{q}}{\hat{P}} q'
$$

66

where:

$$\beta_F' = \frac{1}{(1-\bar{M}^2)}\left[P'(1-\bar{M}-\bar{M}^2) + \rho'\bar{M} + V'\left\{ \frac{1}{2} + \frac{3}{2}\bar{M} - \bar{M}^2[1 + (1+\bar{M})\frac{\gamma}{2}] \right\} \right]$$

$$\beta_G' \equiv \frac{1}{(1-\bar{M}^2)}\left[P'(1+\bar{M}-\bar{M}^2) + \rho'\bar{M} + V'\left\{ \frac{1}{2} - \frac{3}{2}\bar{M} - \bar{M}^2[1 + (1-\bar{M})\frac{\gamma}{2}] \right\} \right]$$

$$\beta_E' \equiv P' + V'$$

(92)

Taking the Laplace transform with respect to time, with zero initial conditions, and letting subscripts 1 & 2 stand for the upstream and downstream stations respectively (see Figure 40), the general solution to equations (91) becomes:

$$[P_2' + \gamma M_2 V_2']e^{s\int_0^l \frac{dx}{V+C}} - [P_1'+\gamma M_1 V_1'] + \frac{(\gamma-1)}{S}\int_0^l \frac{\bar{q}}{\bar{P}}\beta_F'(x,s)\frac{d}{dx}e^{s\int_0^x \frac{dx}{V+C}}dx$$

$$= \frac{(\gamma-1)}{S}\int_0^l \frac{\bar{q}}{\bar{P}}q'(x,s)\frac{d}{dx}e^{s\int_0^x \frac{dx}{V+C}}dx$$

$$[P_2' - \gamma M_2 V_2']e^{s\int_0^l \frac{dx}{V-C}} - [P_1'-\gamma M_1 V_1'] + \frac{(\gamma-1)}{S}\int_0^l \frac{\bar{q}}{\bar{P}}\beta_G'(x,s)\frac{d}{dx}e^{s\int_0^x \frac{dx}{V-C}}dx$$

(93)

$$= \frac{(\gamma-1)}{S}\int_0^l \frac{\bar{q}}{\bar{P}}q'(x,s)\frac{d}{dx}e^{s\int_0^x \frac{dx}{V-C}}dx$$

$$[P_2' - \gamma\rho_2']e^{s\int_0^l \frac{dx}{V}} - [P_1'-\gamma\rho_1'] + \frac{(\gamma-1)}{S}\int_0^l \frac{\bar{q}}{\bar{P}}\beta_E'(x,s)\frac{d}{dx}e^{s\int_0^x \frac{dx}{V}}dx$$

$$= \frac{(\gamma-1)}{S}\int_0^l \frac{\bar{q}}{\bar{P}}q'(x,s)\frac{d}{dx}e^{s\int_0^x \frac{dx}{V}}dx$$

In equations (93) the first equation describes downstream running sonic waves of the form $P' + \gamma M V'$, traveling at sonic speed plus throughflow velocity. The second equation describes upstream running sonic waves of the form $P' - \gamma M V'$, traveling at sonic speed minus throughflow velocity. The third equation describes entropy waves, $P' - \gamma\rho'$, drifting downstream at throughflow velocity.

67

The entropy waves become more apparent from the expression for the entropy of an ideal gas:

$$\frac{\Delta S}{C_v} = S' = P' - \gamma \rho'$$ (94)

The entropy waves are related to temperature by:

$$\gamma T' = S' + (\gamma-1) P'$$ (95)

It is through equation (95) that the drifting hot and cold combustion products, or entropy waves, are accounted for in the rumble model. Temperature changes produced as the entropy waves strike the exhaust nozzle create waves which then travel back upstream at sonic speed.

Equations (93) are not useful until the integrals are evaluated, which will require definitions of $V(x)$, $C(x)$, $q(x)$, $P(x)$ and some assumptions that will allow integration of $q'(x,S)$, $\beta_F'(x,S)$, $\beta_G'(x,S)$, and $\beta_K'(x,S)$. To complete the solution the augmentor is divided into several "short" sections, each of length ℓ, for each of which it can be assumed:

(a) $\quad \dfrac{d \, \bar{P}(x)}{dx} = 0$

(b) $\quad \dfrac{d \, \bar{T}(x)}{dx} = $ constant

(c) $\quad q'(x,t) = q'\left(0, \, t - \displaystyle\int_0^x \frac{dx}{\bar{V}} \right)$

(d) $\quad \dfrac{\bar{q}(x)}{\bar{P}(x)} = $ constant

The small static pressure drop in an augmentor justifies assumption (a). A linear temperature rise throughout a section of length ℓ is a good approximation, which justifies assumption (b). Assumption (c) is the equation for a "drifting burning particle" releasing heat at a constant volumetric rate as it drifts down the augmentor. A more detailed explanation of this assumption will be provided in part c (Development of Combustion Equations). To justify the constant steady-state heat release rate (q) consider the steady-state version of the energy equation (third in equations (88)).

$$\bar{V} \left[\frac{1}{\bar{P}} \frac{d\bar{P}}{dx} - \frac{\gamma}{\bar{\rho}} \frac{d\bar{\rho}}{dx} \right] = (\gamma-1) \frac{\bar{q}}{\bar{P}}$$

With appropriate substitutions, the equation reduces to:

$$\frac{\bar{q}}{\bar{P}} = \left(\frac{\gamma}{\gamma-1} \right) \frac{R}{\bar{P}} \frac{W}{A} \frac{dT}{dx} - \frac{\bar{V}}{\bar{P}} \frac{d\bar{P}}{dx}$$

Since $\dfrac{d\bar{P}}{dx} = 0$ and $\dfrac{dT}{dx} = $ constant, then

$$\frac{\bar{q}}{\bar{P}} = \text{constant} = \frac{\gamma}{\gamma-1} \frac{C_1 M_1}{\ell} \left(\frac{T_2}{T_1} - 1 \right)$$ (96)

For a "short" section of length ℓ the integration of $\beta_F'(x,S)$ in equations (93) can be carried out as follows:

$$\int_0^\ell \frac{\bar{q}}{\bar{P}} \beta_F(x,S) \frac{d}{dx} e^{S \int_0^x \frac{dx}{\bar{V}+C}} dx \approx \frac{\bar{q}}{\bar{P}} \beta_F(o,S) \int_0^{\ell/2} \frac{d}{dx} e^{S \int_0^x \frac{dx}{\bar{V}+C}} dx$$

$$+ \frac{\bar{q}}{\bar{P}} \beta_F'(\ell,S) \int_{\ell/2}^\ell \frac{d}{dx} e^{S \int_0^x \frac{dx}{\bar{V}+C}} dx$$

Similar treatment allows integration of $\beta_G'(x,S)$ and $\beta_E'(x,S)$ in equation (93). To determine how "short" a section must be for the solution to be valid, the resulting rumble model was exercised repeatedly while decreasing the section length (by adding more stations in the combustion zone). As the section length decreases, the result will rapidly approach an exact solution. It was found that section lengths shorter than about 20 inches were unnecessary.

With the above assumptions, equation (93) becomes:

$$[P_2 + \gamma \bar{M}_2 V_2] - [P_1 + \gamma \bar{M}_1 V_1']e^{-\tau_F S} - (\gamma-1)\frac{\bar{q}}{\bar{P}} \beta'_{F_1} \left[\frac{e^{-\tau_F S} - e^{-\tau_{F_2} S}}{S} \right]$$

$$+ (\gamma-1) \frac{\bar{q}}{\bar{P}} \beta'_{F_2} \left[\frac{1-e^{-\tau_{F_2} S}}{S} \right] = (\gamma-1) \frac{\bar{q}}{\bar{P}} q_1' \left\{ \bar{M}_1 \left[\frac{e^{-\tau_F S} - e^{-(\tau_{E_1} + \tau_{F_2})S}}{S} \right] \right.$$

$$\left. + M_2 \left[\frac{e^{-(\tau_{F_2} + \tau_{E_1})S} - e^{-\tau_E S}}{S} \right] \right\}$$

(97)

$$[P_1 - \gamma \bar{M}_1 V_1'] - [P_2 + \gamma \bar{M}_2 V_2']e^{-\tau_G S} + (\gamma-1) \frac{\bar{q}}{\bar{P}} \beta'_{G_1} \left[\frac{1-e^{-\tau_{G_1} S}}{S} \right]$$

$$(\gamma-1) \frac{\bar{q}}{\bar{P}} \beta'_{G_2} \left[\frac{e^{-\tau_G S} - e^{-\tau_{G_1} S}}{S} \right]$$

$$= (\gamma-1) \frac{\bar{q}}{\bar{P}} q_1' \left\{ \bar{M}_1 \left[\frac{1-e^{-(\tau_{G_1}+\tau_{E_1})S}}{S} \right] + \bar{M}_2 \left[\frac{e^{-(\tau_{G_1}+\tau_{E_1})S} - e^{-(\tau_G + \tau_E)S}}{S} \right] \right\}$$

$$[P_2 - \gamma \rho_2] - [P_1 - \gamma \rho_1']e^{-\tau_E S} - (\gamma-1) \frac{\bar{q}}{\bar{P}} \beta'_{E_1} \left[\frac{e^{-\tau_E S} - e^{-\tau_{E_2} S}}{S} \right]$$

$$+ (\gamma-1) \frac{\bar{q}}{\bar{P}} \beta'_{E_2} \left[\frac{1-e^{-\tau_{E_2} S}}{S} \right] = (\gamma-1) \frac{\bar{q}}{\bar{P}} q_1' \tau_E e^{-\tau_E S}$$

where:

$$\tau_F \equiv \int_0^r \frac{dx}{V+C} \qquad \tau_G \equiv -\int_0^r \frac{dx}{V-C} \qquad \tau_E \equiv \int_0^r \frac{dx}{V}$$

$$\tau_{F_1} \equiv \int_0^{r/2} \frac{dx}{V+C} \qquad \tau_{G_1} \equiv -\int_0^{r/2} \frac{dx}{V-C} \qquad \tau_{E_1} \equiv \int_0^{r/2} \frac{dx}{V} \tag{98}$$

$$\tau_{F_2} = \tau_F - \tau_{F_1} \qquad\qquad\qquad \tau_{E_2} = \tau_E - \tau_{E_1}$$

$$\beta_{F_1} = \frac{1}{(1-M_1^2)}\left[P_1(1-M_1-M_1^2) + \rho_1 M_1 + V_1\left\{ \frac{1}{2} + \frac{3}{2}M_1 - M_1^2\left[1 + (1+M_1)\frac{\gamma}{2}\right] \right\} \right]$$

$$\beta_{F_2} \equiv \frac{1}{(1-M_2^2)}\left[P_2(1-M_2-M_2^2) + \rho_2 M_2 + V_2\left\{ \frac{1}{2} + \frac{3}{2}M_2 - M_2^2\left[1 + (1+M_2)\frac{\gamma}{2}\right] \right\} \right]$$

$$\beta_{G_1} = \frac{1}{(1-M_1^2)}\left[P_1(1+M_1-M_1^2) - \rho_1 M_1 + V_1\left\{ \frac{1}{2} - \frac{3}{2}M_1 - M_1^2\left[1 + (1-M_1)\frac{\gamma}{2}\right] \right\} \right]$$

$$\beta_{G_2} \equiv \frac{1}{(1-M_2^2)}\left[P_2(1+M_2-M_2^2) - \rho_2 M_2 + V_2\left\{ \frac{1}{2} - \frac{3}{2}M_2 - M_2^2\left[1 + (1-M_2)\frac{\gamma}{2}\right] \right\} \right] \tag{99}$$

$$\beta_{E_1} = P_1 + V_1$$

$$\beta_{E_2} = P_2 + V_2$$

For convenience in programming equations (96) on the computer the following identity substitutions were made:

$$\beta_{F_1} \quad PF_1 P_1 + RF_1\rho_1 + VF_1 V_1$$

$$\beta_{F_2} \quad PF_2 P_2 + RF_2\rho_2 + VF_2 V_2$$

$$\beta_{G_1} \quad PG_1 P_1 + RG_1\rho_1 + VG_1 V_1 \tag{100}$$

$$\beta_{G_2} \quad PG_2 P_2 + RG_2\rho_2 + VG_2 V_2$$

where by definition:

$$PF_1 = \frac{1}{(1-\bar{M}_1^2)} \quad [1-\bar{M}_1-\bar{M}_1^2]$$

$$RF_1 = \frac{\bar{M}_1}{(1-\bar{M}_1^2)}$$

$$VF_1 = \frac{1}{(1-\bar{M}_1^2)} \left\{ \frac{1}{2} + \frac{3}{2} \bar{M}_1 - \bar{M}_1^2 \left[1 + (1+\bar{M}_1) \frac{\gamma}{2} \right] \right\}$$

$$PF_2 = \frac{1}{(1-\bar{M}_2^2)} \quad [1 - \bar{M}_2 - \bar{M}_2^2]$$

$$RF_2 = \frac{\bar{M}_2}{(1-\bar{M}_2^2)}$$

$$VF_2 = \frac{1}{(1-\bar{M}_2^2)} \left\{ \frac{1}{2} + \frac{3}{2} \bar{M}_2 - \bar{M}_2^2 \left[1 + (1+\bar{M}_2) \frac{\gamma}{2} \right] \right\}$$

$$PG_1 = \frac{1}{(1-\bar{M}_1^2)} \quad [1-\bar{M}_1-\bar{M}_1^2]$$

$$RG_1 = \frac{-\bar{M}_1}{(1-\bar{M}_1^2)}$$

$$VG_1 = \frac{1}{(1-\bar{M}_1^2)} \left\{ \frac{1}{2} - \frac{3}{2} \bar{M}_1 - \bar{M}_1^2 \left[1 + (1-\bar{M}_1) \frac{\gamma}{2} \right] \right\}$$

$$PG_2 = \frac{1}{(1-\bar{M}_2^2)} \quad [1 + \bar{M}_2 - \bar{M}_2^2]$$

$$RG_2 = \frac{-\bar{M}_2}{(1-\bar{M}_2^2)}$$

$$VG_2 = \frac{1}{(1-\bar{M}_2^2)} \left\{ \frac{1}{2} - \frac{3}{2} \bar{M}_2 - \bar{M}_2^2 \left[1 + (1-\bar{M}_2) \frac{\gamma}{2} \right] \right\}$$

(101)

The time constants in equations (98) were evaluated based upon the steady-state through-flow and sonic speed profiles created by the linear temperature gradient.

$$V(x) = V_1 \left[1 + \left(\frac{T_2}{T_1} - 1 \right) \frac{x}{\ell} \right]$$

$$C(x) = C_1 \sqrt{1 + \left(\frac{T_2-T_1}{T_1} \right) \frac{x}{\ell}}$$

(102)

71

Then the time constants in equations (98) become:

$$\tau_F \equiv \frac{\ell/C_1}{\left(\dfrac{T_2}{T_1} - 1\right)} \frac{2}{\bar{M}_1} \ell n \left[\frac{1 + M_1 \sqrt{T_2/T_1}}{1 + M_1} \right]$$

$$\tau_G \equiv \frac{\ell/C_1}{\left(\dfrac{T_2}{T_1} - 1\right)} \frac{2}{\bar{M}_1} \ell n \left[\frac{1 - \bar{M}_1}{1 - \bar{M}_1 \sqrt{T_2/T_1}} \right]$$

$$\tau_E \equiv \frac{\ell/C_1}{\left(\dfrac{T_2}{T_1} - 1\right)} \frac{1}{\bar{M}_1} \ell n \left[\frac{T_2}{T_1} \right]$$

$$\tau_{F_1} \equiv \frac{\ell/C_1}{\left(\dfrac{T_2}{T_1} - 1\right)} \frac{2}{\bar{M}_1} \ell n \left[\frac{1 + \bar{M}_1 \sqrt{\frac{1}{2}(1 + T_2/T_1)}}{1 + \bar{M}_1} \right]$$

$$\tau_{G_1} \equiv \frac{\ell/C_1}{\left(\dfrac{T_2}{T_1} - 1\right)} \frac{2}{\bar{M}_1} \ell n \left[\frac{1 - \bar{M}_1}{1 - \bar{M}_1 \sqrt{\frac{1}{2}(1 + T_2/T_1)}} \right]$$

$$\tau_{E_1} \equiv \frac{\ell/C_1}{\left(\dfrac{T_2}{T_1} - 1\right)} \frac{1}{\bar{M}_1} \ell n \left[\frac{1}{2}(1 + T_2/T_1) \right]$$

(103)

This completes the development of the wave equations.

Equations (97) are applied throughout the augmentor between any two stations between which there is no discontinuity. The station designations used for the rumble model are shown in Figure 40. In applying the equations, the general subscripts 1 and 2 are replaced by the actual upstream and downstream station numbers, respectively. Referring to Figure 40, they are applied between stations (1) — (2), (2) — (3), (4) — (5), (5) — (10) and (10) — (11). Between stations (1) through (5) and between stations (10) — (11) there is no heat addition, and so the heat addition terms q/P are set to zero. The heat addition terms for the combustion zone, stations (5) — (10), are discussed in part C.

Discontinuities occur at the pressure drop locations, stations (2) and (3). These are modeled as small incompressible resistive pressure drops of zero length. The continuity and energy equations are also applied.

$$P_2 - P_3 \approx \frac{\rho_2 V_2^2}{2}$$

$$W_2 = W_3$$

(104)

$$T_2 = T_3$$

The equations are linearized and normalized as before to yield:

$$P_2' - \left[1 - \left(\frac{\bar{P}_2 - \bar{P}_3}{\bar{P}_2} \right) \right] P_3' = \left(\frac{\bar{P}_2 - \bar{P}_3}{\bar{P}_2} \right) (\rho_3' + 2V_3')$$

$$\rho_2' + V_2' = \rho_3' + V_3'$$ (105)

$$P_2' - \rho_2' = P_3' - \rho_3'$$

In applying equations (105) to a given pressure drop the general subscripts 2 and 3 are replaced by the actual upstream and downstream station numbers, respectively. For convenience in programming, equations (105) were combined with the wave equations (97) to eliminate the need for two stations at each pressure drop. It is the combined equations which appear in the rumble model listing.

A junction occurs where the core stream and fan stream enter the augmentor and form the overall augmentor stream (stations (3), (3H) and (4)). Again applying continuity, momentum and energy:

$$W_3 + W_{3H} = W_4$$

$$\left(\frac{P - P_4}{P} \right)_{\substack{\text{FAN SIDE} \\ \text{OR} \\ \text{CORE SIDE}}} \approx \left(\frac{W\sqrt{T}}{P} \right)^2_{\substack{\text{FAN SIDE} \\ \text{OR} \\ \text{CORE SIDE}}}$$ (106)

$$W_3 T_3 + W_{3H} T_{3H} = W_4 T_4$$

The linearized and normalized versions become:

$$\rho_4' + V_4' = \left(\frac{BPR}{1+BPR} \right) \rho_3' + \left(\frac{BPR}{1+BPR} \right) V_3' + \left(\frac{1}{1+BPR} \right) \rho_{3H}' + \left(\frac{1}{1+BPR} \right) V_{3H}'$$

$$P_3' - \left[1 - \left(\frac{\bar{P}_3 - \bar{P}_4}{\bar{P}_3} \right) \right] P_4' = 2 \left(\frac{\bar{P}_3 - \bar{P}_4}{\bar{P}_3} \right)\left(\frac{BPR}{1+BPR} \right) V_3'$$

$$+ \left(\frac{\bar{P}_3 - \bar{P}_4}{\bar{P}_3} \right) \left(\frac{BPR}{1+BPR} \right) \rho_3' + 2 \left(\frac{\bar{P}_3 - \bar{P}_4}{\bar{P}_3} \right)\left(\frac{1}{1+BPR} \right) V_{3H}'$$

$$+ \left(\frac{\bar{P}_3 - \bar{P}_4}{\bar{P}_3} \right) \left(\frac{1}{1+BPR} \right) \rho_{3H}'$$ (107)

$$P_{3H}' - \left[1 - \left(\frac{\bar{P}_3 - \bar{P}_4}{\bar{P}_3} \right) \right] P_4' = 2 \left(\frac{\bar{P}_3 - \bar{P}_4}{\bar{P}_3} \right)\left(\frac{BPR}{1+BPR} \right) V_3'$$

$$+ \left(\frac{\bar{P}_3 - \bar{P}_4}{\bar{P}_3} \right) \left(\frac{BPR}{1+BPR} \right) \rho_3' + 2 \left(\frac{\bar{P}_3 - \bar{P}_4}{\bar{P}_3} \right)\left(\frac{1}{1+BPR} \right) V_{3H}'$$

$$+ \left(\frac{\bar{P}_3 - \bar{P}_4}{\bar{P}_3} \right) \left(\frac{1}{1+BPR} \right) \rho_{3H}'$$

$$V_4' + P_4' = \left[\frac{BPR\,(T_3/T_H)}{1 + BPR\,(T_3/T_H)} \right] P_3' + \left[\frac{BPR\,(T_3/T_H)}{1 + BPR\,(T_3/T_H)} \right] \cdot V_3'$$

$$+ \left[\frac{1}{1 + BPR\,(T_3/T_H)} \right] P_{3H} + \left[\frac{1}{1 + BPR\,(T_3/T_H)} \right] \cdot V_{3H}'$$

73

For the Swirl augmentor, the momentum equations at stations (3) - (4) and (3H) - (4) are modified to account for the possibility of different pressure drops across the fan and core swirl vanes. The linearized version of the momentum equations for the Swirl augmentor becomes:

$$P'_3 - \left[1 - \left(\frac{\bar{P}_3 - \bar{P}_4}{\bar{P}_3}\right)\right] P'_4 = 2\left(\frac{\bar{P}_3 - \bar{P}_4}{\bar{P}_3}\right) V'_3 + \left(\frac{\bar{P}_3 - \bar{P}_4}{\bar{P}_3}\right) \rho'_3$$

$$P_{3H}' - \left[1 - \left(\frac{\bar{P}_{3H} - \bar{P}_4}{\bar{P}_{3H}}\right)\right] P'_4 = 2\left(\frac{\bar{P}_{3H} - \bar{P}_4}{\bar{P}_{3H}}\right) V'_{3H} + \left(\frac{\bar{P}_{3H} - \bar{P}_4}{\bar{P}_{3H}}\right) \rho'_{3H}$$

(108)

Definition of the upstream and downstream boundary conditions, at the fan and at the nozzle, respectively, will complete the acoustic equations. The fan was assumed to be delivering a constant mass flowrate through the fan OD (defined as that portion of the fan between the fan splitter and fan tip) and through the fan ID (defined as that portion of the fan between the centerline and the fan splitter). It was also assumed that the temperature of the fan discharge flow could be taken as time invarient (also, because of the low Mach number at fan discharge, total and static temperatures can be used interchangeably). To account for the presence of a core engine, and explore any possible attendant interaction with fan duct acoustics, a simple first order lag representation of the core engine was incorporated into the rumble model. The core engine was represented as a compressor delivering constant corrected air flow (corrected to compressor face conditions) into a lumped volume. Flow out of the volume exited through a choked turbine to emerge at station (3H). The resulting transfer function for the core engine is:

$$\frac{W'_{3H}}{P_C'} = \frac{1}{1 + \tau_{CORE} S}$$

(109)

Where:

W'_{3H} = mass flowrate at station (3H)

P'_C = static pressure at the compressor face

τ_{CORE} = core engine time constant

A default value of τ_{CORE} = 0.005 seconds is built into the rumble model. A different value can be input by the user, and is calculated as the mass of air in the core engine volume divided by the mass flowrate of air through the core engine. Proximity of the fan splitter to fan discharge also affects the boundary condition at the fan. Two cases were considered and are built into the rumble model. In the first case, called the "proximate" splitter configuration, the fan splitter is assumed to be so close to fan discharge that no communication can occur between the fan duct and the core engine across the fan splitter. For this case, the boundary condition at the fan becomes:

$$P'_C - W'_{3H} = 0$$
$$W_1' = \rho'_1 + V_1' = 0$$
$$T_1' = P_1' - \rho_1' = 0$$

(110)

74

In the second case, called the "remote" splitter configuration, the fan splitter is assumed to be sufficiently remote from fan discharge to allow perfect communication between the fan duct and the core engine across the fan splitter. For this case, the boundary condition at the fan becomes:

$$P'_C = P'_1$$

$$W'_1 = \rho'_1 + V'_1 = -\frac{P'_1}{BPR}$$

(111)

$$T'_1 = P'_1 - \rho'_1 = 0$$

$$W'_{sH} = \frac{P'_1}{1 + \tau_{CORE} S}$$

This completes the definition of the upstream boundary condition. It is of interest to note that entropy waves are created by sonic wave reflections at the upstream boundary. Since an entropy perturbation is $S'_1 = P'_1 - \gamma \rho'_1$, and at the boundary $\rho'_1 = P'_1$, then $S'_1 = (1 - \gamma) P'_1$. A similar argument will show that entropy waves are also created at the pressure drops (stations (2) and (3)). These are automatically accounted for in the rumble model, but are of minor importance compared to the entropy waves created in the combustion zone by combustion disturbances.

The downstream boundary condition is based upon the presence of a "short" nozzle just downstream of station (11), for which:

$$\frac{W \sqrt{T_o R}}{A P_o} = \phi (P_R)$$

(112)

where:

$$\phi = \frac{\left[\left(P_R^{\frac{\gamma-1}{\gamma}} - 1 \right) \left(\frac{2}{\gamma-1} \right) \right]^{\frac{1}{2}}}{P_R^{\frac{\gamma+1}{2\gamma}}}$$

$$P_R = P_o / \text{nozzle throat static pressure}$$

$$P_R \leq \left(\frac{\gamma+1}{2} \right)^{\frac{\gamma}{\gamma-1}}$$

When linearized, the downstream boundary condition becomes:

$$V_{11}' = \frac{1}{2} \quad (P_{11}' - \rho_{11}') + (KNOZ) P_{11}'$$

(113)

where:

$$KNOZ = \frac{\left[1 + \left(\frac{\gamma+1}{2} \right) \bar{M}_{11} \right] \left(\frac{P_R}{\phi} \frac{\partial \phi}{\partial P_R} \right)}{[1 - \bar{M}_{11}{}^2 (1+\gamma)] \left(\frac{P_R}{\phi} \frac{\partial \phi}{\partial P_R} \right)}$$

$$\frac{P_R}{\phi} \frac{\partial \phi}{\partial P_R} = \left[\frac{P_R{}^{\frac{\gamma-1}{\gamma}}}{2 \left(P_R{}^{\frac{\gamma-1}{\gamma}} - 1 \right)} - \frac{\gamma+1}{2 (\gamma-1)} \right] \left(\frac{\gamma-1}{\gamma} \right)$$

It is also of interest to note that for choked flow,

$$P_R \geq \left(\frac{\gamma+1}{2} \right)^{\frac{\gamma}{\gamma-1}},$$

then KNOZ = 0 and:

$$V_{11}' = \frac{1}{2}(P_{11}' - \rho_{11}') = \frac{1}{2} T_{11}' \tag{114}$$

substituting from equation (102):

$$V_{11}' = \frac{1}{2\gamma} S_{11}' + \frac{(\gamma-1)}{2\gamma} P_{11}' \tag{115}$$

This equation directly relates how entropy waves, as well as pressure disturbances, striking a choked nozzle will produce a velocity disturbance.

This completes the acoustic equation development. These equations describe the response of pressure, velocity and density throughout the augmentor to a disturbance in combustion. Development of the corresponding combustion equations, which describe how combustion throughout the augmentor will respond to disturbances in pressure, velocity and density, is presented in the following section.

c. Development of Combustion Equations

Development of the combustion equations for the V-gutter flameholder augmentor is presented first. Then the combustion equations for Vorbix and Swirl augmentors are presented.

For the V-gutter flameholder augmentor two combustion streams, the fan stream and the core stream, are treated. This is necessary to be able to account for the different combustion characteristics of the fan and core streams. The two streams can have different flameholder designs and fuel-air ratios as well as different flameholder approach temperatures and velocities, causing the two streams to have different efficiency vs. fuel-air ratio characteristics. In addition, the fan stream is preceded by a long fan duct which can exhibit lon-

grounded resonance at the low frequencies associated with rumble. The core stream is preceded by a short section terminating at turbine discharge, which is much less responsive at low frequencies.

The basic approach taken for the rumble model was to model combustion disturbances in the fan and core streams independently, accounting for the individual properties of each stream. The resulting two combustion disturbances (calculated as volumetric heat release rate disturbances) were then simply added to form a single overall disturbance. The overall disturbance was then distributed evenly over the total cross-sectional area of the augmentor, which was taken to consist of a single overall stream with mean mixed properties. This approach accounts for the different combustion characteristics of the fan and core streams, while avoiding the complexities associated with a rigorous treatment of the radial as well as the axial distribution of combustion throughout the augmentor.

Experience with modeling the combustion process as a plane heat addition with all combustion taking place in zero length, had shown that the resulting predictions of rumble were sensitive to the axial location chosen for the plane. Since combustion actually takes place over a distance of 30 to 60 inches, it was decided that the axially distributed nature of the burning should be accounted for. This was accomplished by dividing the combustion zone into a number of axial sections, each of length ℓ, as explained in part b, "Development of Acoustic Equations."

Combustion equations used in the rumble model are based upon an extension of empirical steady-state processes to the case of time variant flow. A schematic of the steady-state processes is shown in Figure 41. Consider first that the augmentor contains only the fan stream. An identical set of equations will exist for the parallel core stream. Following a particle of air as it moves through the augmentor, the following steps will occur:

- Particle of air picks up fuel as it crosses the spraybar.

- Particle drifts at through-flow velocity to the flameholder, station (4).

- Particle is ignited by the flameholder wake as it drifts from the flameholder, to the beginning of the combustion zone, station (5) (defined as the location where the bulk fluid temperature begins to rise sharply).

- Particle drifts and burns from station (5) to the end of the combustion zone, station (10) (defined as the location where bulk fluid temperature ceases its sharp rise).

It was determined (see equation (96)) that for a linear temperature gradient, the steady-state volumetric heat release rate in a section of length ℓ in the augmentor could be taken as independent of axial position. This implies that at steady state, a particle of fuel-air mixture drifting and burning through a section of the augmentor, has a volumetric heat release rate that is independent of axial position. The rate can be computed directly from the flowrate, ideal temperature rise, efficiency, and combustion zone volume of the augmentor.

$$q = \frac{C_p}{v} W T_i \eta \qquad (116)$$
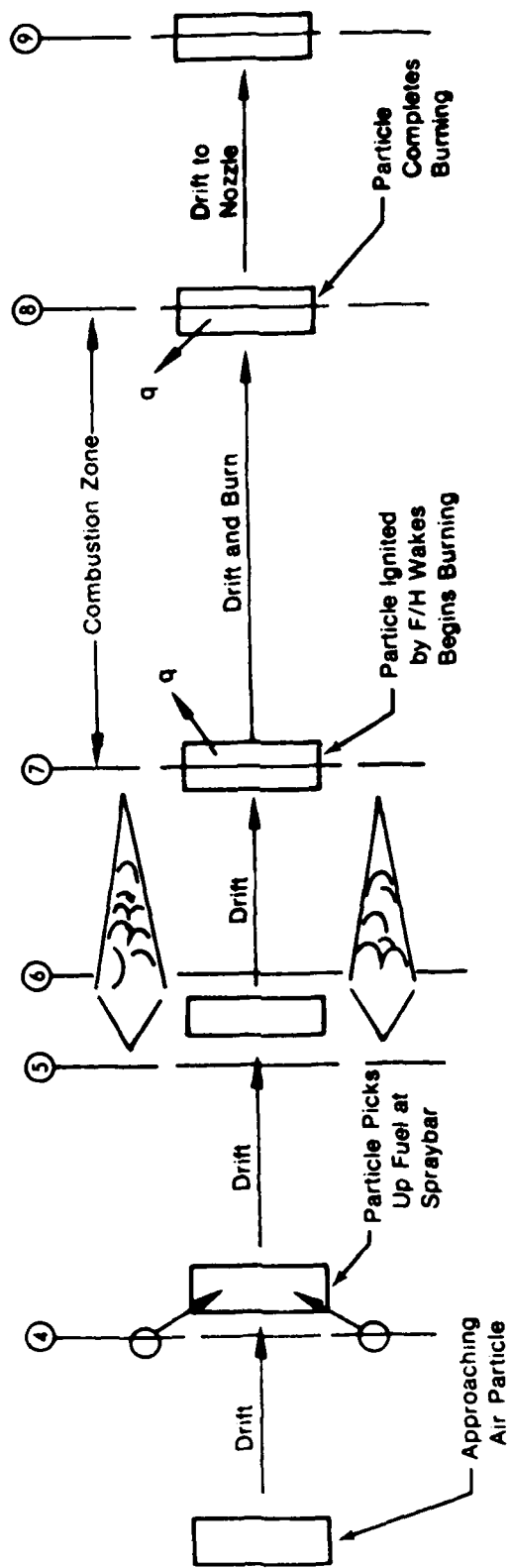
Figure 41. Steps in Augmentor Combustion Process

FD 1-4860

78

For small perturbations in operating parameters the quasi-steady treatment requires a period ... of relation between independent ... and process, and the relation ... is also used to compute the rate when W, T, and γ are subjected to instantaneous approach conditions. The resulting equation will model combustion as it will or behaves in a quasi-steady manner. The volumetric heat release rate at any position in the combustion zone will reach the steady state value corresponding to instantaneous conditions at the flameholder and at the spraybar after a delay. The delay is the time required to purge the old combustion gases and refill with new combustion gases traveling at through flow velocity.

For the fan stream, instantaneous approach conditions are taken to be the instantaneous conditions at station (3). Because of the large pressure drop in the fuel spraybar injector changes in fuel flow in response to augmentor pressure at the spraybar are small compared to changes in air flow. Consequently, fuel flow can be considered constant, and the fuel-air ratio of the particle as it crosses the spraybar is determined by changes in air flow only.

$$FA_{S/B} = \frac{\text{constant}}{W_a} \tag{117}$$

A period of time, τ_{DC}, is required for the particle to drift from the spraybar to the flameholder. Therefore, the fuel-air ratio of the particle when it reaches the flameholder can be expressed as:

$$FA_c(t) = FA_{S/B} (t - \tau_{DC}) \tag{118}$$

At the ignition plane (flameholder) the particle has a "potential" volumetric heat release rate of:

$$q_c = \frac{C_F}{v_c} W_a T_{ic} \eta_c \tag{119}$$

The ideal temperature rise is a function of the fuel-air ratio of the particle (effects of approach temperature and pressure are negligible). The efficiency is assumed to be a function of the fuel-air ratio and the approach pressure, temperature and velocity.

$$T_{ic} = fcn(FA_c) \tag{120}$$

$$\eta_c = Vfcn(FA_c, P_a, T_a, V_a) \tag{121}$$

The particle crossing the flameholder will begin burning after a time ℓ_4/∇_4, which is the time required to drift from Station (4) to (5) while being ignited. When it begins burning at Station (5), the heat release rate of the particle will be (X = 0 at Station (5)):

$$q(o,t) = q_c (t - \ell_4/\nabla_4) \tag{122}$$

At some station, X distance downstream of Station (5), the local heat release rate will become that of the particle after an additional time delay,

$$\tau_b = \int_0^x dx/\nabla(x),$$

79

which is the time required to drift from Station (5) a distance X at through-flow velocity $\bar{V}(X)$. Then, at a location X in the combustion zone, the heat release rate will be:

$$q(x,t) = q(o, t - \tau_E) \tag{123}$$

The linearized versions of equations (117) through (121), written in terms of the Laplace transform of the normalized variables are:

$$FA'_{s,B} = -W'_s$$

$$FA'_c = FA'_{s/B} \, e^{-\tau_{DC} S}$$

$$q'_c = W'_s + T'_I + \eta'$$

$$T'_{Ic} = \left[\frac{FA}{T_I}\frac{\partial T_I}{\partial FA}\right]_c FA'_c \tag{124}$$

$$\eta'_c = \left[\frac{FA}{\eta}\frac{\partial \eta}{\partial FA}\right] FA'_c + \left[\frac{P}{\eta}\frac{\partial \eta}{\partial P}\right]_c P'_s + \left[\frac{T}{\eta}\frac{\partial \eta}{\partial T}\right]_c T'_s + \left[\frac{V}{\eta}\frac{\partial \eta}{\partial V}\right]_c V'_s$$

solving for q'_c:

$$q'_c = \left[1 - \left\{\left[\frac{FA}{T_I}\frac{\partial T_I}{\partial FA}\right]_c + \left[\frac{FA}{\eta}\frac{\partial \eta}{\partial FA}\right]_c\right\} e^{-\tau_{DC} S}\right] W'_s$$

$$+ \left[\frac{P}{\eta}\frac{\partial \eta}{\partial P}\right]_c P'_s + \left[\frac{T}{\eta}\frac{\partial \eta}{\partial T}\right]_c T'_s + \left[\frac{V}{\eta}\frac{\partial \eta}{\partial V}\right]_c V'_s \tag{125}$$

A corresponding equation for the core stream can be directly written by changing subscript "C" to subscript "H", and changing the reference approach station from (3) to (3H).

$$q'_H = \left[1 - \left\{\left[\frac{FA}{T_I}\frac{\partial T_I}{\partial FA}\right]_H + \left[\frac{FA}{\eta}\frac{\partial \eta}{\partial FA}\right]_H\right\} e^{-\tau_{DH} S}\right] W'_{sH}$$

$$+ \left[\frac{P}{\eta}\frac{\partial \eta}{\partial P}\right]_H P'_{sH} + \left[\frac{T}{\eta}\frac{\partial \eta}{\partial T}\right]_H T'_{sH} + \left[\frac{V}{\eta}\frac{\partial \eta}{\partial V}\right]_H V'_{sH} \tag{126}$$

The total volumetric heat release rate (subscript "T") is formed by adding the heat release rates of the fan and core streams:

$$q_t v_T = Q_t = Q_C + Q_H = q_C v_C + q_H v_H \tag{127}$$

or, in normalized form:

$$q'_t = \left[\frac{Q_C}{Q_t}\right] q'_C + \left[\frac{Q_H}{Q_t}\right] q'_H \tag{128}$$

Equation (128) computes the instantaneous volumetric heat release rate of a particle of combined fan stream and core stream fuel-air mixture when the particle reaches the flameholder. The term "potential" is applied because the particle has not yet been ignited. The particle is ignited by the flameholder wake as it drifts a distance ℓ_4 at velocity V_4. The particle begins releasing the "potential" heat at Station (5), as defined by equation (122). To

... ... Gi... of the core stream has now been added to the augmentor (only the fan stream was originally being considered), so the total heat release of both streams is being treated equation (122) is rewritten as:

$$q(o,t) = q_t (t - \ell_4 / \nabla_4)$$ (129)

Linearized:

$$q'(o,t) = q_t (t - \ell_4 / \nabla_4)$$ (130)

Equation (130) simply adds a delay into the system which allows tailoring the axial location of the beginning of the combustion zone. For convenience in programming the equations, this delay is added to the drift delay in the combustion zone (τ_E) to form an overall particle drift delay from the flameholder.

$$\tau_Q = \ell_4 / \nabla_4 + \tau_E$$ (131)

The particle then releases heat throughout the combustion zone as defined by equation (123), the linearized version of which is:

$$q'(x,t) = q'(o, t - \tau_E)$$ (132)

This equation represents the augmentor heat release based on steady-state conditions. To accurately model the combustion process in the augmentor, the dynamics of the flameholder wake must be included. These dynamics were incorporated in the heat release term as a first order lag:

$$q_{out/dynamic} = \frac{q_{out/steady\text{-}state}}{1 + \tau S}$$ (133)

The dynamics involved in calculating the flameholder wake time constant τ are discussed in Section II.B-2.

Equation (131) was presented in part b, (Development of Acoustic Equations), and used to evaluate integrals in equation (93). The combustion equations require that the following information about the steady-state operating point:

$$\left[\frac{Q_C}{Q_t} \right], \left[\frac{Q_H}{Q_t} \right], \left[\frac{FA}{T_i} \frac{\partial T_i}{\partial FA} \right]_{C,H}, \left[\frac{FA}{\eta} \frac{\partial \eta}{\partial FA} \right]_{C,H},$$

$$\left[\frac{P}{\eta} \frac{\partial \eta}{\partial P} \right]_{C,H}, \left[\frac{T}{\eta} \frac{\partial \eta}{\partial T} \right]_{C,H}, \text{ and } \left[\frac{V}{\eta} \frac{\partial \eta}{\partial V} \right]_{C,H}$$

The heat release rate ratios Q_C/Q_T and Q_H/Q_T are computed in the program from conditions known about each augmentor stream:

$$\frac{Q_C}{Q_t} = \frac{(BPR \, T_{ic} \, \eta_C)}{(BPR \, T_{ic} \, \eta_C) + (T_{iH} \, \eta_H)}$$

  (134)

$$\frac{Q_H}{Q_t} = \frac{(T_{iH} \, \eta_H)}{(BPR \, T_{ic} \, \eta_C) + (T_{iH} \, \eta_H)}$$

81

The partial derivative terms $\left[\dfrac{FA}{T_i}\dfrac{\partial T_i}{\partial FA}\right]_{C.H}$ are computed in the program from a

subroutine curvefit of the ideal temperature rise curve. A graphical definition of the term is supplied in Figure 42. The partial derivative terms involving efficiency are computed in the Flameholder Combustion Model and supplied directly to the rumble model. Alternately, they may be computed from empirical data and be input by the user. The graphical definition of terms is similar to that of Figure 42.
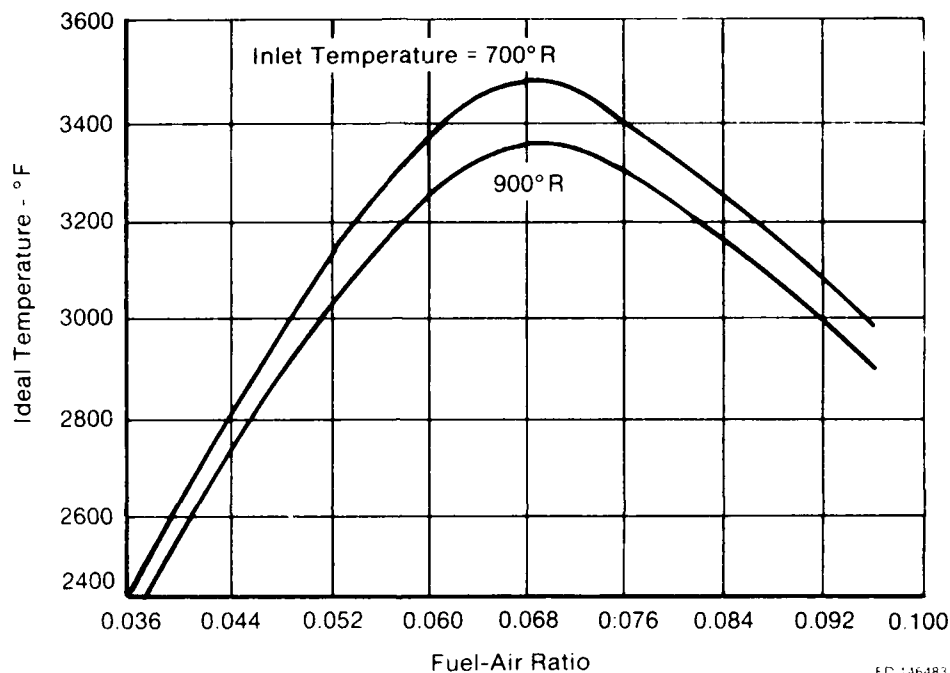
Figure 42. Ideal Temperature Rise for Constant Pressure Combustion of Hydrocarbon Fuels

This completes the combustion equation development for the V-gutter flameholder model. All of the above equations apply to the Vorbix and Swirl augmentors except as noted below.

For the Vorbix and Swirl augmentors, independent heat release rates for the fan and core streams cannot be identified because of the flow mixing. In addition, the effects of pilot fuel-air ratio on augmentor combustion efficiency must be accounted for. Equation (119) is again applied, but on an overall basis only.

$$q_t \doteq \frac{Cp}{v} W_4 T_1 \eta \tag{135}$$

The overall fuel-air ratio is computed from total mixed air flow at station (4).

$$FA = \frac{constant}{W_4} \tag{136}$$

82

The overall ideal temperature rise is a function of overall fuel-air ratio. The efficiency is assumed to be a function of overall fuel-air ratio, pilot fuel-air ratio and pressure at station (4)

$$T_i = fch(FA) \tag{137}$$

$$\eta = fch(FA, FAP, P_4) \tag{138}$$

Then for the Vorbix and Swirl augmentors, the instantaneous "potential" volumetric heat release rate of a particle of mixture when the particle reaches station (4) is:

$$q_t = \left[1 - \left[\frac{FA}{T_i} \frac{\partial T_i}{\partial FA} \right] - \left[\frac{FA}{\eta} \frac{\partial \eta}{\partial FA} \right] \right] W_4$$

$$+ \left[\frac{FAP}{\eta} \frac{\partial \eta}{\partial FAP} \right] FAP' + \left[\frac{P}{\eta} \frac{\partial \eta}{\partial P} \right] P_4' \tag{139}$$

Equation (139) applies to both the Vorbix and Swirl augmentors, and is equivalent to equation (128) for the V-gutter augmentor. The Vorbix and Swirl augmentors differ in pilot location. The Swirl has the pilot at fan duct exit, so that airflow through the Swirl pilot is proportional to fan duct exit flow, W_3. The vorbix has the pilot near midspan, radially, and slightly aft of Stations (3) and (3H), so that airflow through the Vorbix pilot is proportional to total flow. W_4. Then, since fuel flow into both pilots is constant:

$$\text{Swirl:} \quad FAP' = - W_3' \tag{140}$$
$$\text{Vorbix:} \quad FAP' = - W_4'$$

For convenience in programming, W_4 can be replaced by:

$$W_4 = W_3 + W_{3H}$$

$$W_4 = \left[\frac{BPR}{1 + BPR} \right] W_3 + \left[\frac{1}{1 + BPR} \right] W_{3H} \tag{141}$$

Substituting (109) and (110) into (108):

$$\text{Swirl:} \quad q_t = \left\{ \left(1 - \left[\frac{FA}{T_i} \frac{\partial T_i}{\partial FA} \right] - \left[\frac{FA}{\eta} \frac{\partial \eta}{\partial FA} \right] \right) \left(\frac{BPR}{1 + BPR} \right) - \left(\frac{FAP}{\eta} \frac{\partial \eta}{\partial FAP} \right) \right\} W_3$$

$$+ \left\{ \left(1 - \left[\frac{FA}{T_i} \frac{\partial T_i}{\partial FA} \right] - \left[\frac{FA}{\eta} \frac{\partial \eta}{\partial FA} \right] \right) \left(\frac{1}{1 + BPR} \right) \right\} W_{3H}$$

$$+ \left[\frac{P}{\eta} \frac{\partial \eta}{\partial P} \right] P_4' \tag{142}$$

$$\text{Vorbix:} \quad q_t = \left\{ \left(1 - \left[\frac{FA}{T_i} \frac{\partial T_i}{\partial FA} \right] - \left[\frac{FA}{\eta} \frac{\partial \eta}{\partial FA} \right] - \left[\frac{FAP}{\eta} \frac{\partial \eta}{\partial FAP} \right] \right) \left(\frac{BPR}{1 + BPR} \right) \right\} W_3$$

$$+ \left\{ \left(1 - \left[\frac{FA}{T_i} \frac{\partial T_i}{\partial FA} \right] - \left[\frac{FA}{\eta} \frac{\partial \eta}{\partial FA} \right] - \left[\frac{FAP}{\eta} \frac{\partial \eta}{\partial FAP} \right] \right) \left(\frac{1}{1 + BPR} \right) \right\} W_{3H}$$

$$+ \left[\frac{P}{\eta} \frac{\partial \eta}{\partial P} \right] P_4' \tag{143}$$

83

Equations (142) and (143) replace equation (128). All other combustion equations are identical to those developed for the V-gutter flameholder augmentor. The partial derivatives in equations (142) and (143) must be computed from empirical data and be input by the user.

This completes development of the combustion equations. For the solution technique, based upon applying the Nyquist criterion to the open loop transfer function (OLTF), the OLTF is formed by renaming q_t' to q'_{IN} in equation (130) and by renaming q_t' to q'_{OUT} in equations (128), (142), and (143).

d. Phase I Results

Phase I of this program addressed the areas within the current model which had shown the need for improvement. In the systems dynamics portion of the model these areas included:

- The effect of liquid fuel droplet dynamics in the spraybar-to-flameholder region.

- The modification of the model to account for different combustion characteristics in the fan and core streams.

- The addition of a first order lag on the heat release rate due to flameholder wake dynamics.

These modifications and their impact on the output of the rumble model are discussed in this section.

(1) Liquid Fuel Droplet Dynamics in Spraybar-to-Flameholder Region

The rumble model, as developed ur   the Lo-Frequency Augmentor Instability Investigation, predicted the first mode of rumble at higher frequencies than experienced during the FSER tests. Also, a second or third mode of rumble was predicted that was not observed during the FSER tests (Figure 43). One possible explanation is that there is a lag in the heat release rate (Q out) that is not accounted for in the model. The model assumes gaseous fuel particles that move in phase with the air flow between the spraybars and the flameholders. In fact, liquid particles exist in this region and should exhibit a lag in directional change which would cause a lag in the heat release rate. During the Lo-Frequency Augmentor Instability Investigation a lag was incorporated on the heat release rate (Q out) to verify the assumption. The rumble model was exercised at several altitude test points with lags ranging from 0.001 to 0.008 sec. A lag of 0.003 sec indicated best agreement with test results. Figure 44 presents the same test point as presented in Figure 43 with a 0.003 sec lag on the heat release rate. The second and third rumble modes are not predicted and the first mode of rumble at 52 Hz is in perfect agreement with FSER test results.
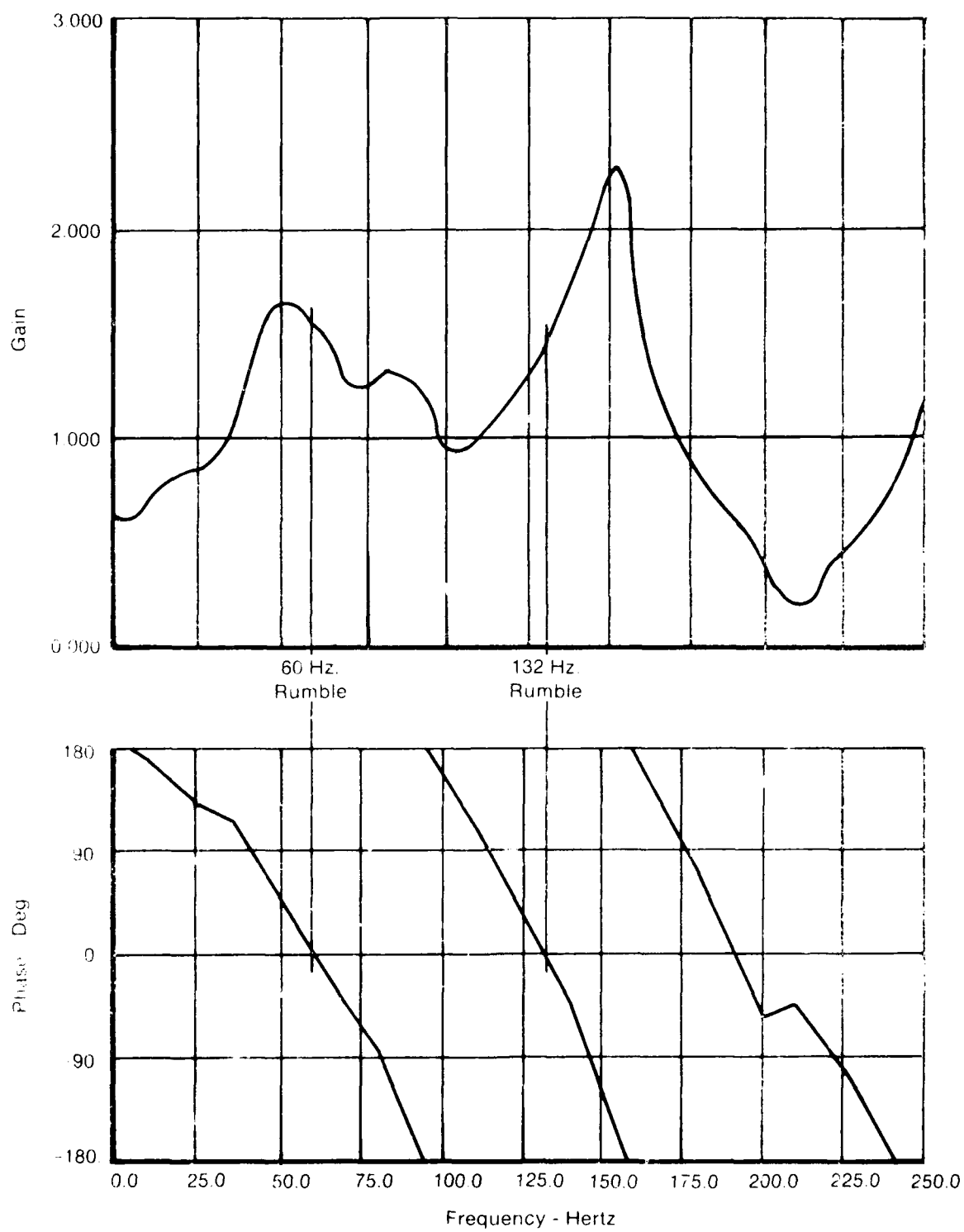
Figure 43. Original Rumble Model Output. Rumble at 60 Hz and 132 Hz.
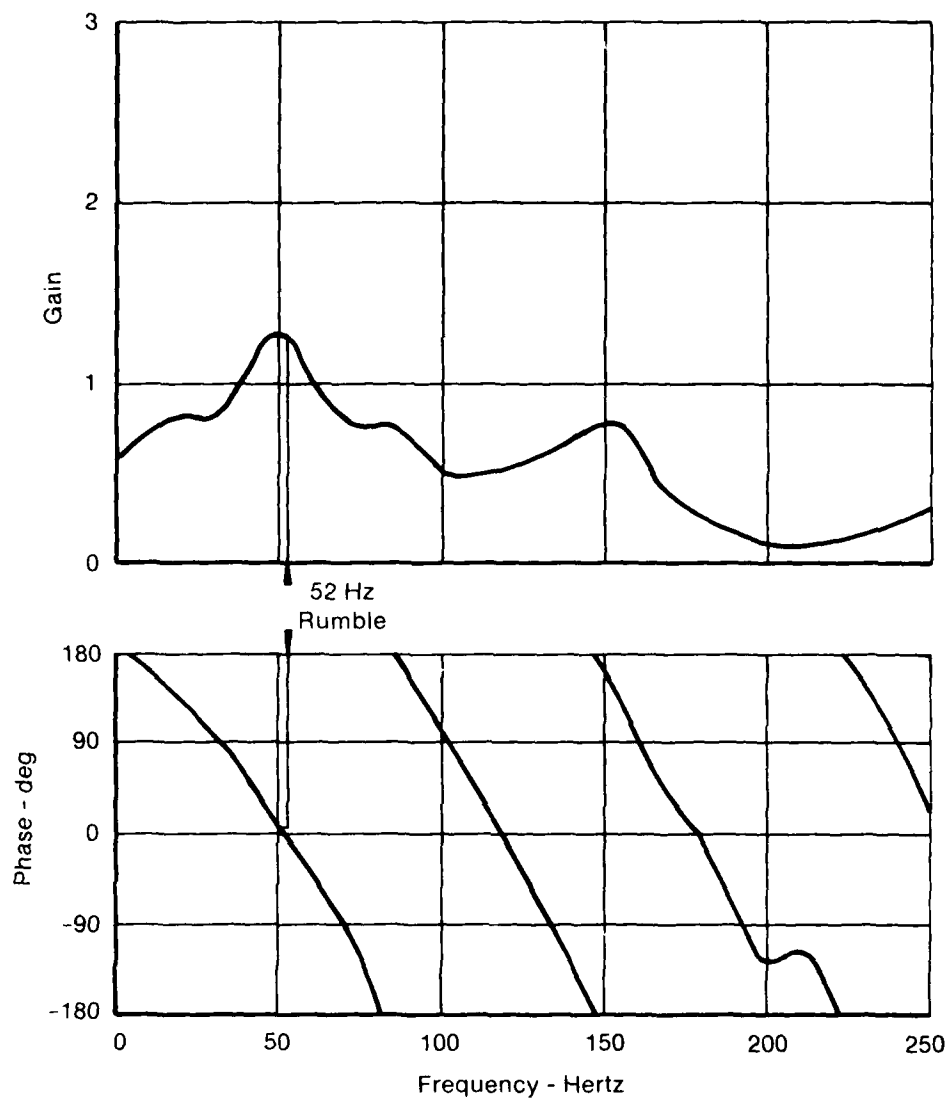
Figure 44. Original Rumble Model With 0.003 sec Lag on Q_{out}. Rumble at 52 Hz.

FD 141410

86

During Phase I of this contract, an analytical investigation was conducted into the physics of the liquid fuel particle dynamics in the spraybar/flameholder region. The augmentor fuel system model was used to predict liquid fuel particle sizes for various augmentor/flight conditions. The droplet dynamics were modeled by applying the equation $F = ma$, where F is the drag force on the droplet, m is the mass of the droplet and a is the acceleration of the droplet. This results in a first order differential equation for the velocity of the fuel droplet:

$$\frac{dV_f}{dt} + \frac{1}{\tau_d} V_f = \frac{1}{\tau_d} V_a, \tag{144}$$

where V_f is the fuel droplet velocity, V_a is the velocity of the airstream, and τd is the fuel droplet time constant which is a function of the droplet diameter and the drag coefficient, $\tau d = f (d, C_D)$. In the frequency domain, using normalized variables

$$\left[\; (\;)' \quad \frac{\Delta (\;)}{(\;)} \right] \; . \tag{145}$$

the fuel droplet velocity is given by:

$$V_f = \frac{V_a'}{1 + \tau_d S} \; . \tag{146}$$

The fuel air ratio is given by:

$$FA = \frac{W_f}{W_a} \tag{147}$$

where W_f and W_a are the fuel flow rate and air flow rate, respectively. Linearized, this becomes $FA' = W_f' - W_a'$ where

$$W'_f = 0_f + V_f' + 0' \text{ and } W_a' = \rho_a' + V_a' + {}'0 \tag{148}$$

and ρ_f and ρ_a are the fuel and air densities.

Making these substitutions, the equation for the fuel-air ratio becomes:

$$FA' = \frac{V_a'}{1 + \tau_d S} - \rho_a' - V_a' \text{ or } FA' = \frac{- \tau_d S}{1 + \tau_d S} V_a' - \rho_a' \tag{149}$$

This is the equation that was added to the rumble model.

In the original model, fuel flow was assumed constant and the change in fuel-air was given by $FA' = - V_a' - \rho_a'$.

The effect of droplet dynamics is to modify the effect in air velocity by the term

$$\frac{\tau_d S}{1 + \tau_d S} \tag{150}$$

Physically, this term is a high pass filter and attenuates frequencies below

$$\frac{1}{2\pi\tau_d} \tag{151}$$

87

Results of the rumble model with the addition of fuel droplet dynamics (τ_d = 0.0053 sec) are shown in Figure 45. Instabilities occur at 75 Hz, 147 Hz and 232 Hz, which do not agree with engine data. The combustion lag shown in the figure acts as a low pass filter. Therefore, the addition of fuel droplet dynamics, which acts as a high pass filter, was not expected to give results in agreement with test data. The effect of adding both fuel droplet dynamics and the 0.003 sec combustion lag was also evaluated. Figure 46 shows that this combination is stable.

These results indicate that the model, with the addition of fuel droplet dynamics, does not agree with engine test data. Therefore, fuel droplet dynamics can be eliminated as a critical factor in the prediction of rumble.

(2)   Account for Different Combustion Characteristics in the Fan and Core Streams

When the rumble model was extended to account for the fan and core stream of a turbofan engine, certain assumptions were made to simplify the wave equations. One of these assumptions was that downstream of the flameholder, the fan and core streams are mixed and come to a common temperature at Station 4 (Figure 47). The temperature gradient was assumed to be linear throughout the augmentor. The overall heat release of the combined fan and core streams was assumed to begin at Station 5 and end at Station 10.

During Phase I of this contract, the rumble model was extended to account for the fact that the fan stream and core stream have different axial temperature profiles. Figure 48 shows typical augmentor temperature profiles for various augmentor fuel/air ratios. Since it is required in the rumble model that the temperature rise is linear between two sections in the augmentor, the actual temperature profile had to be modified. The temperature profile was broken up into a series of linear gradients which approximated the actual temperature profile. It was found that a profile formed by combining a core stream temperature rise occurring over the first three sections of the augmentor and a fan stream temperature rise occurring over the last four sections gave the best approximation. Figure 49 shows the individual fan and core stream temperature profiles used in the rumble model, and Figure 50 shows the combined profile. This improved temperature profile reflects the different combustion characteristics of the fan and core streams.

Data from FX217-18 engine tests at AEDC were used to verify model changes. The flight point and flameholder design selected were 0.8/30K and Frithorn flameholder (Run 70/1100). Engine data indicated that this was a stable operating point.

The original rumble model (see AFAPL-TR-78-82) and the rumble model with the improved augmentor temperature profile were both run using FX217-18 data from Run 70/1100 at 0.8/39K. The combustion model was executed using a single streamtube analysis to generate input for the rumble model. Figure 51 gives the output of the original rumble model. An instability is predicted at 57 Hz. Engine test data indicates stable operation at this point so the prediction of the original rumble model is incorrect.

The output of the rumble model with the improved augmentor temperature profile is shown in Figure 52.

The plot indicates an instability at 60 Hz. This is not in agreement with test data. However, since this improved temperature profile is a better model of the actual combustion process, it was incorporated into the model as a permanent change.
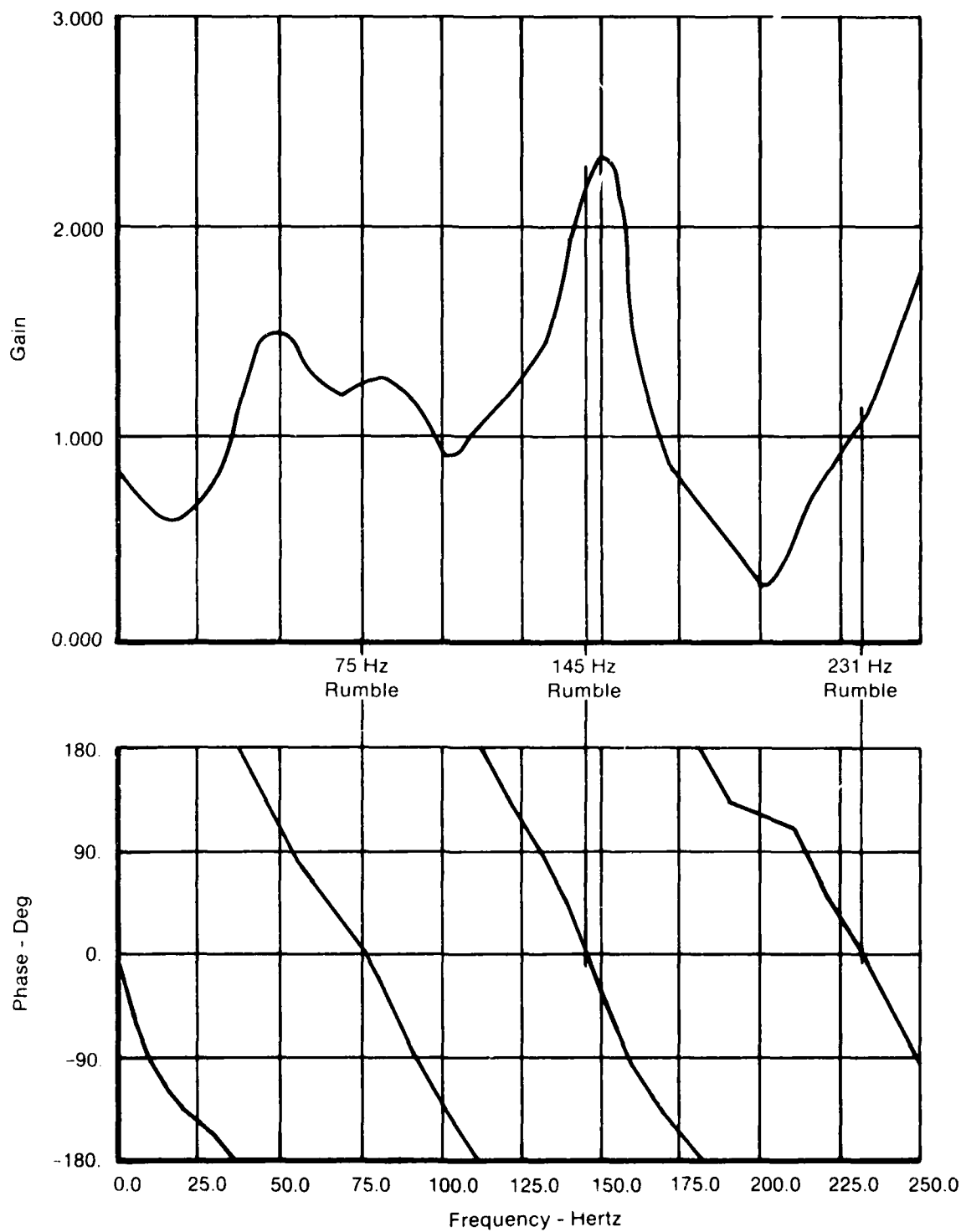
Figure 45. Rumble Model Output With the Addition of Fuel Droplet Dynamics ($\tau_d = 0.0053$)
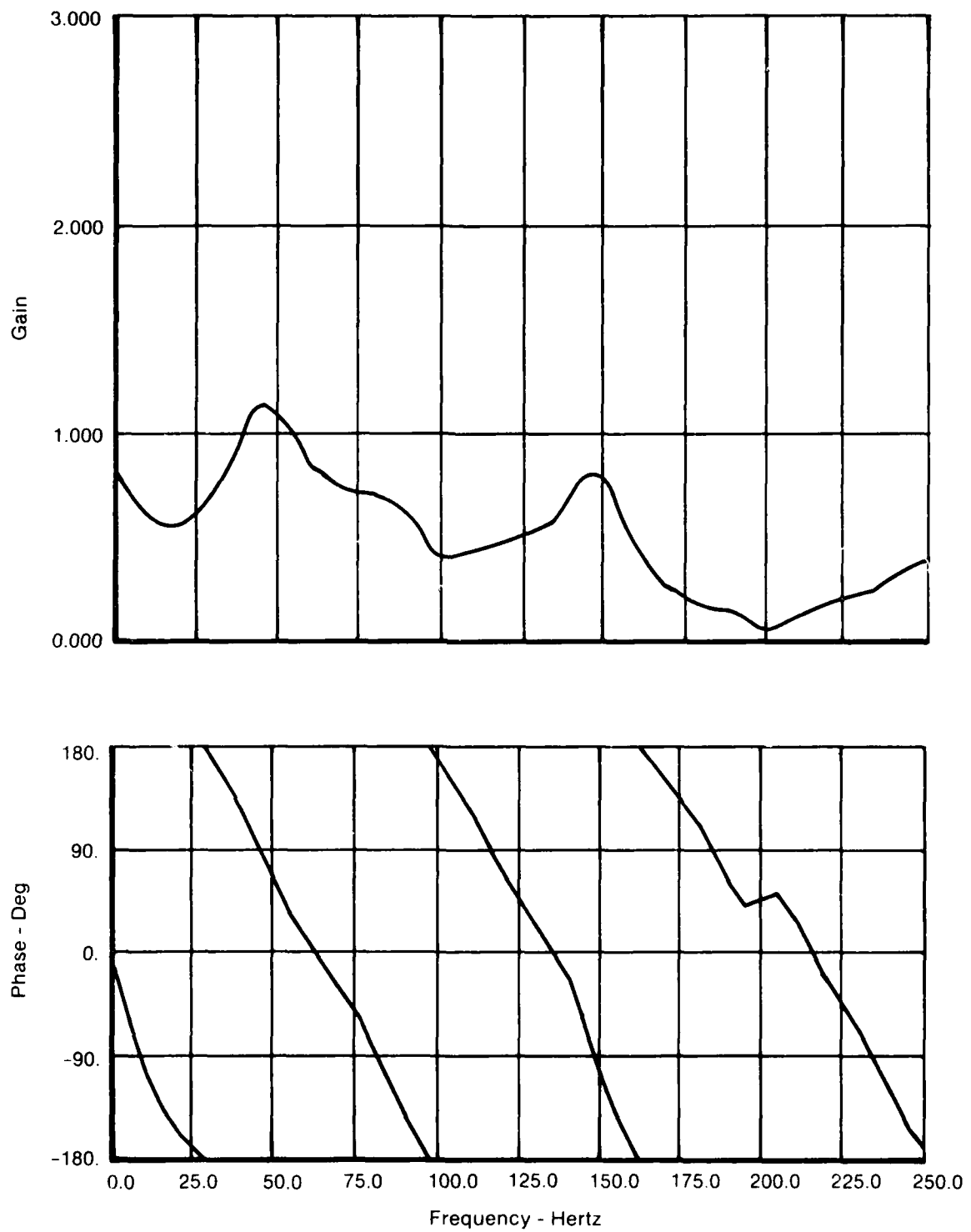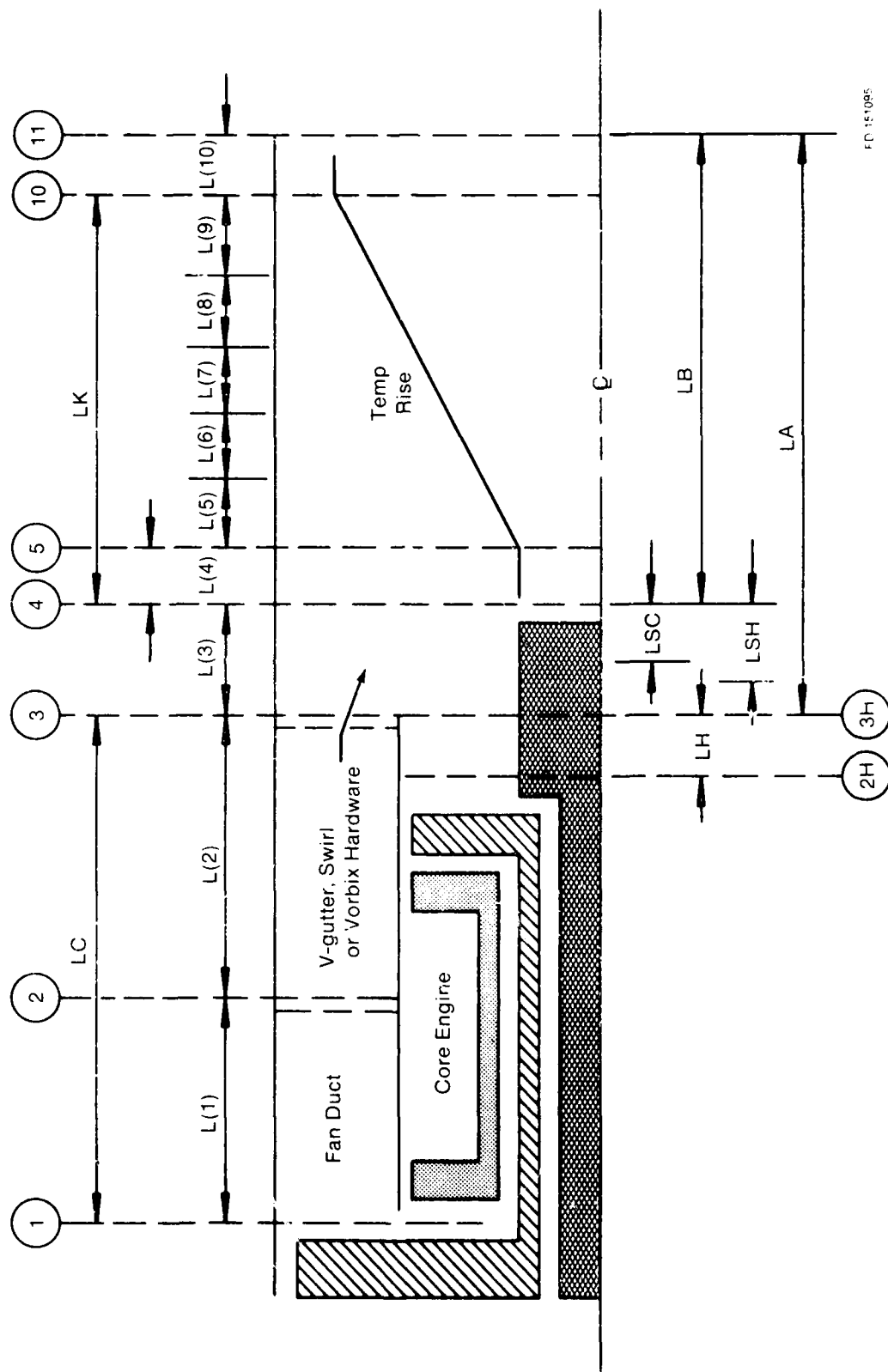
FD 230868

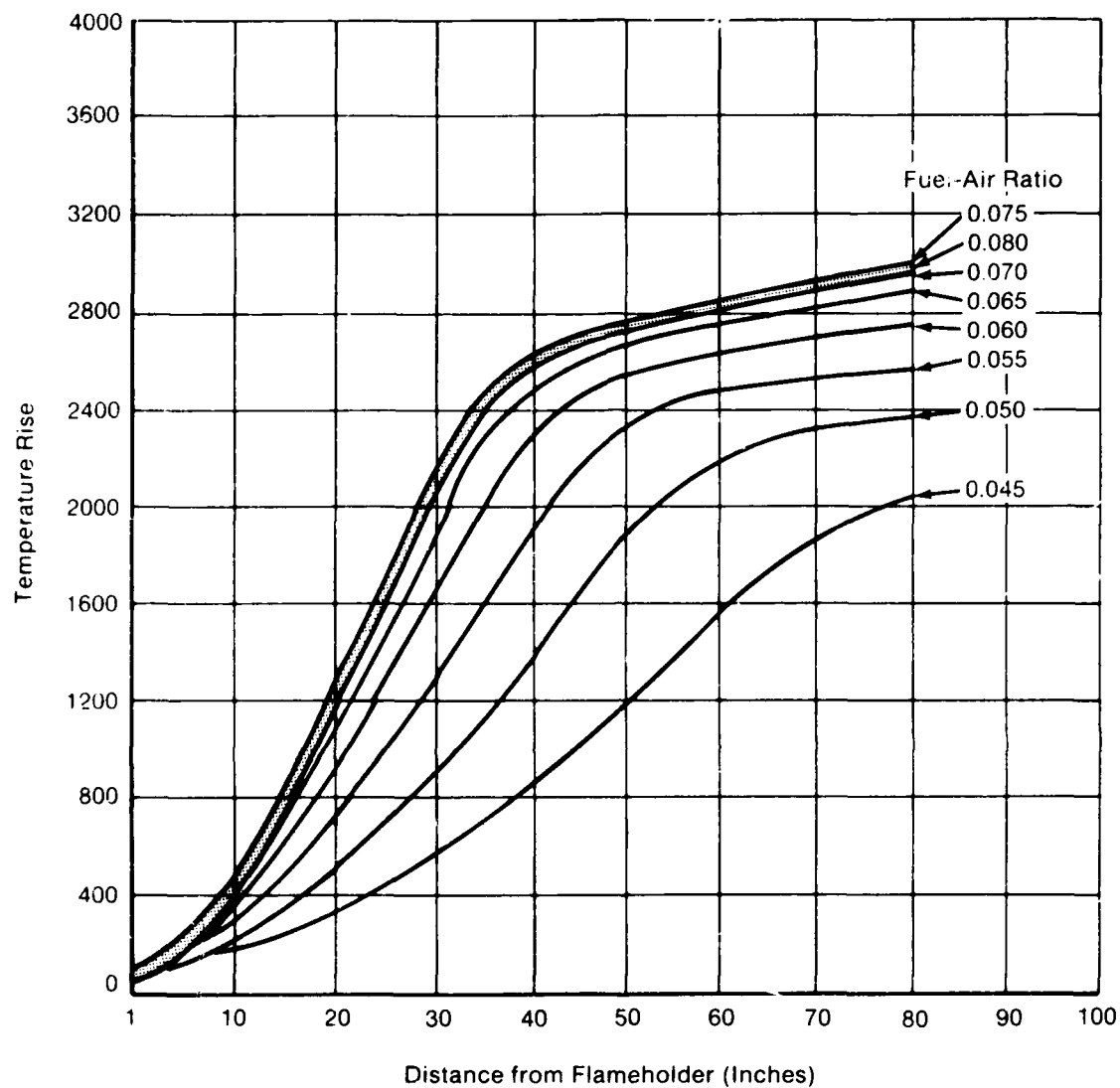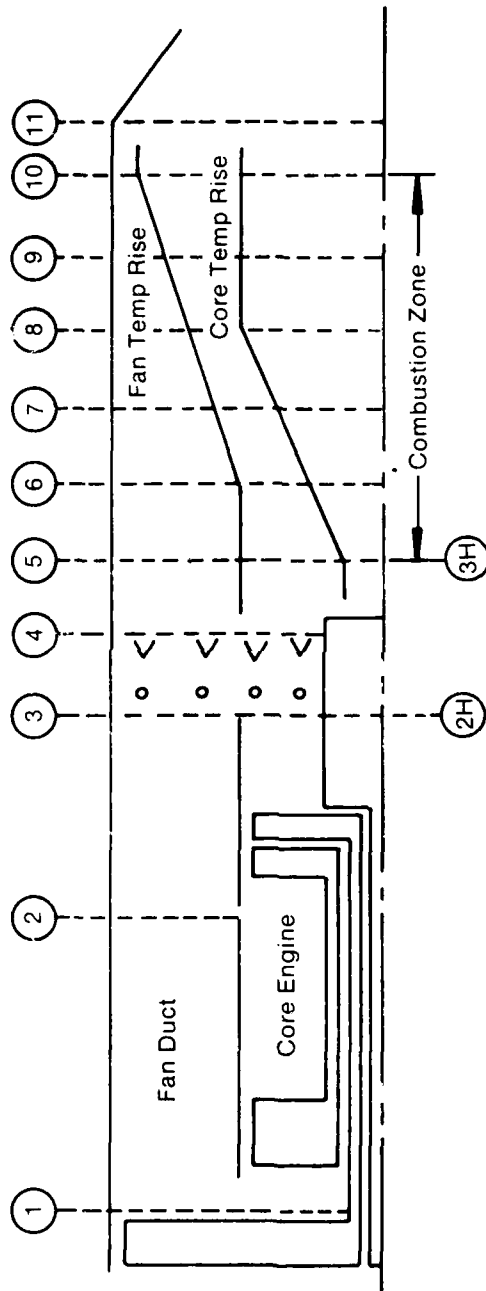*Figure 46. Rumble Model Output With Fuel Droplet Dynamics (τ_d = 0.0053) and 0.003 sec Lag on Q_{out}*

Figure 47. Original Model of Augmentor Temperature Rise

91

Figure 48. *Typical Combustion Temperature Profiles*

FD 151432

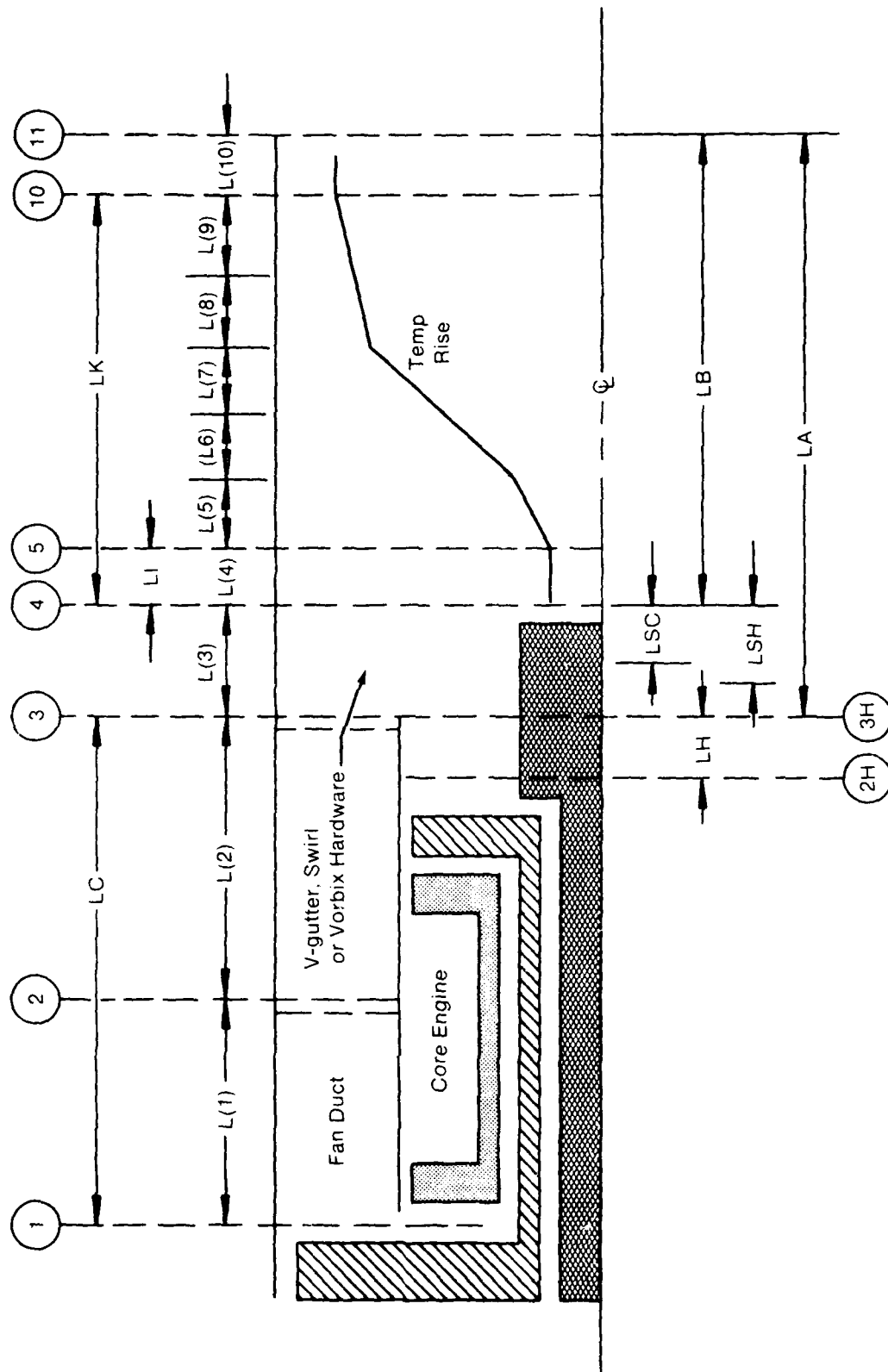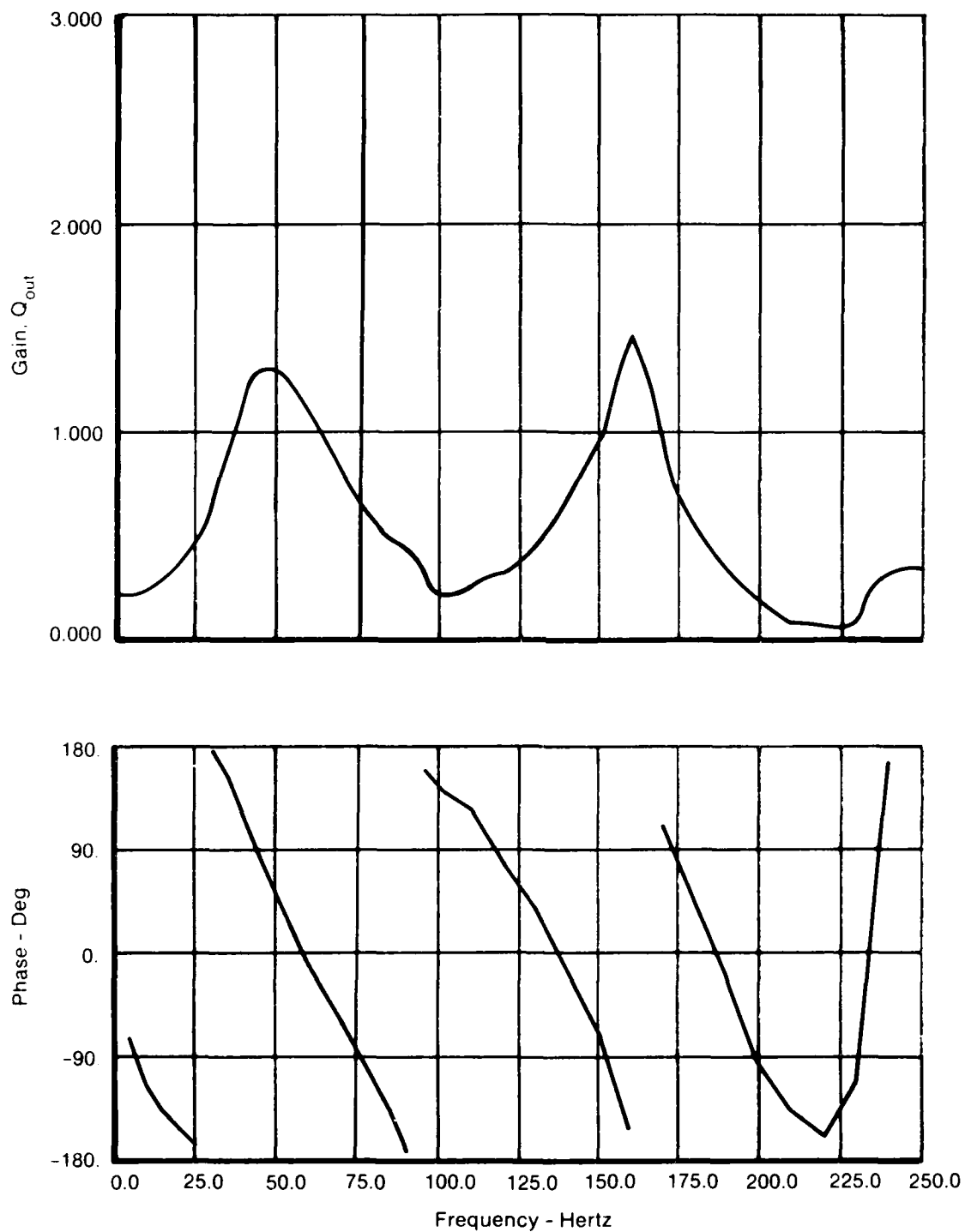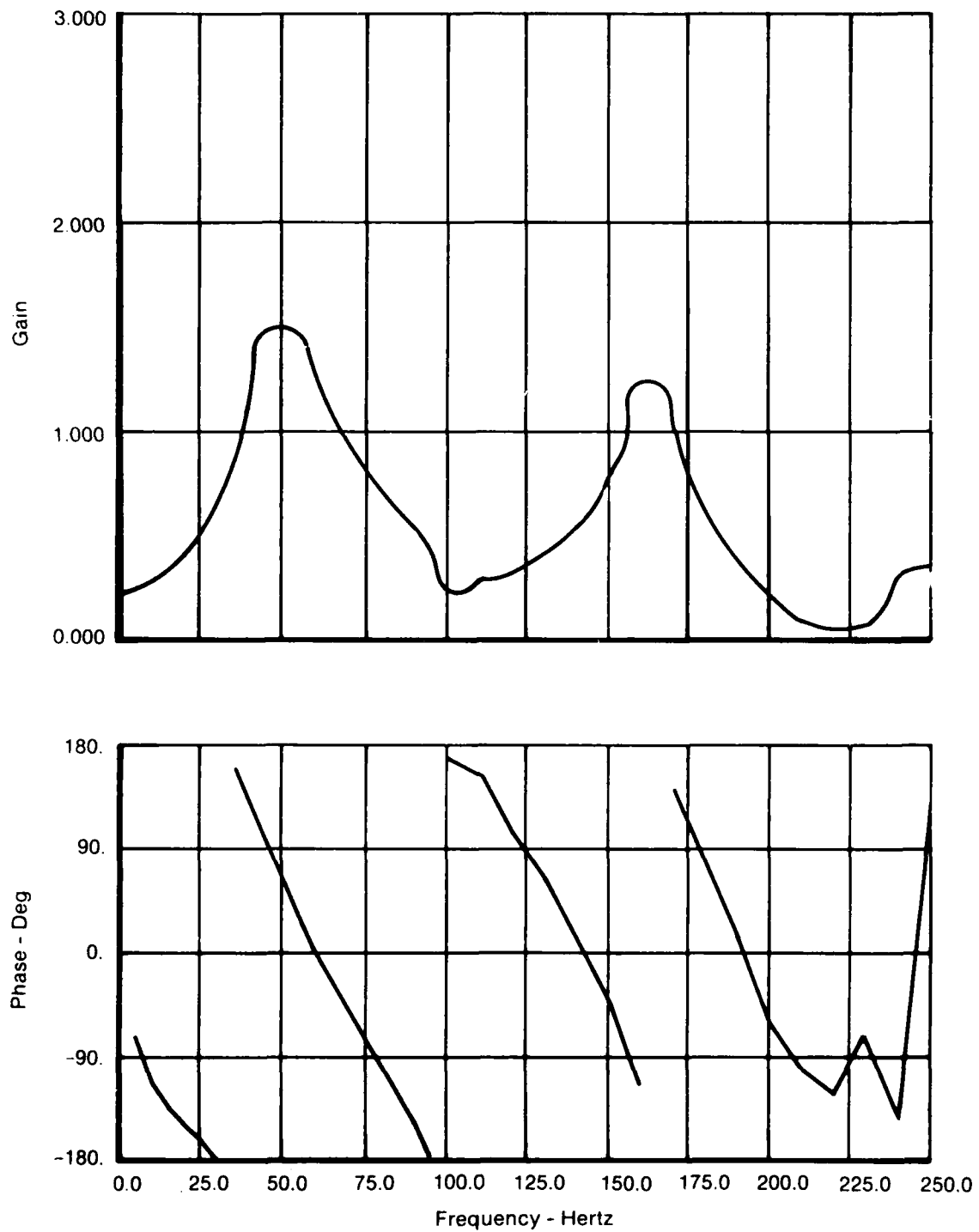*Figure 49. Individual Fan and Core Stream Temperature Rise*

FD 170204

93

Figure 50. Improved Model of Augmentor Temperature Rise

94

FD 230870

*Figure 51. Original Rumble Model. Frithorn Flameholder, Single Stream-
tube Analysis, 0.8/39K*

95

Figure 52. Rumble Model With Improved Augmentor Temperature Profile. Frithorn Flameholder, Single Streamtube Analysis, 0.8/39K

FD 230871

(3) Lag on Heat Release Rate (Q_{out})

Since the addition of fuel droplet dynamics in the spraybar-to-flameholder region did not result in the appropriate lag on the heat release rate, another source of this lag was sought. It was found that there is a lag associated with the dynamics of the flameholder wake region. The dynamics involved in the calculation of this flameholder wake time constant are discussed in detail in Section II.B-2. This lag was incorporated into the rumble model as a single first order lag on the total (duct plus core) heat release rate based on steady-state conditions:

$$Q_{out\ dynamic} = \frac{Q_{out\ steady\ state}}{1 + \tau S} \tag{152}$$

Where τ is the flameholder wake time constant.

The individual time constants for each streamtube in the duct and core streams were averaged to give a single overall time constant. Typical values of this time constant are 0.003 to 0.005 sec.

Figure 53 shows the output of the rumble model for the Frithorn flameholder at 0.8/39K with the addition of the improved augmentor temperature gradient and the lag on the heat release rate. Again, the combustion model was run using a single streamtube analysis. The flameholder wake time constant calculated for this case is 0.005 sec. The frequency has shifted to lower values and the gain at the high frequencies has been reduced. These are the expected results of the addition of a first order lag on the heat release rate. The output indicates that this is a stable condition which agrees with engine test data.

e. Refined Model Evaluation

Phase II of the current program concentrated on comparison of the refined rumble model with available engine test data taken on the F100(3). These data were measured at the AEDC test cells on engine FX217-18 with two different flameholder configurations, identified as F100(3) Bill of Material and a revised design called "Frithorn." The Phase I results presented the refined rumble model output at a flight point of 0.8 Mach number and 39,000 ft altitude (0.8/39K), using a single fan and single core streamtube. The Phase II results utilize multiple streamtubes to evaluate fuel-air ratio distribution. Combinations of 0.8/39K and 0.8/45K flight points and the two flameholder configurations were evaluated.

(1) Multistreamtube Analysis

The combustion model was executed using a multistreamtube analysis in the core and duct for the Frithorn flameholder at the flight point 0.8/39K. This analysis allowed the user to model the radial and circumferential variations in geometry and aerodynamics. The analysis consisted of 48 fan duct streamtubes and 64 core streamtubes. The results of the improved rumble model using the multistreamtube combustion model output are shown in Figure 54. The model indicates that this is a stable operating point which agrees with test data. The gain in the heat release rate is slightly lower than the gain calculated using a single streamtube combustion model. Since the fuel-air ratios vary significantly in any engine, it is recommended that the multistreamtube analysis be used.
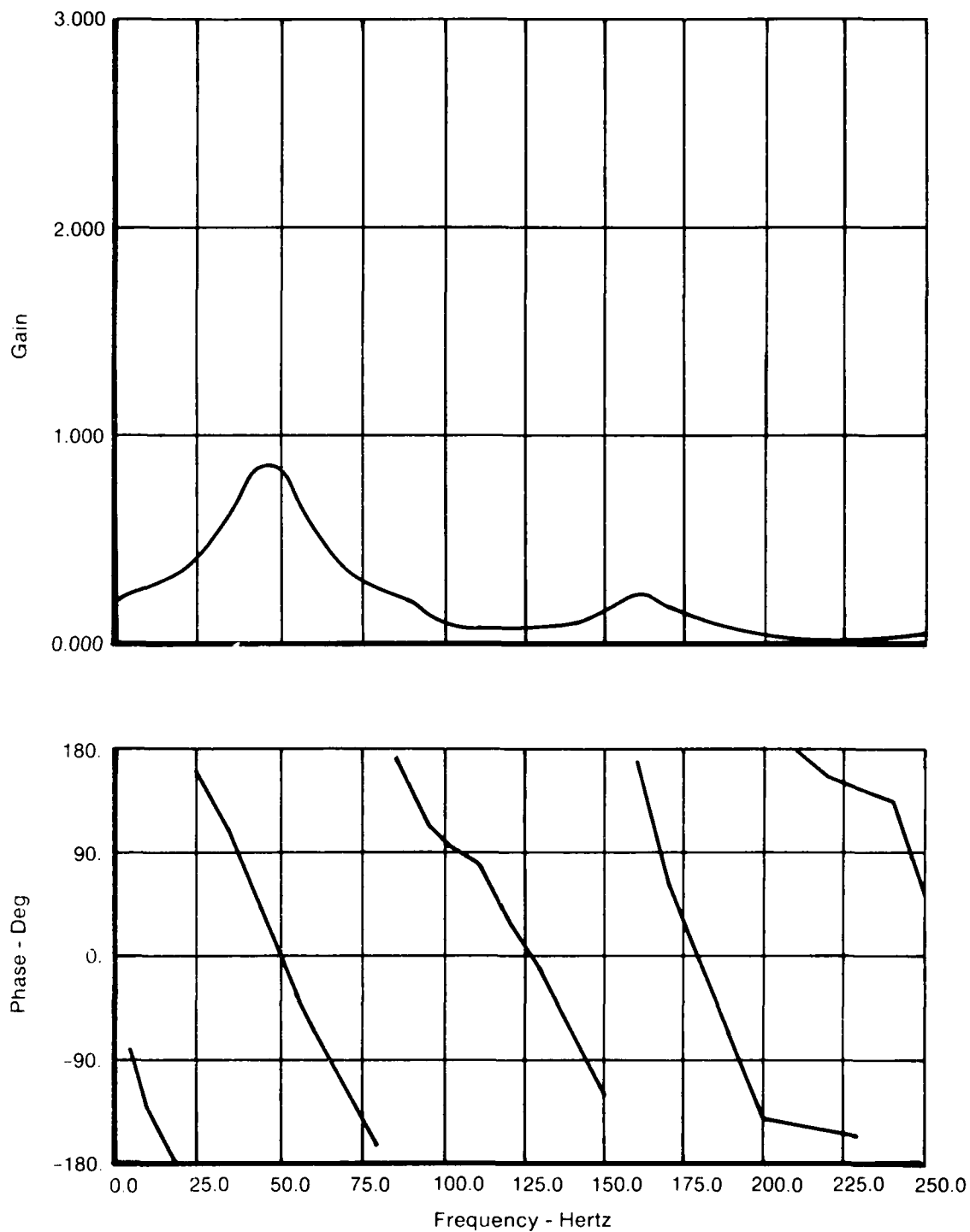
Figure 53. *Rumble Model With Improved Augmentor Temperature Gra-*
dient and Lag on Q_{out} *— Frithorn Flameholder, 0.8/39K, Single*
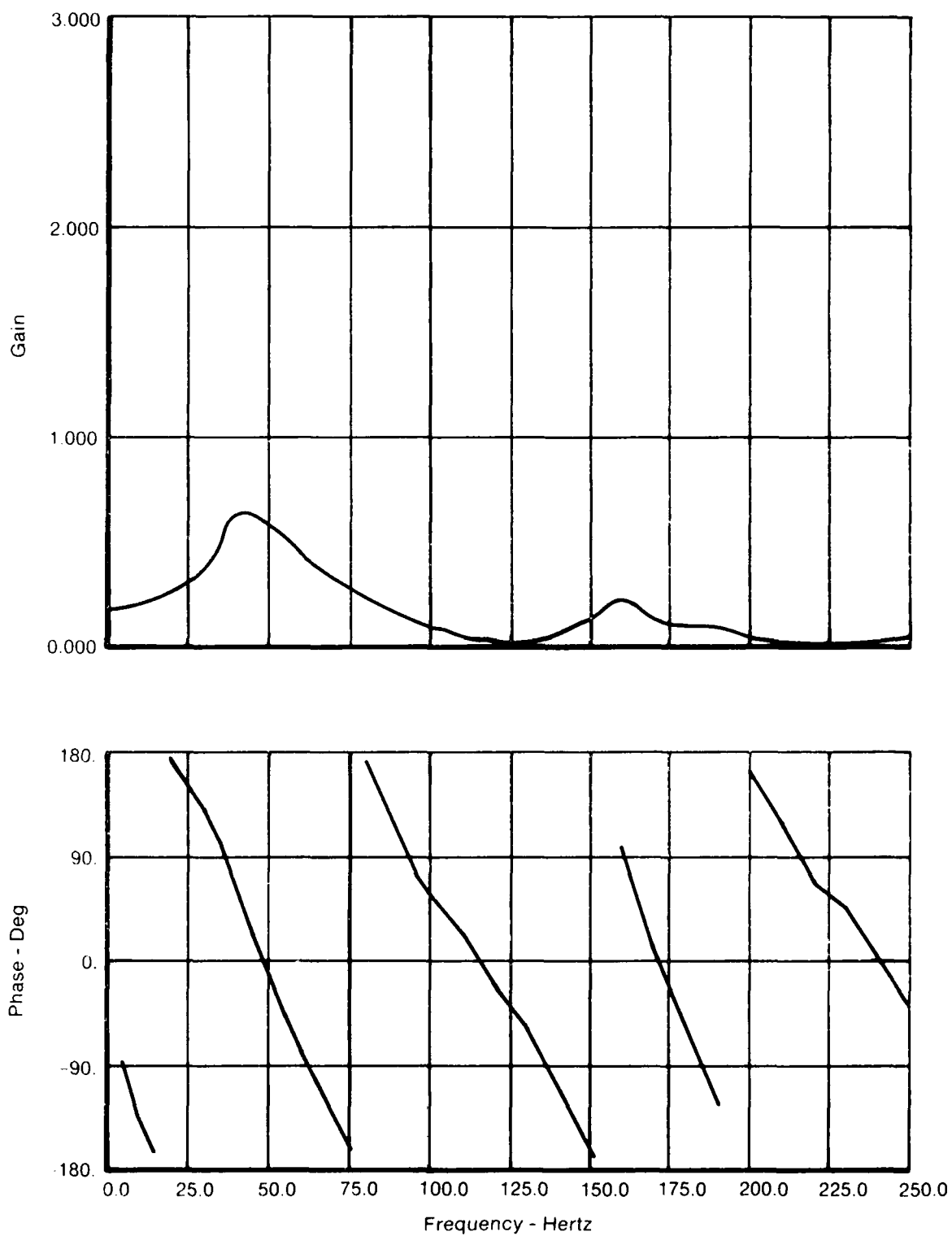*Streamtube Analysis*

FD 230872

Figure 54. *Rumble Model With Improved Augmentor Temperature Gradient and Lag on Q_{out} — Frithorn Flameholder, 0.8/39K, Multistreamtube Analysis*

FD 230873

99

(2) Analysis of Additional Data

For further verification the model was executed using data from various other combinations of flameholder/flight conditions.

Using a multistreamtube combustion analysis, the model predicted rumble at 48 Hz for the Frithorn flameholder at 0.8/45K (see Figure 55). FX217-18 engine data indicated a rumble blowout at 0.8/41K (Figure 56). The spectrum analysis at the bottom of Figure 56 indicates that the rumble frequency is approximately 50 Hz.

The gain calculated in the rumble model at 0.8/39K is 0.6 and the gain at 0.8/45K is 1.4. Somewhere between these two points the model would predict the transition from stable operation to rumble. Assuming a linear variation in gain from 0.8/39K to 0.8/45K, we expect the model to predict rumble starting at approximately 0.8/42K. The altitude predicted for the onset of rumble for the Frithorn flameholder is in good agreement with test data. The rumble frequency predicted by the model also compares well with engine data. Table I gives a summary of the results for the Frithorn flameholder.

The model was run for the B/M flameholder at 0.8/39K. Figure 57 shows the rumble model output for this case. The model predicts rumble (gain ~2) at 48 Hz. When execution of the rumble model was attempted at 0.8/45K, an error was encountered. The combustion model indicated that the rich limit on fuel-air ratio in the duct was exceeded. Therefore, the rumble model could not be run at this flight condition.

Engine data from FX217-18 for the B/M flameholder at 0.8/39K indicates stable operation. A rumble blowout occurred at 0.8/49K (see Figure 58). The spectrum analysis shows the frequency of rumble to be approximately 50 Hz.

Rumble model predictions for the B/M flameholder do not agree with FX217-18 test data. The model predicts rumble at 0.8/39K while engine data indicates stable operation. The combustion model is predicting a value of −7 for ZEFC

$$\left(\frac{FA}{\eta} \frac{\delta\eta}{\delta FA} , \text{ duct} \right)$$

for this case. ZEFC is a main factor involved in the prediction of rumble. This large negative value of ZEFC is the reason for the model prediction rumble at 0.8/39K for the B/M flameholder. Also, the combustion model would not generate any output for the flight point 0.8/45K. The engine was operating at this point. Therefore, the combustion model results do not agree with engine data for the B/M flameholder.
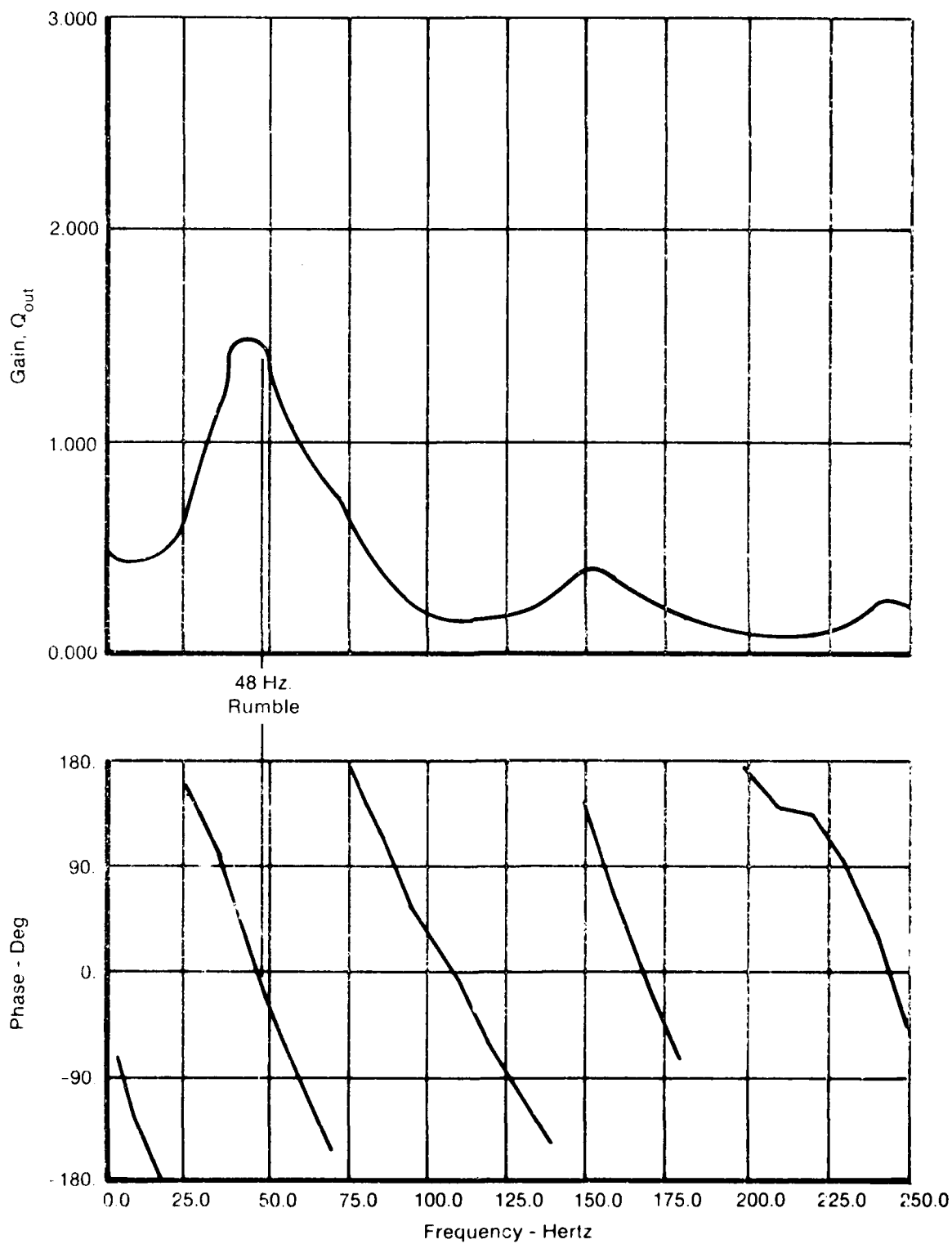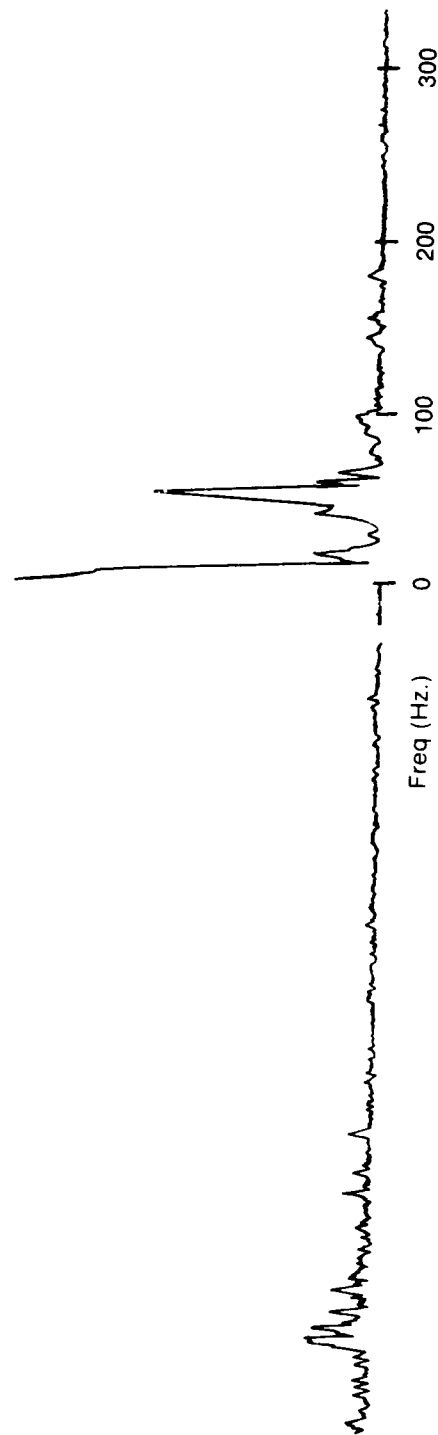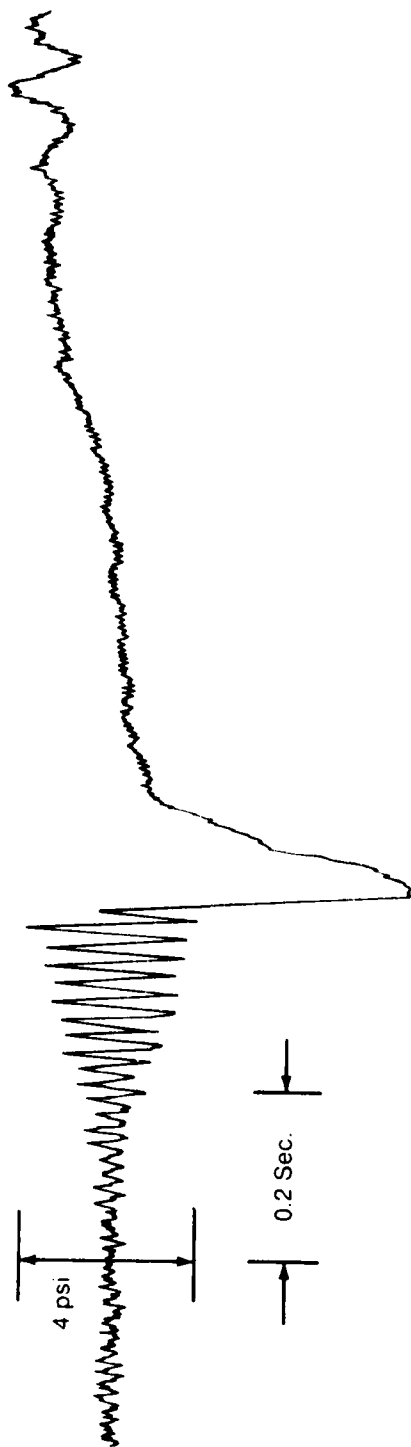
Figure 55. *Rumble Model — Frithorn Flameholder, 0.8/45K, Multistream-tube Analysis*

FD 230874

101

Figure 56. FX217-18, Run 70/1100, Frithorn Flameholder, 0.8/41K Augmentor Kistler AK03

FD 230875

102

TABLE I.   FRITHORN FLAMEHOLDER

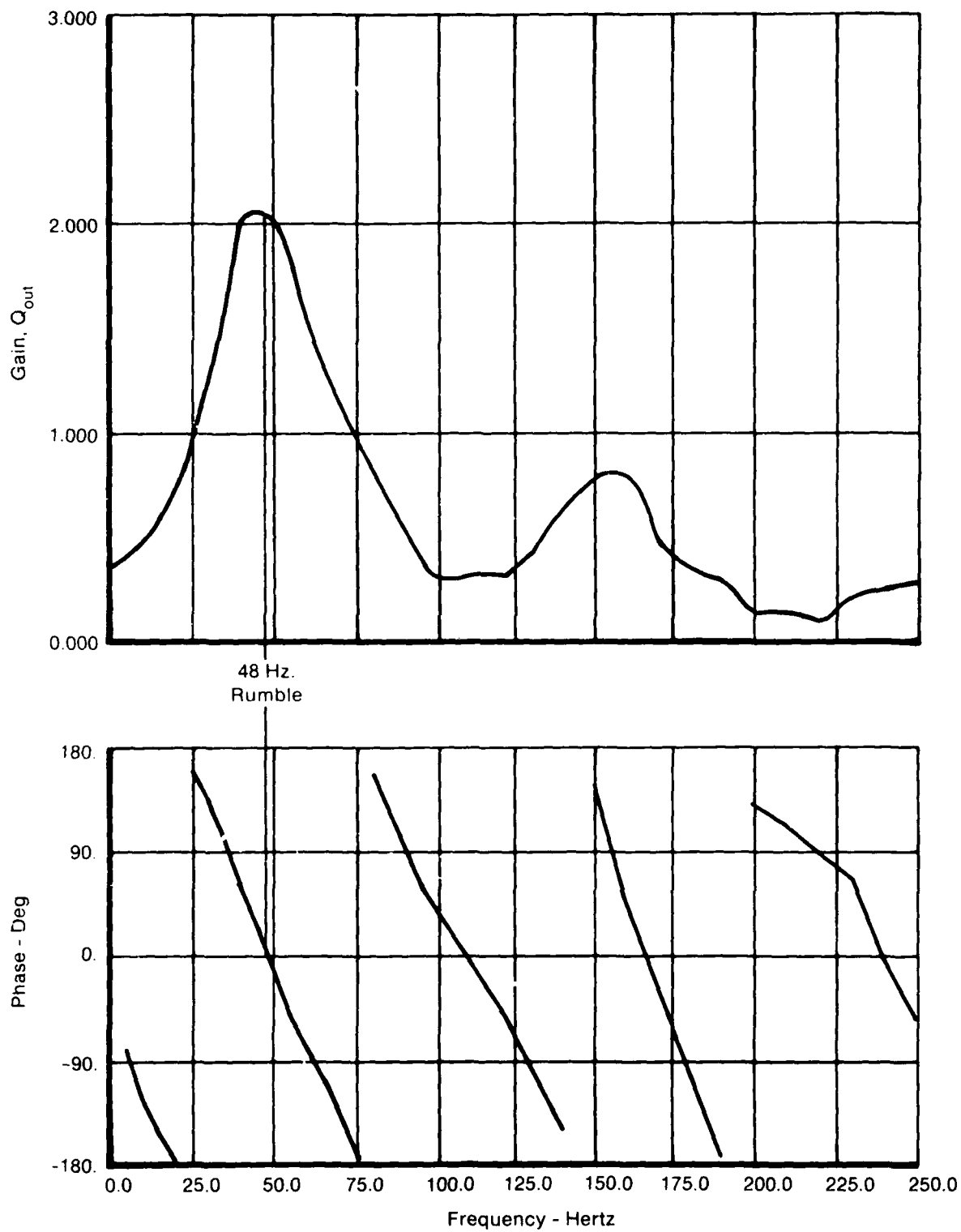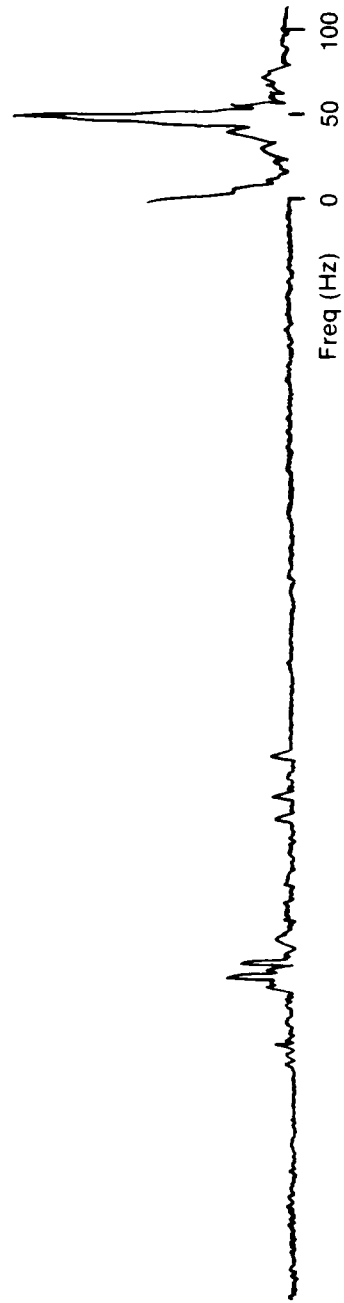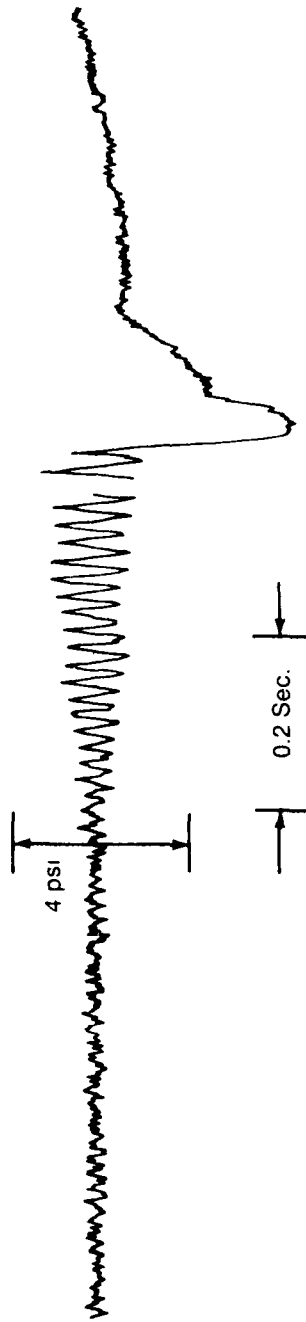|	Altitude for Rumble at 0.8 Mach No. (ft)	Rumble Frequency (Hz)
Engine Data — FX217-18	41K	50
Rumble Model	42K	48

Figure 57.   *Rumble Model — B/M Flameholder, 0.8/39K, Multistreamtube
Analysis*

FD 230876

104

Figure 58. FX217-18, Run 69/1090. B/M Flameholder, 0.8/48K Augmentor Kistler AK03

FD 230877

C. CONCLUSIONS

The Augmentor Stability Management Program has resulted in an extended and improved design system for turbofan augmentors. The program is capable of design evaluation for performance or stability. The results of the various submodels are in excellent agreement with experimental data from several sources.

The combustion model uses a unique solution for stability and efficiency which explains the relative effects of fuel-air ratio, geometry and inlet conditions. The model has shown reasonable correlation with full scale engine test data. The full program is a viable design system for engine design and development.

Perhaps the most important conclusions are drawn from the sensitivity of the results to variations in inlet conditions. To design a stable, high efficiency turbofan augmentor fuel system and flameholder, the designer must have accurate quantitative definition of the inlet profiles. This information should be considered an early priority item in an engine development program.

REFERENCES

1. Kaminski, W. R., and G. P. Beduerftig, "Regenerative Heat Sink Experimental Investigation," Pratt & Whitney Aircraft, Florida Report No. 2895, July 1968.

2. Glickstein, M. R. and R. H. Whitesides, Jr., "Forced Convection Nucleate and Film Boiling of Several Aliphatic Hydrocarbons," ASME Paper 67-HT-88, 9th National Heat Transfer Conference, Seattle, Washington, August 1967.

3. Starkman, E. S., et al., "Expansion of a Very Low Quality Two-Phase Fluid Through a Convergent - Divergent Nozzle," *Journal of Basic Engineering,* June 1964.

4. Longwell, J. P., and M. A. Weiss, "High Temperature Reaction Rates in Hydrocarbon Combustion," Industrial and Engineering Chemistry, 1955.

5. Gater, R. A., and M. R. L'Ecuyer, "Correlation of Liquid-Film Cooling Mass Transfer Data," *International Journal of Heat and Mass Transfer,* Vol. 15, 1972.